1964

Deformation behaviors of niobium and tantalum at low temperatures

Dale Stephen Cowgill
Iowa State University

DEFORMATION BEHAVIORS OF NIOBIUM AND TANTALUM AT LOW TEMPERATURES

by

Dale Stephen Cowgill

A Dissertation Submitted to the
Graduate Faculty in Partial Fulfillment of
The Requirements for the Degree of
DOCTOR OF PHILOSOPHY

Major Subject: Metallurgy

Approved:

Signature was redacted for privacy.

In Charge of Major Work

Signature was redacted for privacy.

Head of Major Department

Signature was redacted for privacy.

Dean of Graduate College

Iowa State University
Of Science and Technology
Ames, Iowa

1964

TABLE OF CONTENTS

STATEMENT OF THE PROBLEM

The character of the mechanical properties of niobium metal changes from ductile at room temperature to brittle at low temperature. Other transition metals, vanadium, chromium, molybdenum, tungsten and iron, also exhibit a change from ductile to brittle mechanical behavior over some temperature range. The transition metal tantalum, sister element of niobium, does not exhibit such behavior.

The purpose of this investigation is to examine the deformation behavior of niobium in the transition temperature range, and to compare this behavior with that of tantalum under equivalent conditions. The comparison is intended to determine whether the differences in low temperature mechanical behaviors of niobium and tantalum are related to macroscopically distinguishable changes in their modes of plastic deformation.

DEVELOPMENT OF THE PROBLEM

Shank (98) has reported on a survey of information pertaining to structural failures, which would be classed as brittle in modern terminology, starting with steel bars in 1879, water standpipes in New York in 1886, including the Boston Molasses Tank Disaster in 1919, and more recent failures of bridges in Belgium and Canada in the 1950's.

Reports of the failures of steel bars in the nineteenth century attributed failure to brittleness inherent in the steel. The standpipes, molasses tank and other early structural failures were attributed to design inadequacies. When the bridges failed, both inherent material properties and complex variables of design and environment were known to be involved in catastrophic brittle failure of steel structures.

The first observations of brittle fracture in structural steels were made early in the history of Bessemer steel production. In 1864, Joseph Kirkaldy published the results of testing of materials carried out in his laboratories in London. The report included information on various materials of construction and, in particular, compared the mechanical properties of Bessemer steel with other irons and steels. Kirkaldy noted that Bessemer steel, which was ductile at room temperature and slow load rates, exhibited very little ductility when loaded rapidly. In modern terms, Kirkaldy

noted that increased strain rate promoted brittleness. This report was probably the first formal recognition of the problem of brittleness in ductile steel. Todhunter's discussion (109) of Kirkaldy's report includes the following quotation which indicates that Kirkaldy recognized brittleness to be a function of the testing or loading conditions as well as the nature of the material.

> "The appearance of the same bar may be completely changed from wholly fibrous to wholly crystalline, without calling in the assistance of any of those agents already referred to - viz., vibration, percussion, heat, magnetism, etc. and may be done in three different ways: first, by alternating the shape of the specimen so as to render it more liable to snap; second, by treatment making it harder; and third, by applying the strain (stress) so suddenly as to render it more liable to snap from having less time to stretch."

Shank (98) reported that Bessemer steel in use for naval construction was found to fracture under low load when impact and "severe" weather were its combined environment. Thus, as early as 1879, increased brittleness in steels loaded at reduced temperature was recognized.

The water standpipe failures in 1886, 1898, and 1904, also discussed by Shank, were examples of brittle failure of rivited structures. While attributing the actual cause of failure to faulty material used in marginally designed situations, the observers of the time emphasized that fracture seemed to have been initiated at the stress concentrations caused by rivit holes and fixtures. Thereafter, existence

of stress concentration was carefully examined in structural failures. This recognition of embrittlement of ductile metals by stress concentration led later workers to develop notched-bar impact tests for evaluation of the toughness of steels.

In 1886 Maitland (75) reported on properties of gun steels as determined by extensive tests at the Royal Gun Factory, Woolrich, England. Maitland tried to produce fractures of the same type as observed when guns failed during firing, i.e., "crystalline" fractures. He first used gun powder to apply high strain rates to rods of the steels and obtained much higher ductility, as expressed by reduction in area, than from slow tensile tests. He even managed to obtain failure by necking in more than one site in a single rod. He found, however, that when identical material in the form of a cylinder was strained by exploding gun powder inside, the fracture was crystalline. In the ensuing discussion of the paper, Strohmeyer attributed the crystallinity to straining under biaxial tension and noted that triaxial tension would produce even more drastic brittleness. Strohmeyer also noted that the facets of the crystalline fracture usually exhibited "feather" markings which pointed toward the source of the fracture. Apparently little attention was paid to Strohmeyer's remarks, because rediscovery of these characteristic markings was one of the few conclusive points determined from the Molasses Tank

Disaster in 1919.

In January, 1919, a Boston molasses tank containing about 2,500,000 gallons of molasses collapsed, drowning twelve persons in molasses and killing others in the attendant destruction. Several horses were killed, and the Boston Elevated Railway was damaged. Litigation of course followed. Shank mentions that one side went to great lengths to prove that an explosion caused the disaster, while the opponents contended that the design was faulty. In his summary, the court auditor noted that both sides were supported by the highest authorities in the field and that,

> "... Amid this swirl of polemical scientific waters it is not strange that the auditor has at times felt that the only rock to which he could safely cling was the obvious fact that at least one-half of the scientists must be wrong."

The present state of knowledge about brittle failure might be summarized in the same way.

Even though both low temperature and stress concentration had been previously recognized as contributing to material brittleness and both were added to marginal design in the molasses tank, no additional factors were recognized. However, Strohmeyer's "feathers" were observed under certain conditions in laboratory tests on the tank steel from the tank and were called "chevrons". It seems reasonable to expect that the spectacular accident would have stimulated some more consideration of deformation and fracture.

In the 1920's, scientists and engineers turned their attention to the fundamental causes of fracture, brittle and ductile; and two useful approaches were proposed to explain brittle fracture and the transition of ductile to brittle behavior.

Cleavage fracture, i.e. fracture in which two planes of atoms in a crystal separate without appreciable plastic deformation, was recognized as a characteristic of brittle failure of structures and as a reproducible mode of failure in iron and steel. Ductile fracture was recognized as flow of metal by layers (perhaps crystallographic planes) sliding past one another until fracture occurred. Ludwik (70) postulated that cleavage fracture occurred in a metal when stress normal to the potential cleavage planes reached some critical value, and that this critical stress increased very little with decreasing temperature. He observed that the critical shear stress necessary to produce plastic flow increased rapidly with decreasing temperature. As test temperature was decreased, the stress necessary to produce plastic flow would increase until at a particular temperature stresses for plastic flow and for cleavage would be the same. Then at lower temperatures the stress required for flow would be greater than that for cleavage and cleavage fracture would occur instead of plastic flow. Figure 1 illustrates this proposal. Any change in the conditions of the material

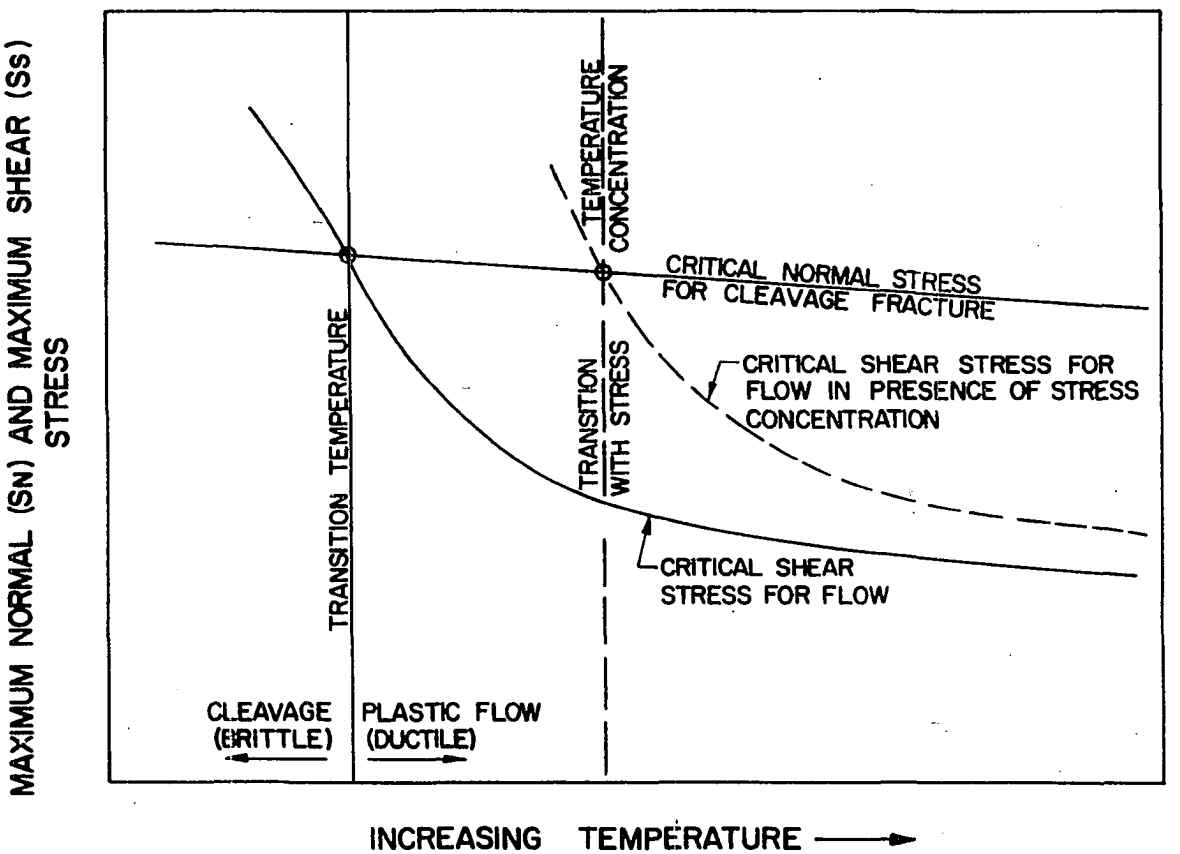

Figure 1. Illustration of Ludwik's explanation for the ductile-to-brittle transition

or the test, such as stress concentration, which will raise the yield stress at a given temperature will raise the temperature at which brittle failure occurs (Figure 1). This approach is still quite useful, even though it provides no information about the fundamental mechanisms involved.

A. A. Griffith (46) in 1924 calculated the conditions necessary for fracture in isotropic elastic media. The basis of his calculation was that the elastic strain energy introduced in an elastic medium by the presence of a crack or a dicontinuity was converted to energy of the surfaces formed by a growing crack when some critical stress was applied to the medium. Then for a crack pre-existing in an elastic medium, the stress required to cause the crack to grow would be

$$S = \sqrt{\frac{E\,\gamma}{2\,c}} \qquad (1)$$

where E is the elastic modulus, γ is the surface energy of the crack and c is the crack length. Griffith then tested his theory by introducing cracks of various sizes into glass fibers and determining the stress required for fracture. The fracture stresses were found to agree with the above expression. This model requires that a crack pre-exist in the material when the load is applied. Calculations applying Griffith's expression to metals showed that cracks of readily observable size would be required. Since metals do not

generally contain such cracks but do fail, the model was obviously not sufficient. Griffith's expression, however, has been the starting point from which expressions involving terms combining energy consumed in plastic work with the crack surface energy were determined to fit experimental results.

At about the same time the explanations for brittle fracture were being proposed, x-rays were being employed for determination of the crystallography of slip and fracture. Elam (32) examined brass and determined that slip, i.e. flow by sliding layers of metal, occurred predominately on {110} planes in brass, and that cleavage in brass occurred predominately on {100} planes, and occasionally on {110} planes. Workers examining iron (32, 105) observed slip which was interpreted as occurring on {110}, {112}, and {123} planes or on planes with no integral indices at all. Cleavage was found (30) to occur on {100} planes in iron. Elam (31) proposed that such non-crystallographic slip and wavy slip bands which were occasionally observed in body-centered cubic metals could be explained by slip on non-parallel {110} planes. At that time it was also known that tungsten could fail by cleavage or, under some conditions such as elevated temperature, by slip.

In 1934, the dislocation theory was applied to metals by Taylor, Orowan and Polanyi. From then until World War II, very little attention was given to fracture and fracture

mechanisms. Early in World War II the first all-welded Liberty and Victory Ships were put into service. By 1944, some 500 of these ships had experienced large fractures ranging from cracked deck plates to breaking in half. This violent presentation of the phenomena of brittle fracture led the American Academy of Sciences and the National Research Council to formulate the Ship Structures Committee in 1943 for the purpose of ascertaining the cause of the frequent failures and recommending changes which would obviate such failures in future ship structures. The committee itself was comprised of representatives from industry, from the Navy and from universities; therefore, the results of progress made by the committee were widely disseminated both formally and informally.

In 1957, Parker summarized the knowledge accumulated by the Ship Structures Committee into a very readable book entitled, Brittle Behavior of Engineering Structures (84). Parker's book summarizes both the knowledge of failures in structures and the knowledge concerning the separate variables, e.g. composition, strain rate, stress state, etc., which had been studied in research projects initiated or supported by the Ship Structures Committee. As we have seen, the effects of certain variables were separately recognized long before the formation of study committees.

Parker discussed the effects of composition, prior

mechanical treatment, heat treatment and size and shape on the brittle behavior of steel. It was noted that the interstitial impurities, carbon, hydrogen, oxygen and nitrogen, were effective in raising the temperature at which brittle failure occurred. The effects of prior working and heat treatment were such that resulting large grain size or second phase particles tended to raise the ductile-to-brittle transition temperature. The effect of shape was directly associated with stress concentration. The size effect was that the larger a piece, the more likely it was to be brittle. Even after subtracting or accounting for the effects of residual stress, of variations in prior working, and of variations in microstructure, the size effect, although small, was still present.

Parker used the Griffith and Ludwik models in his descriptions of the mechanisms of failure. In 1957 and 1958, Stroh (104), Cottrell (25), and Petch (87) presented different but similar dislocation theories of the brittle fracture of metals. In all three theories, some plastic flow was required to initiate fracture. Dislocation theory was utilized by Cottrell (110) to show that coalescence of immobile dislocations in the crystallographic plane most favorable for cleavage could result in Griffith type critical micro-cracks. Stroh (103) showed that dislocation pile-ups at grain boundaries could produce slip or micro-cracks in adjacent

grains. He also postulated (102) a mechanism, later observed experimentally, by which sub-boundary arrays of dislocations could move under stress to produce a crack in single crystals. The point of interest was that dislocation theory could account for crack formation, and Griffith's model corrected for plastic deformation could account for propogation.

Cottrell and Bilby (26) provided an early explanation of strengthening due to interstitial or substitutional solute impurities. Cottrell derived an expression for the energy of interaction between dislocations in a metal and solute impurities in the vicinity of the dislocations. By means of this model and experimental data from iron with carbon and nitrogen, Cottrell was able to explain observed yield points in steels.

Cottrell was also able to empirically derive an expression relating strain rate to test temperature necessary to produce a yield point in iron. This relationship also involves the diffusion coefficient for carbon in iron, thereby directly relating temperature, strain rate and interstitial effects on yield strength of iron.

Cracknell and Petch (28) observed that the yield strength of iron varied as the inverse root of the grain size. From this observation, the so-called Petch Equation

$$\sigma_y = \sigma_o + k_y \, d^{-1/2} \qquad (2)$$

was proposed to relate the grain size, 2d, to the yield strength, σ_y. The parameter σ_o, taken as a measure of the stress required to move a free dislocation through a lattice, depends on the composition of the material and the strain rate and temperature of testing. The parameter k_y is a measure of the stress necessary to propagate slip or dislocation motion across a grain boundary. It was observed that the fracture stress of iron below the transition temperature followed a similar relationship. Therefore, the parameters σ_o and k_y have become standard terms in studies of yielding and brittle behavior.

Cottrell (25), Stroh (101) and Petch (86) proposed different mechanisms of dislocation behavior which led to the same grain size relationship empirically obtained by Cracknell and Petch. Cottrell then applied this relationship to a modification of Griffith's expression in which the surface energy term, γ, appears. Cottrell's expression, Equation 3,

$$(\sigma_o \, d^{1/2} + k_y) \, k_y = \beta \gamma G \qquad (3)$$

where the constant β depends on the specimen geometry and G is the elastic shear modulus, may be rearranged to

$$\sigma_o \, d^{1/2} = \frac{\beta \gamma G}{k_y} - k_y \, . \qquad (4)$$

Equation 4 provides a criterion for brittle fracture of a given material for which the grain size or σ_o is varied.

The effects of strain rate, temperature and composition on the brittle transition are introduced with σ_o. Cottrell's surface energy term is an "effective" energy which is obtained by applying experimental values to Griffith's equation (Equation 1). Since it is easier to obtain brittle fracture than to obtain these values independently, the surface energy, γ, is often calculated from experimental data and treated as the third parameter in yield and fracture studies.

Included in Parker's summary was the point that the ductile-to-brittle transition in mechanical properties was found in body-centered cubic metals and in hexagonal close-packed metals, and not in face-centered cubic metals.

During and after the second world war, interest in non-ferrous metals increased rapidly, especially for aircraft and space applications where low weight was required and high temperatures were often encountered. In the 1950's, it was recognized that the so-called refractory metals, vanadium, niobium, tantalum, tungsten, molybdenum, chromium, and their alloys might be useful materials for high temperature applications. It was also recognized that these materials were body-centered cubic and, therefore, likely to exhibit brittleness at low temperatures. Tungsten and chromium had long been considered brittle materials except at elevated temperatures, and their change from brittleness to ductility was related to the corresponding change found in steel. In

1957, Wessel (113) reported on studies of niobium, tantalum, iron and molybdenum at low temperatures in which it was found that niobium exhibited a ductile-to-brittle transition at about -125°C, but that tantalum remained ductile to at least -200°C.

Studies by Pugh (92) and Bechtold (8) on tantalum also showed that for various grain sizes, strain rates, and purities, tantalum remained ductile down to liquid nitrogen temperatures. In his review of the state of metallurgy at low temperatures in 1957, Barrett (6) reported that tests by Basinsky at 4.2°K proved tantalum remained ductile.

Magnusson and Baldwin (74) examined the effects of temperature and strain rate on the low temperature properties of twelve metals including the six refractory metals excepting niobium, and confirmed the existence of a brittle-to-ductile transition in tungsten, molybdenum, chromium and vanadium but found none in tantalum. At that stage in study of refractory metals, it was known that even though the same variables affected the other low temperature mechanical properties of niobium in the same ways, niobium exhibited a ductile-to-brittle transition and tantalum did not. Since this study is concerned with comparison of tantalum and niobium, subsequent work on mechanical properties of the other transition metals will not be further traced.

Mechanical properties of tantalum at low temperatures

have been reported by several investigators. Barrett and Bakish (7) reported observation of a few cleavage facets in tantalum deformed by impacting at liquid nitrogen temperatures. They identified the cleavage faces as {110} planes with {100} planes occasionally observed. Adams and Iannucci (1) observed cleavage facets in tantalum fractured at room temperature, -78°C and -196°C. They did not identify the cleavage planes but observed the markings in materials containing less than 200 ppm total interstitials with grain sizes of 0.011, 0.023 and 0.016 cm average diameter at all three temperatures. Cleavage traces were observed at strain rates of 1.09×10^{-3} and 9.96×10^{-2} in/in/sec at all three temperatures. It should be noted that other samples of tantalum having the same grain sizes and composition and tested at the same strain rates and temperatures exhibited no cleavage. Derivation of useful information from comparison of results of the two investigations on tantalum is practically impossible, and comparison of results of tantalum investigations with results of niobium investigations are even less fruitful. No other investigators have reported cleavage in tantalum at low temperatures for purities investigated.

Koo (65) investigated grain size effects in tantalum deformation and found that k_y decreased from 5.2×10^6 dynes/$cm^{3/2}$ at 77°K to 2.3×10^7 dynes/$cm^{2/3}$ at 298°K. The room temperature value was about the same as k_y for iron and much

higher (10 times) than k_y for niobium. Gilbert, et al. (43) evaluated k_y from grain size versus yield strength plots and by Lüder's strain extrapolation. For tensile tests in the range from 78°K to 293°K, they found k_y between 8.1×10^7 and 1.6×10^7 dynes $cm^{2/3}$. They concluded that for impurities greater than 75 ppm, total dislocation substructure had no effect on yielding.

The effect of strain rate on yielding of tantalum at low temperatures was determined by Bechtold (8) who found that yield strength at 78°K increased only 10 per cent when strain rate was increased from 2.8×10^{-4} per second to 5×10^{-1} per second.

The effects of solute atoms were investigated by Bechtold (8), Wilcox and Huggins (116), Imgram, et al. (57) and Hahn, et al. (48). In summary, findings of these investigators are that nitrogen and oxygen are the most effective solute atoms for increase of yield strength, while hydrogen interacts with dislocations to produce low temperature strain-aging.

Determinations of the mechanisms of deformation at low temperatures were made by Ferriss, et al. (38) who investigated slip in tantalum, by Koo (65), and by Anderson and Bronisz (4) who investigated twinning behavior of tantalum. Hull, et al. (55) and Lement, et al. (69) investigated the effect of dislocation distribution or substructure on the mechanical behavior of tantalum. In all cases, deformation

was by slip on {101} planes in <111> directions and by twinning on {112} planes. Ferriss, et al. tested single crystals at 77°K, 195°K and room temperature and found that the slip traces were sharper and less often crossed as the testing temperature was decreased. Koo observed that larger grain size promoted twinning at a given temperature and that oxygen additions inhibited twinning.

Investigations into the low temperature behavior of niobium started much later than those for tantalum but have proceeded at a much faster rate. Tantalum has been available and used for many years in applications where superior chemical corrosion resistance was required, but the potential application of niobium was not developed until alloys with high temperature strength and relatively low density were required for aircraft and space applications.

In 1957, Wessel and Lawthers (114) investigated the low-temperature properties of niobium and found that it underwent a ductile-to-brittle transition at about -125°C. Several other authors have observed brittle behavior in niobium. Begley (9), Leadbetter and Argent (68), and McHargue and McCoy (71) observed the brittle behavior while examining the effect of oxygen on the mechanical properties of niobium. Churchman (21) and Adams, et al. (2) found the transition to be at lower temperatures in higher purity niobium used in their investigations. Imgram, et al. (58) obtained cleavage

fracture in tests of notched specimens and compared these with unnotched specimens in which no cleavage was observed.

In the first account of the ductile-to-brittle transition in niobium, Wessel and Lawthers (114) observed that cleavage fracture occurred on {100} planes in niobium at temperatures below -125°C. Their tensile tests were conducted at a strain rate of 1×10^{-3} in/in/sec on material having grain sizes of 4, 120 and 700 grains/mm^2. They found that higher strain rate failed to produce cleavage in the expected temperature range. The material having the largest grain size contained about 450 ppm interstitials and showed mixed shear (ductile) and cleavage fracture at -125°C and total cleavage in tests conducted at -150°C and -196°C. The material with an average grain size of 120 grains/mm^2 exhibited only cleavage in tests conducted at -150, -175 and -196°C; however, the total interstitial content was about 1650 ppm with 1330 ppm oxygen. Increasing the purity to 1480 ppm including 1060 ppm oxygen and decreasing the grain size to 700 grains/mm^2 lowered the temperature at which cleavage first appeared to -175°C. Mixed shear and cleavage were observed in this metal at -175, -185 and -196°C, and one test at -186°C failed with no detectable shear. Reducing the interstitial content to 780 ppm at the smallest grain size resulted in all shear failures except at -196°C where some cleavage was also observed.

Churchman (21) tested niobium at low temperatures using

a tensile strain rate of 4×10^{-4} in/in/sec and obtained cleavage fracture in large grain specimens at -180°C. The average grain size was 3 to 10 grains/mm^2, and the interstitial purity was recorded as less than 600 ppm total. Nitrogen content was reported as less than 100 ppm. Carbon and hydrogen contents were not reported, and the oxygen content was estimated by hardness tests to be between 400 and 500 ppm. Churchman examined seven cleavage facets and found that failure had occurred on {100} planes in three instances and on {110} planes in the other four. He also noted that x-ray patterns from the {110} planes indicated somewhat more surface plastic deformation than in the cases of {100} planes. Material of the same composition but with 5600 grains/mm^2 exhibited no cleavage at -180°C but exhibited some twinning.

Kocks and Maddin (64), in tests on single crystal niobium at room temperature, observed cleavage fracture on {100} planes.

Adams, et al. (2) observed cleavage in niobium containing about 1500 ppm total interstitials at -253 and -196°C. Using a strain rate of 2×10^{-4} in/in/sec, they observed total cleavage fracture for a grain size of 0.071 cm at -253°C. At the same temperature and strain rate, grain sizes of 0.015, 0.004 and 0.003 cm exhibited mixed cleavage and shear fractures with fracture preceded by twinning in all cases.

The only analysis attempted indicated that the cleavage plane was (100). Tests at -196°C at the same strain rate resulted in total shear failures for all grain sizes; however, increasing the strain rate to 6.18×10^{-2} in/in/sec induced cleavage fracture in the 0.071 cm grain size material. Even at this greater strain rate, smaller grain material fractured entirely by shear even though total elongation was less than 10 per cent. Adams, et al. also analyzed their results in terms of the Cottrell equation for transition temperature and found their results to be consistent with his analysis.

Leadbetter and Argent (68) also observed cleavage facets mixed with shear in tests conducted on niobium at -196°C. Two grain sizes, 0.019 cm and 0.027 cm average grain diameters, were tested at a strain rate of 4.5×10^{-5} in/in/sec. The purity of this material was about 150 to 350 ppm total interstitials. Finer grain material also tested at this temperature and strain rate exhibited no cleavage. No identification of cleavage planes was reported.

Maddin and Chen (72, 73) found that slip in niobium single crystals occurred primarily on {110} planes or on combinations of {110} planes in both tension and compression. Some slip traces which were composed of short, unconnected traces were identified as traces of slip on {110} or {112} or {123} planes or combinations of all three sets of planes. Determination of change in pole orientation by x-ray asterism

led the investigators to the conclusion that the slip was basically {110} < 111>.

Churchman (21), Adams, et al. (2), and Leadbetter and Argent (68) also observed twinning in association with the brittle behavior at low temperatures. McHargue and McCoy (71) associated cleavage with twinning only in the presence of hydride platelets, and Wellings and Maddin (112) observed twinning in high purity materials in which no cleavage fracture was obtained. In both these investigations, increased purity of the niobium led to increased tendency toward twinning. Thus the effect of interstitials on twinning is precisely contrary to their effect on brittle failure.

Schwartzberg, et al. (96) determined that additions of tungsten and molybdenum raised the ductile-to-brittle transition temperature. Limited and inconclusive work by Begley and Platte (11) was carried out on the effects of substitutional solutes on mechanical properties of niobium. The effect of interstitial solutes on low temperature properties of niobium has been described by several authors, with the general conclusion as indicated by Hahn, et al. (48) that the order of decreasing effectiveness in raising the transition temperature was nitrogen, oxygen, hydrogen and carbon. Evans (37) investigated the effect of nitrogen on the yield behavior of niobium at room temperature and found an increase in strength even above maximum solid solubility.

Hiltz[1] conducted notch impact tests at low temperatures and found nitrogen to be more than twice as effective as oxygen in raising the transition temperature, and, for both interstitials, the transition temperature was increased even after maximum solid-solubility was attained. Begley and Bechtold (10), Begley and Platte (11), Leadbetter and Argent (68), Wilcox and Huggins (116), and Imgram, et al. (57) investigated the effect of oxygen on the mechanical properties of niobium for various oxygen concentrations and testing conditions.

Imgram, et al. (57), and Wilcox, et al. (115) also evaluated the effects of hydrogen on niobium. In both cases, hydrogen was found to increase "brittleness", but the effect of increased strain rate on alloys containing dissolved hydrogen was to decrease brittleness. That is precisely the effect found in hydrogen embrittlement of steel and is contrary to the effects of the other interstitial elements.

In keeping with Kirkaldy's observation that increased strain rate promoted brittle behavior in steel, Wessels and Lawthers (114), Mincher and Sheely (77), Gregory, et al. (45), Adams, et al. (2), Wilcox and Huggins (116), Leadbetter and Argent (68), and Wilcox, et al. (115) found that increased strain rate either increased the yield strength a few per

---

[1]R. H. Hiltz. Thompson Ramo Woolridge, Inc., Cleveland, Ohio. Effect of interstitials on slow-bend transition in niobium. Private communication. 1962.

cent, or raised the transition temperature in niobium, or both. The increase in strength with strain rate agrees with observations in other body-centered cubic metals and with the theories presented by Cottrell (25), and Cracknell and Petch (28); however, none of the investigators utilized the information to write an expression equating temperature and strain rate effects as was done by Cottrell for iron.

The parameters found in Petch's grain size versus yield strength equation have been evaluated for niobium at various temperatures and purities by Adams, et al. (2), Churchman (21), Dyson, et al. (29), Gregory, et al. (45), Johnson (59), Leadbetter and Argent (68), Mincher and Sheely (77), and Wilcox and Huggins (116). The general observations of these investigators was that the dependence of the yield strength of niobium on grain size was about 10^6 dynes $cm^{3/2}$, lowest of the refractory metals. Negative variation of yield strength with decreasing grain size has been reported and has been attributed by Lement, et al. (69) to substructure variations due to differing annealing conditions and to inability of the grain size plot to represent conditions due to variation in grain size within individual samples.

A detailed study of the relation of substructure to mechanical properties of refractory metals is being carried out by Lement, et al. (69) in which transmission electron microscopy has been used to ascertain the dislocation

arrangement and behavior under various mechanical testing conditions.

In summary, the low temperature mechanical properties of niobium and tantalum have been extensively investigated for a number of years. The large number of variables found to affect mechanical behavior of these materials and the even larger variety of test conditions employed by various investigators have made it very difficult to make accurate predictions concerning the mechanical behavior of either metal.

The variety of testing conditions already indicated precludes systematic determination of the effects of interstitials on either yielding or brittle behavior in these materials. The effects of interstitials on the mechanisms of deformation have been discussed by several authors, but the variety of testing conditions discussed precludes derivation of conclusive results from direct comparisons.

The one area in which testing conditions have maintained some semblance of consistency among various investigators has been the selection of testing temperatures. In nearly every case, the testing was carried out at temperatures obtained by immersion in convenient, common, constant boiling liquids and mixtures. The only problem generated by such consistency is that actual deformation behaviors in intermediate temperature ranges are unknown and, hence, assumed to be the same as the

behavior at the actual testing temperatures.

Cleavage fracture in both niobium and tantalum has been identified as occurring on {110} and {100} crystallographic planes under a variety of conditions. Slip deformation has also been reported to occur on {110} planes as well as {112} and {123} planes in both niobium and tantalum; however, no investigations have determined both slip and cleavage characteristics under the same conditions, even though modern theory requires the slip to initiate cleavage.

Information on deformation behavior in the ductile-to-brittle transformation range for niobium has not been reported, and equivalent information concerning tantalum deformation is unavailable. This investigation was initiated to provide equivalent information for both metals.

DETERMINATION OF EQUIVALENT CONDITIONS

The validity of comparison of deformation behaviors of niobium and tantalum depends on attainment of "equivalent" conditions. For two different elements equivalence must be met in two areas: material equivalence and test equivalence.

Material Equivalence

Examination of the general properties of niobium and tantalum reveals many similarities in physical, chemical and mechanical properties and, as would be expected, a few dissimilarities. The most striking mechanical dissimilarity is the object of this investigation. Table 1 summarizes some of the common physical properties of tantalum and niobium and includes the ratios of the values of these properties. For our purposes, the identity of crystal structures and lattice sizes is probably of most interest.

The chemical similarity of the two metals is evident from their occurrence in nature as mixed oxides or minerals and from the difficulty in effecting chemical separation of these two metals. Another aspect of the chemical behavior of more interest to us is alloying behavior. Table 2 summarizes the intermediate phases, their crystal structures and the solid solubilities of several alloying elements for which phase diagrams are available for both niobium and tantalum. The table shows that differences in alloying behavior are

Table 1. Comparison of some physical properties of niobium (76) and tantalum (76, 78)

Property	Values		
	Niobium	Tantalum / Niobium	Tantalum
Atomic number	41	1.78/1	73
Atomic weight	92.91	1.95/1	180.95
Density, g/cm^3	8.6	1.93/1	16.6
Crystal structure	b.c.c.	--	b.c.c.
Lattice parameter, Å	3.300	1.00/1	3.303
Atom diameter, Å	2.853	1.00/1	2.854
Modulus of elasticity, 25°C, in tension, million psi	15.0	1.80/1	27.0
in shear, million psi	5.44	1.84/1	10.0
Poisson's ratio, 25°C	0.38	0.92/1	0.35
Melting temperature, °K	2733	1.20/1	3269
Coefficient of linear thermal expansion, 0-100°C, x 10-6 cm/cm/°C	7.2	0.90/1	6.5
Thermal conductivity, 20°C, cal/cm^2/cm/°C/sec	0.125	1.04/1	0.130
Heat capacity, 0°C, cal/deg/mole	6.012	1.00/1	6.024
Coefficient of electrical resistivity, 0-100°C, μ ohm cm/°C	0.00395	0.97/1	0.00383
Magnetic susceptibility, 25°C, x 10-6 cgs units	2.20	0.38/1	0.827
Quantum states of valence electrons	$4d^4 5s^1$		$5d^3 6s^2$

Table 2. Alloying behavior of niobium and tantalum[a]

Alloying element	Intermediate phases: Formula Nb	Formula Ta	Crystal structure Nb	Crystal structure Ta	Solid solubility maxima: Atom per cent Nb	Atom per cent Ta	Temperature °K Nb	Temperature °K Ta
Boron	Nb_3B	Ta_3B	--	--	< 6.5	5.0	1880	2070
	Nb_2B	Ta_2B	--	tet.				
	Nb_3B_2	Ta_3B_2	tet.	--				
	NbB	TaB	ortho.	ortho.				
	Nb_3B_4	Ta_3B_4	ortho.	ortho.				
	NbB_2	TaB_2	hex.	hex.				
Carbon	Nb_2C	Ta_2C	hex.	hex.	5.9	0.3	2500	3070
	NbC	TaC	f.c.c.	f.c.c.				
Chromium	$NbCr_2$	$TaCr_2$	f.c.c.	f.c.c./hex.	33.2	21.6	1990	2250
Cobalt	$NbCo_2$	$TaCo_2$	cubic/hex	cubic/hex.	--	--	--	--
		$TaCo_3$		f.c.c./hex				
Hafnium	none	none			> 40	100	1920	> 1770
Hydrogen	?	Ta_3H	--	tet./ortho.	85	40	373	> 373
Iron	Nb_9Fe		--		5	7	2020	1910
	Nb_3Fe_2		cubic					
	$NbFe_2$	$TaFe_2$	hex.	hex.				

[a]Compiled from diagrams presented by English (35), Hansen (51) and Elliott (33, 34).

Table 2. (Continued)

Alloying element	Intermediate phases: Formula Nb	Formula Ta	Crystal structure Nb	Crystal structure Ta	Solid solubility maxima: Atom per cent Nb	Atom per cent Ta	Temperature °K Nb	Temperature °K Ta
Nickel	$NbNi_3$	$TaNi_3$	ortho.	ortho.	<2	2	1550	1870
Nitrogen	Nb_2N	Ta_2N	h.c.p.	h.c.p.	?	7	--	2270
	$NbN_{0.8}$		hex.					
	$NbN_{0.95}$		h.c.p.					
	NbN	TaN	hex.	h.c.p.				
Oxygen		Ta_4O		ortho	4	>4	2188	>1570
		Ta_2O		ortho.				
	NbO	TaO	cubic	cubic				
	NbO_2	TaO_2	tet.	tet.				
	Nb_2O_5	Ta_2O_5	(3)	(2)				
Plutonium	none	none			0	0		
Rhenium	NbRe	Ta_2Re_3	tet.(σ)	tet.(σ)	45	47	2730	2960
	$NbRe_3$	$TaRe_3$	cubic	cubic				
Silicon	Nb_4Si	Ta_9Si_2	hex.	hex.	4.4	1.2	2140	>1570
		Ta_2Si		tet.				
	Nb_5Si_3	Ta_4Si_3	hex.	hex.				
	$NbSi_2$	$TaSi_2$	hex./ hex.	hex.				
Titanium	none	none			100	100	1150-1990	1150-1990
Tungsten	none	none			100	100	>2570	all

Table 2. (Continued)

Alloying element	Intermediate phases: Formula Nb	Intermediate phases: Formula Ta	Intermediate phases: Crystal structure Nb	Intermediate phases: Crystal structure Ta	Solid solubility maxima: Atom per cent Nb	Solid solubility maxima: Atom per cent Ta	Solid solubility maxima: Temperature °K Nb	Solid solubility maxima: Temperature °K Ta
Uranium	mono-tectoid	none			100	3.1	1170-1370	1450
Vanadium	none	TaV_2		f.c.c.	100	100	all	>1590
Zirconium	mono-tectoid	mono-tectoid			100	1000	>370	1800

minor; and in the case of the interstitial alloying elements carbon, hydrogen, oxygen and nitrogen, the differences occur only in areas where considerable uncertainty exists concerning the number and types of phases which form in a given system.

Figure 2, illustrating the temperature dependence of tensile yield properties of niobium and tantalum, shows that their mechanical behavior is also quite similar, at least in trend if not in particular values. Examination of other mechanical properties shows the same sort of agreement except in the properties illustrated in Figure 3. Figure 3 shows that the ductility of niobium, regardless of the ductility criteria, undergoes a rapid transition over a short temperature range at some temperature below room temperature. Tantalum does lose some ductility, but only by stretching the definition of brittleness can a transformation temperature be identified.

Compositional equivalence

Our concern is with equivalence in mechanical behavior, hence our interest in compositional equivalence is related to the effect of impurities on the mechanical behavior of niobium and tantalum. Present knowledge of mechanical behavior is based on the concept of dislocation motion producing plastic deformation; therefore, any compositional equivalence must deal, at least in part, in terms of dislocations. Since brittle fracture of metals is almost always

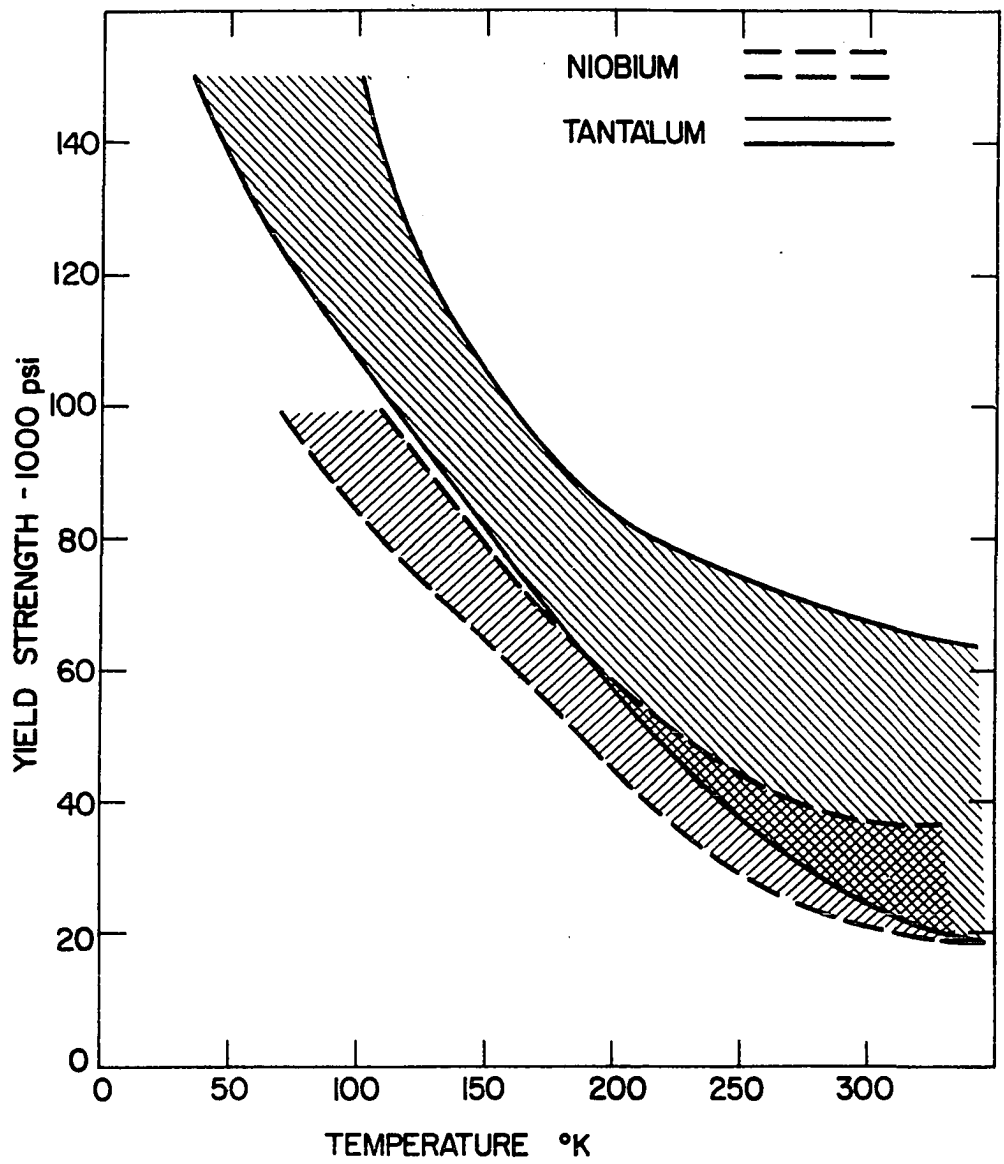

Figure 2. Yield strengths of niobium and tantalum at low temperatures

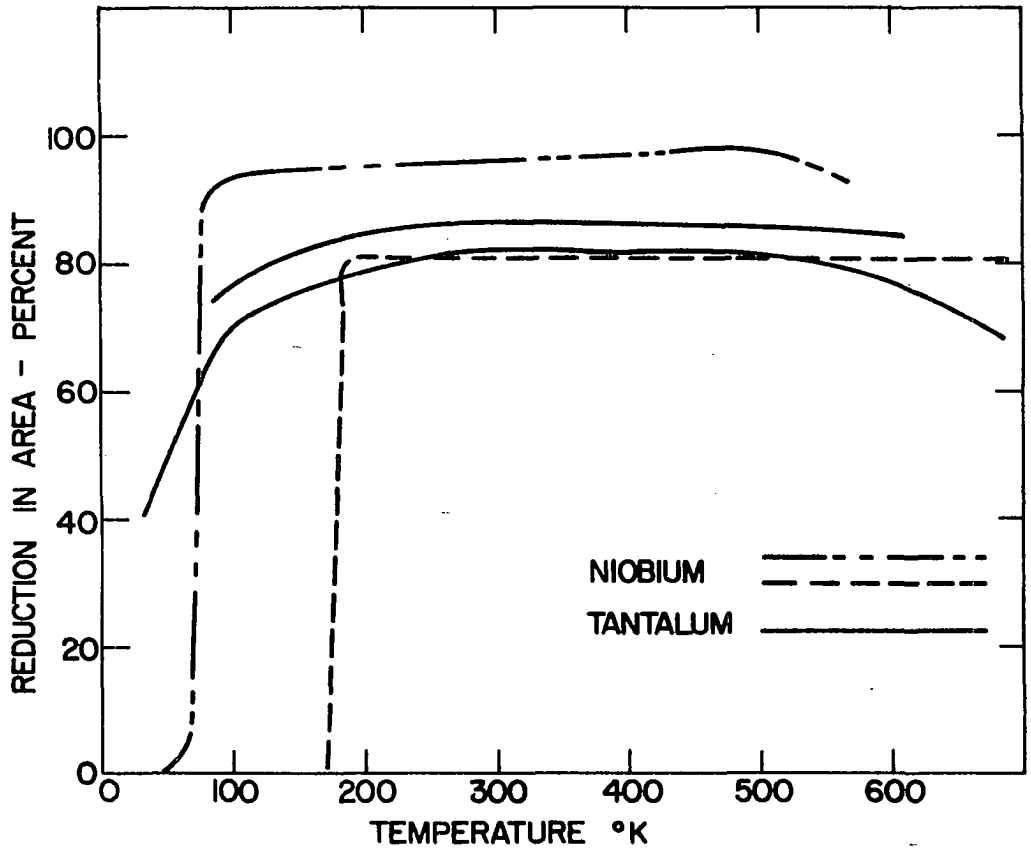

Figure 3. Ductility (as reduction in area) of niobium and tantalum at low temperatures

accompanied by some amount of plastic deformation, and the occurrence of brittle fracture is attributed to inhibition of plastic deformation while subjecting the material to large loads or strains, the effects we must consider are interference of impurities with dislocation motion.

When the amount of impurities in a metal exceeds a certain limit, second phases are formed as particles in the grain boundaries, as particles within the grains of the matrix phase. In either case, the particles block dislocation motion on many slip planes and act to increase flow stress of the alloy. The particles within the grains change the distance of free motion of dislocations, and the alloy behaves as if the grain size of the matrix material were changed. Under certain conditions of heat treatment, impurities may be retained as clusters of atoms which are potential second phase particles. These clusters, known as Guinier-Preston zones, interact with dislocations in much the same way as secondary phases. Second phases may act either as points of rigid stress concentration where dislocation motion is totally restricted and fracture is initiated, or as soft barriers through or around which dislocations may pass with only moderate stress increases. Obviously the effect on brittle behavior depends on the location, number, size and morphology of the particles within a given matrix material. Quantitative evaluation of these four effects has not been reported for any niobium or tantalum

alloy systems and shall not be attempted here. The first step in compositional equivalence, therefore, is avoidance of second phases in the materials. That condition is an ideal, attainment of which depends somewhat on how hard the metal is scrutinized. For our purposes, absence of second phases from microstructures examined by light microscopy will be considered the criterion for single phase material.

Transmission electron microscopic examination of niobium (69, 99, 111) revealed that under some conditions foreign particles were found in materials free of second phases as determined by light microscopy. In high purity materials similar to the ones used in this investigation, the precipitate particles were restricted to dislocation sites; and their effect will be considered as part of the effects of interstitial impurities on dislocation motion.

We must consider two conditions which exist in real single phase materials. The first of these is substitutional solid solution. The effects of substitutional solute elements on some mechanical properties of niobium and tantalum have been described by Hahn, et al. (48) who found that, except for rhenium, all alloying elements investigated tended to raise the ductile-to-brittle transition temperature. In all cases, the effects for small percentages of alloying elements are almost unmeasurable.

Cottrell (110) observed that the lattice in the vicinity

of a dislocation in a crystal possesses elastic strain energy due to the slight displacement of atoms from equilibrium lattice sites. A similar condition is attained in the vicinity of a foreign atom in a lattice of atoms of a different size. The strain around a dislocation varies from compressive around the "extra" plane of atoms to tensile in the opposite region where a plane of atoms was "missing". Location of a large foreign atom in the dislocation region under tensile strain would cause less lattice strain than a dislocation in a uniform region of the lattice; and by shortening "bond" lengths between atoms near the dislocation, the foreign atom would relieve some of the local strain. Cottrell calculated the decrease in lattice strain energy obtained by locating impurity atoms near dislocations and called the energy change the interaction energy, V. Cottrell and Bilby also noted that this interaction energy would provide a potential to attract diffusing atoms so that impurity atoms would tend to collect near dislocations given enough time and enough thermal energy to permit diffusion. Thus, under some conditions, impurities could diffuse to dislocations and relax the local strain energy by interacting with the dislocations. Such relaxation would increase the stress necessary to overcome the energy potential for dislocation motion, and the dislocation would be "pinned" as compared to the unrelaxed state. With this model, yield

point and strain-aging behavior in body-centered cubic metals (in particular, iron) was qualitatively explained.

The expression for interaction energy obtained by Cottrell was

$$V = \frac{4}{3} G r_o^3 e_i \underline{b} \frac{1 + \nu}{1 - \nu} \frac{\sin \alpha}{r} \qquad (5)$$

where G = elastic shear modulus

r_o = atom radius of solvent

$e_i = \frac{r_i - r_o}{r_o}$ and r_i is the atom radius of solute

$\underline{b}$ = dislocation slip distance (Burger's vector)

ν = Poisson's ratio

r, α = spacial coordinates of the solute atom with respect to the dislocation center.

Cottrell and Bilby (26) derived the following expression from the number of solute atoms in the region of the dislocation (about 10 atom distances) after time, t:

$$N = 3n_o \left(\frac{\pi}{2}\right)^{1/3} \left(\frac{ADt}{kT}\right)^{2/3} \qquad (6)$$

where n_o = initial solute concentration

D = diffusion coefficient for the solute atoms

k = Boltzman's constant

T = absolute temperature

$A = \frac{V r}{\sin \alpha}$

Values for lattice strains and diffusion coefficients for substitutional elements in niobium and tantalum are

universally lacking. Therefore, quantitative evaluation of dislocation-substitutional atom interaction is impossible at this time. The information presented by Hahn, et al. (48), however, indicates that the effect of these solute atoms is very small for small amounts of solute. Equivalence, then, can be assumed only if amounts of substitutional alloying elements in niobium and tantalum are very small.

Hahn, et al. (48) presented a thorough review of the effect of interstitial elements on the ductile-to-brittle transition behavior in refractory metals. Their survey is in the form of generalizations which, "are presented in the form of propositions ... and will be discussed and documented where possible" (p. 1). Thus, even though considerable experimental work concerning the effect of interstitials on brittle behavior has been carried out, the variation in reported conditions and results makes generalizations somewhat speculative. The principal problem involved in determining the effect of interstitials on refractory metals is the uncertainty of solid-solubility in these metals. Hahn, et al., chose to describe the solubility as, "interstitial contents likely to be maintained in solid-solubility in group V-A and VI-A after moderate cooling rates" (p. 3). The "likely" is based on, "estimates of the equilibrium solubility on the temperature where $D = 10^{-11}$ cm^2/sec." D is the diffusion coefficient of the interstitial in the metal in

question and is at least as uncertain as the solubility. Table 3 lists the values considered by Hahn, et al., to be likely solubility limits for niobium (columbium) and tantalum. The values for oxygen in niobium and nitrogen in tantalum are higher than values reported for room temperature solubility.

Table 3. Maximum room temperature solid solubility of interstitials in niobium and tantalum after moderate cooling rates[a]

	Solubility, ppm			
	Hydrogen	Carbon	Nitrogen	Oxygen
Niobium	9000	100	300	1000
Tantalum	4000	70	1000	200

[a]Compiled from data presented by Hahn, et al. (48).

Figure 4 illustrates the findings of Hiltz on the effect of oxygen, nitrogen and carbon on the slow-bend transition temperature of niobium. His tests were conducted as slow-bend tests on recrystallized material and showed nitrogen to be most effective and carbon least effective in raising the ductile-to-brittle transition temperature. One of the propositions by Hahn, et al., generalized the order of embrittlement of refractory metals by interstitials to be hydrogen (most potent), nitrogen, oxygen and carbon (least potent).

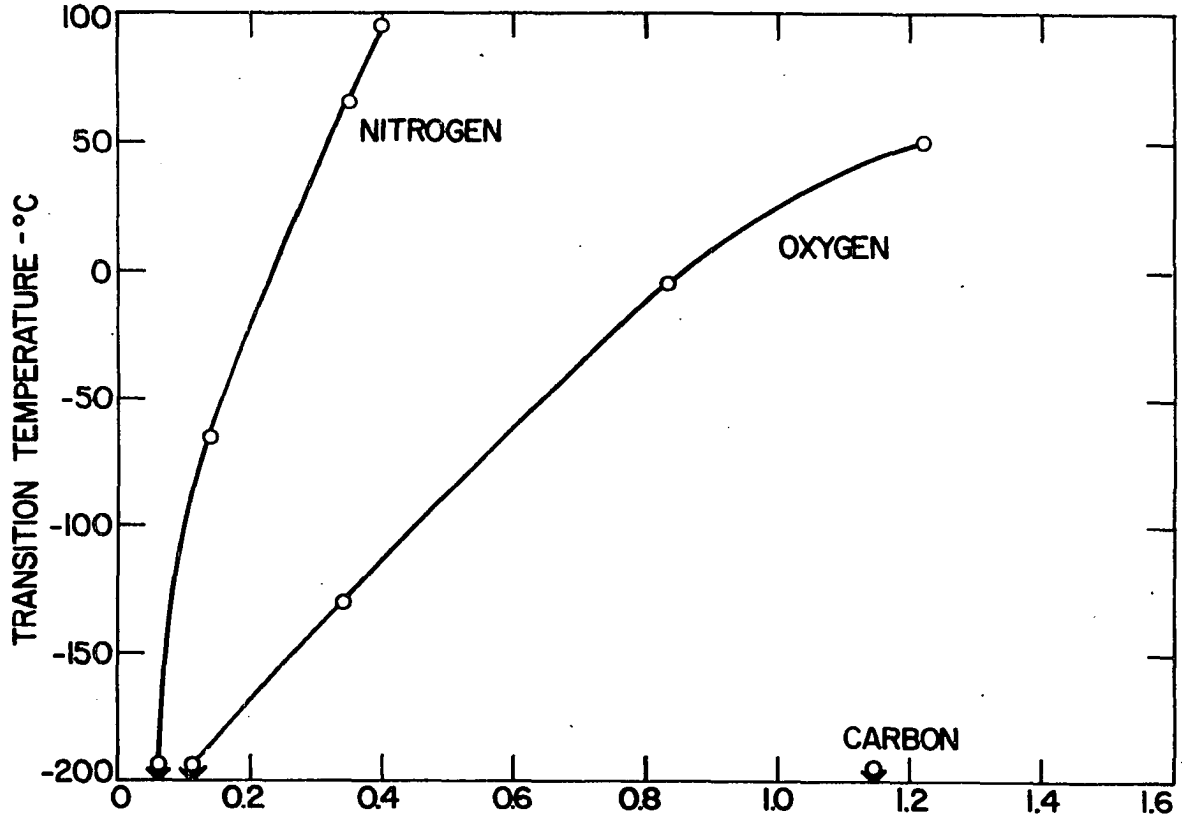

Figure 4. Effect of carbon, nitrogen and oxygen in the ductile-to-brittle transition temperature of niobium (after Hiltz)

Interaction of interstitials with dislocations may be treated in terms of the Cottrell equation (Equation 5, above), and in this case information on solubility, lattice strain and diffusion behavior of interstitials in refractory metals is partially available (5, 17, 63, 88, 89, 90, 97). Table 4 summarizes the values of average lattice strain in niobium and tantalum due to the interstitial elements carbon, hydrogen and nitrogen. Equivalence in terms of interstitial solutes can then be taken as compositions in tantalum and niobium which produce equivalent interaction of dislocation with interstitials, i.e. produce equal dislocation pinning. Examination of Equation 3 shows that values for the elastic shear modulus, Poisson's ratio, the dislocation Burger's vector and lattice strain due to solute atoms are required. Experimental values are available for values of shear modulus and Poisson's ratio at room temperature and for shear modulus at temperatures above room temperature. Since the brittle transition occurs below room temperature, modulus values in that range would be useful to determine equivalent conditions; however, none have been reported. The variation in elastic modulus with temperature for both materials has been summarized by Tietz, et al. (107). No information is available on variations of Poisson's ratio with temperature, and no reasons are known for large changes in these values with temperature; therefore, ratios for niobium and tantalum at room temperature will be

Table 4. Change of average lattice parameter for interstitial solid solutions in niobium and tantalum

Interstitial	Lattice parameter change Å/atom per cent	
	Niobium	Tantalum
Carbon	0.00100	0.00100
Oxygen	0.00267	0.00378
Nitrogen	0.00570	0.00460

considered to be related in the same way at lower test temperatures. The reported slip direction in all body-centered cubic metals has been [111], so the Burger's vector may be taken as $a_o\sqrt{3/2}$, where a_o is the lattice parameter. The Burger's vector for all dislocations will obviously not have precisely this value, but in the absence of contrary information it can be assumed that the distribution of dislocations of given Burger's vector will be essentially the same in the two metals provided that the dislocation densities themselves are similar.

The terms r and α in the Cottrell equation are coordinates which describe the location of the atoms with which the dislocation interacts independently of the lattice structure and hence may be arbitrarily selected at any given temperature.

Equation 7 expresses the conditions necessary for interstitial equivalence in niobium and tantalum.

$$\frac{V_{Nb}}{V_{Ta}} = 1 = \frac{G_{Nb}\ (a_{0Nb})^4\ e_{i-Nb}\ (1+\nu_{Nb})(1-\nu_{Ta})}{G_{Ta}\ (a_{0Ta})^4\ e_{i-Ta}\ (1+\nu_{Ta})(1-\nu_{Nb})} \tag{7}$$

Equation 8 is the form of the expression into which

$$\begin{aligned}(0.5762)(e_{C-Nb}\ \text{x at\%C} + e_{O-Nb}\ \text{x at\%O} + e_{N-Nb}\ \text{x at\%N}) \\ = (e_{C-Ta}\ \text{x at\%C} + e_{O-Ta}\ \text{x at\%O} + e_{N-Ta}\ \text{x at\%N})\end{aligned} \tag{8}$$

composition values for the test materials are to be inserted for evaluation of equivalence. Schoeck and Seeger (94), have presented arguments which show that the effect of interstitials on the deformation of body-centered cubic metals is not entirely due to so-called Cottrell locking, but is a function of Snoek ordering of the interstitial atoms into interstitial sites of minimum strain energy. The expression derived by Schoeck and Seeger for dislocation interstitial interaction is found to dominate only at room temperature and above and hence may be ignored when considering the brittle behavior of niobium.

The theories of Johnston and Gilman (61) and Hahn (47, 49) concern mobility of unpinned dislocations and depend on mobility and generation of fresh dislocations from dislocations present before straining and not pinned at the time the load is applied. The composition enters in determination of

initial free dislocation density and in its effect on dislocation velocity and multiplication under stress. Density of pinned dislocations may be estimated from Cottrell's equation and the concentration of impurity atoms. The magnitude of the impurity effect on the other variables has not yet been determined.

Conrad and Hayes (22) and Gregory (44) consider that yielding is a single thermal activation process and that the mechanism of tearing pinned dislocations from Cottrell atmospheres does not account for the low-temperature yield behavior in body-centered cubic refractory metals. They find that the Peierls-Nabarro, or lattice friction, force on dislocations accounts for experimental results. In the Peierls-Nabarro model, foreign atoms in the lattice present variations in lattice energy which the dislocation must overcome in order to move. The pinned dislocations play no part in yielding or flow and impurities not associated with dislocations are of more direct importance, but the effect of unassociated impurities has not been quantitatively determined. The pinned dislocations also contribute to the Peierls-Nabarro force in that they provide long range static stress fields against which free dislocations must be moved.

In all three models the only measured effect of interstitials is pinning dislocations, whether to slightly inhibit

dislocation motion or to remove them from further contribution. Though admittedly only a rough approximation because true dislocation core conditions are unknown, the Cottrell equation does provide the only means of comparison of effects of interstitial solute atoms on mechanical behavior.

The desired condition in terms of interstitial atoms, then, is that Equation 6 be satisfied for comparable test materials. Compositional equivalence consists of satisfaction of Equation 6 for single phase materials of high purity with respect to substitutional alloying elements.

Structural equivalence

In addition to interaction with alloying atoms, dislocations also interact with each other or with grain boundaries, surfaces or second phases. Since our intention is to eliminate second phases from the alloys to be tested, we can neglect further discussion of that aspect of the problem of structural equivalence.

Petch and coworkers (28, 53, 86) in tests on iron discovered a relationship between the lower yield stress of iron and the grain size. The relationship, Equation 2, is

$$\sigma_y = \sigma_o + k_y d^{-1/2} \qquad (2)$$

characterized by the two yield parameters, k_y and σ_o. The term σ_o may be considered to be the lattice friction stress acting on the dislocation in motion through the crystal.

This in turn is composed of at least two parts, one of which is temperature dependent and generally called the Peierls-Nabarro force, and a non-temperature dependent component which is a function of the impurities, dislocations, etc., in the lattice. Recent work (22, 43, 44, 53), which has attempted to separate the parts of σ_o, indicates that for body-centered cubic materials the Peierls-Nabarro force is responsible for most of the observed increase in yield stress with decreasing temperatures. σ_o is often evaluated by the "grain size" method in which yield stress is plotted against the inverse root of the grain size. The intercept of the plot with the stress axis at infinite grain size is σ_o.

The parameter, k_y, often called the unlocking parameter, is the slope of the plot of lower yield stress versus the negative square root of the grain diameter. According to a model developed by Cottrell (26), k_y is a term which is related to the stress necessary to propogate dislocations across grain boundaries in polycrystalline materials. Petch (40) arrives at the same significance for k_y using a different dislocation model.

If the presence of a yield point is considered to be an irregularity in a naturally smooth stress-strain diagram, one can extrapolate the smooth portion of the diagram above the lower yield elongation back to intersect the elastic portion of the curve. The intersection defines σ_o, the stress

required for motion of free dislocations. The remaining stress up to the lower yield would be σ_a, the stress necessary for motion of dislocations in the presence of some interferring mechanism. Since grain boundaries comprise an interference to dislocation motion, and since the yield strength of polycrystalline materials has been recognized to be a function of grain size since Sorby first identified grains in metals, it is not unreasonable to attempt to relate the stress σ_a to the grain size in a material. Since Petch and coworkers found that yield stress was proportional to the inverse square root of grain size, σ_a conveniently becomes some constant, k_y, times the inverse root of grain size. This procedure, called the extrapolation method, has been used to evaluate σ_o and k_y from individual tensile tests. The requirements for such interpretation are that the diagram be relatively precise so that the lower yield stress is accurately determined and well defined, and that the stress-strain curve be well defined beyond the yield elongation.

Johnson (60) has compared the values of k_y and σ_o obtained by both grain size and extrapolation methods for molybdenum and finds disagreement between the values obtained. He concludes that the stress-strain extrapolation, sometimes called the Lüder's Strain method, is the least satisfactory of the two because of deficiencies in determination of

stress-strain curves. Work by Lement, et al. (69) indicates that the grain size extrapolation methods contain the largest inherent error, since the technique of obtaining a large enough range of grain sizes for reasonable extrapolation consists of annealing the original fine grain material at several temperatures. The resulting substructure is different for each annealing temperature, and Lement, et al. (69) postulate that the substructure determines the true slip length which is the physical condition from which the grain size dependence is obtained. Thus, variation in grain size of a given material is accompanied by a variation in substructure which, however, is not measured or considered in the grain size extrapolation.

The parameter, k_y, for niobium and tantalum has been found to be an order of magnitude smaller than for molybdenum, tungsten, etc., and in some cases has been found by the grain size method to be zero (59) or even negative (69). Since the material for which negative k_y values were obtained by the grain size method exhibited yield points in the stress-strain diagrams, the k_y, if it is truly a measure of the stress required for propagation of dislocations across grain boundaries, cannot be zero. Evans (36) found that strain-annealed niobium exhibited a much stronger grain size yield dependence than did material of the same purity but conventionally annealed. These results then support the

postulates of Lement, et al. (69) and suggest use of the extrapolation method for evaluation of the yield parameters, since that method does not depend on measurement of the structural elements interferring with dislocation motion.

The stress-strain extrapolation technique, however, has serious limitations, one of these being the necessity for well-defined lower yield elongation and subsequent work hardening which is not always obtained. Even when special care is taken, tensile testing of tantalum and niobium at temperatures much below room temperature results in stress-strain diagrams which never exhibit a work hardening region after yield elongation. The usual explanation for such stress-strain behavior is that plastic instability in the form of necking occurs immediately after yielding. Tests on various grain sizes of the same material at these low temperatures often reveal, however, a dependence of yield strength on grain size. If the post-yield portion of the stress-strain curve has a negative slope, extrapolation of that portion will intersect the elastic curve above the lower yield stress and k_y will be negative. In accordance with findings previously mentioned, k_y would be negative. We must conclude, therefore, that the parameters in the Petch equation are ambiguous in the case of niobium and tantalum at low temperatures. Nonetheless, we must determine some equivalence of grain size between the two materials for our

investigation.

The extrapolation difficulties with stress-strain diagrams which show ill-defined transitions from yield elongation to work hardening regions or which have negative work hardening regions can also be observed if strain parameters are used in place of stress parameters. The strain at the end of lower yield elongation is always positive. Since the treatment of the material consists of the arrangement, rearrangement and interaction of dislocations, it seems reasonable for yield elongation to be related in some way to dislocation array in a given material (as is done in the Hahn (47) development). This does not, however, provide a convenient means of measuring σ_o. If σ_o is a constant for a given composition of material, then a plot of yield elongation versus grain size extrapolated to zero yield elongation would give the strain at σ_o. From this strain σ_o could be readily calculated since the theory postulates that σ_o is at most the upper end of the elastic strain range.

Schmidt (93) has presented the results of Savitsky's work on the annealing of tantalum in the form of deformation-temperature-grain size plots which indicate that appreciable grain growth does not occur below 1600°C even though recrystallization occurs as low as 1100 or 1200°C. Page (83) reports that recrystallization in niobium occurs as

low as 900 to 1000°C, and that grain growth becomes noticeable at 1300 to 1400°C. Note that the ratios of temperatures of recrystallization and grain growth to the melting temperatures of the two materials are essentially the same. The work by Lement, et al. (69) on substructures also indicates that the temperatures at which the substructures change from tangled networks to open networks to widely spaced subboundaries for the two materials are in about the same ratio as their melting temperatures. Hull, et al. (55) determined the distribution of dislocations in annealed tantalum in which they found that a well-ordered area of subboundaries replaces subnetworks at temperatures above 1200°C for 30 minute holding periods. The dislocation density in tantalum was reported as somewhat less than $10^{10}/cm^2$ at temperatures above 1400°C. Unfortunately, no comparable discussion of dislocation densities in niobium has been located. From the previous discussion, it appears that treatments of the two metals for the same length of time but at temperatures in the same ratio as their melting temperatures will produce essentially the same structures both in terms of grain size and substructure.

Table 5 is a summary of yield parameter values from Gilbert, et al. (43) and Koo (65) and from a table prepared by Wilcox and Huggins (116) from published test data on niobium and tantalum at low temperatures. Equivalent dislocation-interstitial interaction energies calculated

Table 5. Summary of values for the yield parameters σ_o and k_y for niobium and tantalum

Composition - ppm				Equivalent energies[a]	Test temp. °K	Strain rate 10^{-4} sec.	σ_o 10^8 dyne/cm^2	k_y 10^6 dyne/cm$^{3/2}$
C	N	O	H					
				Niobium				
-	50	60	5	1.60	295	0.10	1.0	52.0
-	20	90	30	1.22	295	0.45	3.4	0.0
-	90	190	61	4.05	295	0.83	6.4	7.9
100	25	50	78	1.46	295	0.83	6.6	9.4
700	500	100	200	12.01	295	2.0	6.9	2.8
-	100	120	15	3.65	295	0.83	7.3	4.2
104	215	230	7	7.08	295	0.83	7.4	2.7
100	140	340	14	6.34	295	0.88	8.3	0.0
-	100	500	-	6.53	295	4.07	9.0	5.0
25	50	53	-	1.02	295	-	9.8[b]	16.0[b]
25	50	53	-	1.02	295	-	9.8	15.1
-	30	70	267	1.71	295	0.83	10.2[c]	8.2[c]
-	50	60	5	1.60	223	0.10	3.1	79.0
700	500	100	200	12.01	195	2.0	12.4	3.8
100	140	340	14	6.34	195	0.88	14.5	0.0

[a]Calculated from Equation 8.

[b]By the extrapolation method.

[c]Fracture stress.

Table 5. (Continued)

Composition - ppm C	N	O	H	Equivalent energies[a]	Test temp. °K	Strain rate 10^{-4} sec.	σ_o 10^8 dyne/cm^2	k_y 10^6 dyne/cm$^{3/2}$
-	100	500	-	6.53	195	4.07	16.9	2.0
25	50	53	-	1.02	195	-	17.0[b]	13.7[b]
25	50	53	-	1.02	195	-	20.2	-2.7
-	100	500	-	6.53	93	4.07	33.4	0.0
-	50	60	5	1.60	88	0.10	14.5	102.0
700	500	100	200	12.01	77	2.0	33.1	5.2
100	140	340	14	6.34	77	0.88	35.8	0.0
700	500	100	200	12.01	77	6160.0	39.0	7.3
25	50	53	-	1.01	77	-	65.6	-36.0
				Tantalum				
18-40	3-12	3-20	0.4-10	0.58-2.21	295	5.0	6.5	23.0
50	101	82	8	10.41	295	1.09	10.8	10.4
50	12	12	-	2.00	295	-	13.0[b]	21.1
50	101	82	8	10.47	295	9.95	14.5	10.4
8	22	14	-	2.08	295	-	15.0[b]	30.6[b]
35	12	12	-	1.78	295	-	16.0	17.9
35	12	12	-	1.78	295	-	17.7[b]	10.9[b]
8	100	14	-	6.87	295	-	18.8[b]	22.4[b]
50	12	12	-	2.00	295	-	19.0	21.1
3	12	147	-	7.06	295	-	19.0[b]	42.6[b]
3	12	96	-	4.88	295	-	19.3	49.0
8	100	14	-	6.87	295	-	19.8	10.9

Table 5. (Continued)

Composition - ppm				Equivalent energies[a]	Test temp. °K	Strain rate $\frac{10^{-4}}{sec.}$	σ_o 10^8 $\frac{dyne}{cm^2}$	k_y 10^6 $\frac{dyne}{cm^{3/2}}$
C	N	O	H					
3	12	96	-	4.88	295	-	26.6[b]	12.6[b]
50	12	12	-	2.00	230	-	23.0[b]	-
8	22	14	-	2.08	230	-	24.0[b]	37.0[b]
3	12	147	-	7.06	230	-	28.5[b]	54.6[b]
3	12	147	-	7.06	230	-	31.0	-
18-40	3-12	3-20	0.4-10	0.58-2.20	203	5.0	13.0	38.0
50	101	82	8	10.47	195	1.09	19.0	10.4
50	101	82	8	10.47	195	9.95	23.5	10.4
35	12	12	-	1.78	195	-	25.2	74.4
8	22	14	-	2.08	195	-	28.0	46.3
50	12	12	-	2.00	195	-	28.0[b]	18.5[b]
8	100	14	-	6.87	195	-	31.2	26.0
8	100	14	-	6.87	195	-	32.0[b]	19.1[b]
3	12	147	-	7.06	195	-	34.0[b]	50.0[b]
35	12	12	-	1.78	195	-	34.0[b]	11.7[b]
3	12	96	-	4.88	195	-	38.2	33.4
3	12	96	-	4.88	195	-	41.0[b]	12.6[b]
50	12	12	-	2.00	150	-	36.0[b]	16.7[b]
50	12	12	-	2.00	150	-	53.0	16.7
8	22	14	-	2.08	150	-	53.0	50.0
3	12	147	-	7.06	150	-	53.0	76.7

Table 5. (Continued)

Composition - ppm				Equiv-alent energies[a]	Test temp. °K	Strain rate 10^{-4} sec.	σ_o 10^8 dyne/cm^2	k_y 10^6 dyne/cm$^{3/2}$
C	N	O	H					
50	12	12	-	2.00	125	-	65.0	34.0
8	22	14	-	2.08	125	-	65.0	39.0
3	12	147	-	7.06	125	-	65.0	80.7
18-40	3-12	3-20	0.4-10	0.58-2.20	77	5.0	28.8	52.0
50	101	82	8	10.47	77	1.09	42.6	10.4
50	101	82	8	10.47	77	9.95	42.6	10.4
35	12	12	8	1.78	77	-	62.5	120.0
8	100	14	-	6.87	77	-	67.5	84.6
3	12	96	-	4.88	77	-	91.0	14.0
50	12	12	-	2.00	77	-	79.0	16.7
8	22	14	-	2.08	77	-	79.0	48.2
3	12	147	-	7.06	77	-	79.0	61.2

from Equation 8 are also listed for each composition. Figure 5 illustrates the range of values reported for k_y, which is supposed to be independent of compositional variations, for both niobium and tantalum. The figure shows that the ranges of k_y for tantalum and niobium overlap; therefore, small grain size variations are not likely to make noticeable differences in otherwise equivalent materials. The conditions desired for structural equivalence, then, are practically identical grain size substructure in both materials.

Test Equivalence

The testing conditions must meet a variety of requirements. First, they must be chosen so as to induce brittle behavior in niobium at some temperature which can be readily attained and maintained. Second, they must provide equivalent, but not necessarily identical, conditions such that the material behavior rather than the testing system characteristics will be observed.

Stress distribution

Since the behavior of interest is the ductile-to-brittle transition range, the most experimentally convenient stress distribution would be that which produced brittleness at the highest temperature. The conditions which produce the maximum transition temperature are those which induce stress concentration and triaxial tensile loading in large specimens,

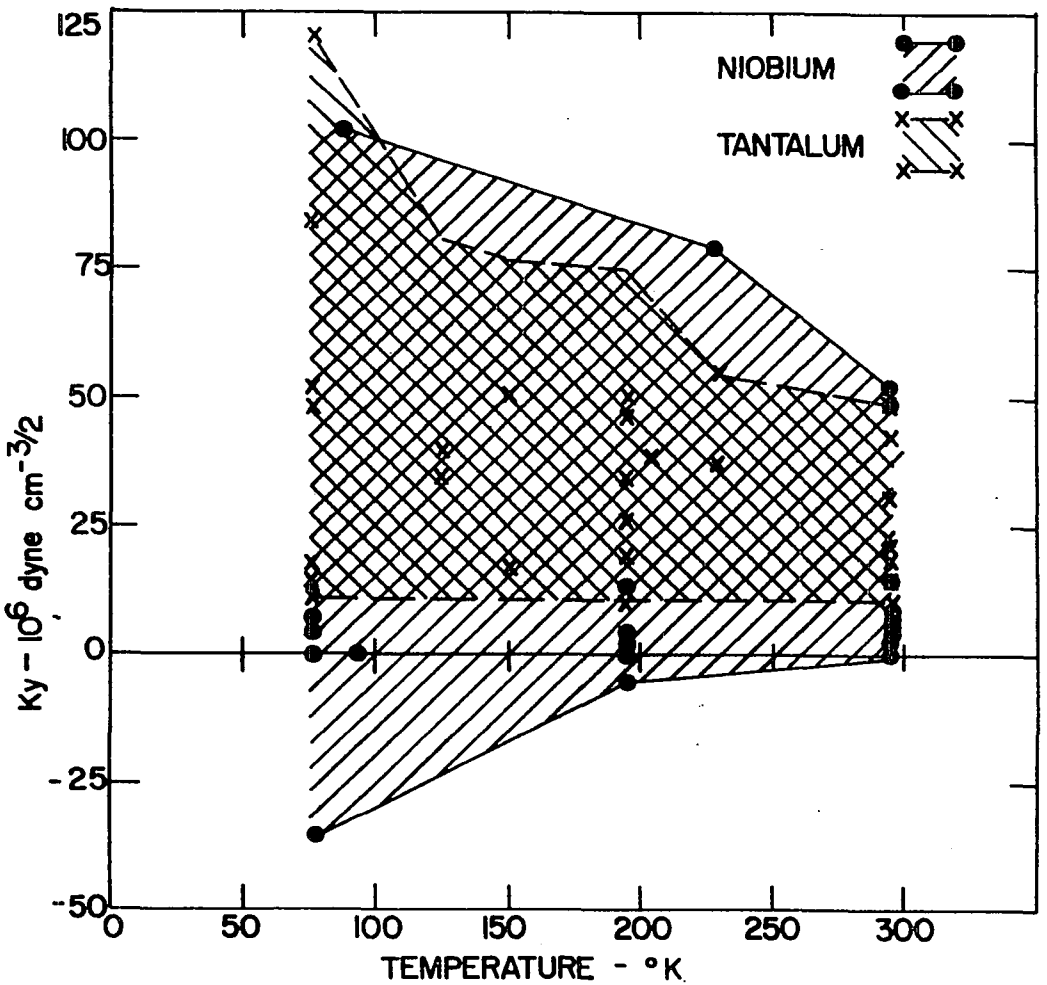

Figure 5. Plot of grain size yield parameter, k_y, for niobium and tantalum at low temperatures

e.g., tensile loading of specimens with sharp notches transverse to the load axis (see Figure 1). These conditions, however, are unsatisfactory on two counts. Small specimens are preferred in order to minimize inhomogenieties in the specimen material. Production of notches in specimens of any size, and particularly in small specimens, introduces the problem of precise reproducibility of the notch geometry. Even in easily machined materials, sharp notches are difficult to reproduce with precision, and the materials under consideration are difficult to machine. Therefore, use of notches to raise the ductile-to-brittle transition range would unnecessarily introduce processing variables as well as complicate observation of resulting deformation. The one specimen configuration which insures highest reproducibility in stress distribution during testing is the uniform cylindrical tensile specimen. Test equivalence can best be maintained by use of small cylindrical tensile specimens loaded so as to insure axiality during testing even though the temperature of interest may be less convenient.

Surface conditions

The effects of surface conditions on brittle behavior arise from two sources: first, roughness of the surface; and second, residual stresses at or near the surface. Surface roughness produces stress concentrations, but of indeterminant magnitude. Reproducibility of test results,

therefore, demands minimum surface roughness. Surface residual stresses arise either from heat treatment in which thermal gradients and/or phase transformations occur, or from mechanical working which produces plastic deformation in a localized region. The best surface condition to insure reproducibility of results would be a surface highly polished after all heat treatment, then treated to remove any plastic deformation resulting from polishing. The most satisfactory methods for minimizing plastic distortion during polishing are standard metallographic techniques. Final removal of distorted surface layers may be accomplished by either polishing or etching by electrolytic or simple chemical methods. In either case, some care must be exercised to avoid contamination of the metals by the etchants.

Interest in the deformation mechanisms also requires the best possible surface so that appearance of slip markings or twin traces may be observed. The surface condition desired for testing equivalence is, therefore, a strain-free, metallographically polished and etched surface.

Temperature and strain rate

With complete material equivalence for niobium and tantalum specimens the yield strengths found in tensile testing at equivalent temperature and strain rate should be the same unless different mechanisms of deformation operate in the two metals. Two kinds of properties obtained from

tensile testing are strength and ductility. Since the object of this investigation is to determine the behavior of niobium and tantalum under conditions where niobium undergoes a ductile-to-brittle transition, the yield strengths are the properties which must be equal to establish equivalent testing conditions.

The yield strengths of niobium and tantalum are generally increased by decreasing temperature or increasing strain rate. Figure 2 shows the ranges of yield strengths of the two metals at low temperatures for various compositions, structures, etc. The ranges overlap at temperatures above 200°K when strengths are plotted as in Figure 2. If strength versus per cent of melting temperature were plotted for both materials, the ranges would overlap over nearly the entire temperature range for which values of yield strength have been reported. Figure 6 shows yield strength versus temperature for specific compositions of niobium and tantalum. The numbers accompanying each line represent the equivalent compositions as calculated from Equation 8. The pairs of lines of nearly equivalent compositions unfortunately are for materials of different grain sizes and structures tested at different strain rates. Ignoring temporarily the strain rate and structural differences, equivalent temperatures for compositions of niobium and tantalum having equivalent dislocation-interstitial interaction energies may be determined by

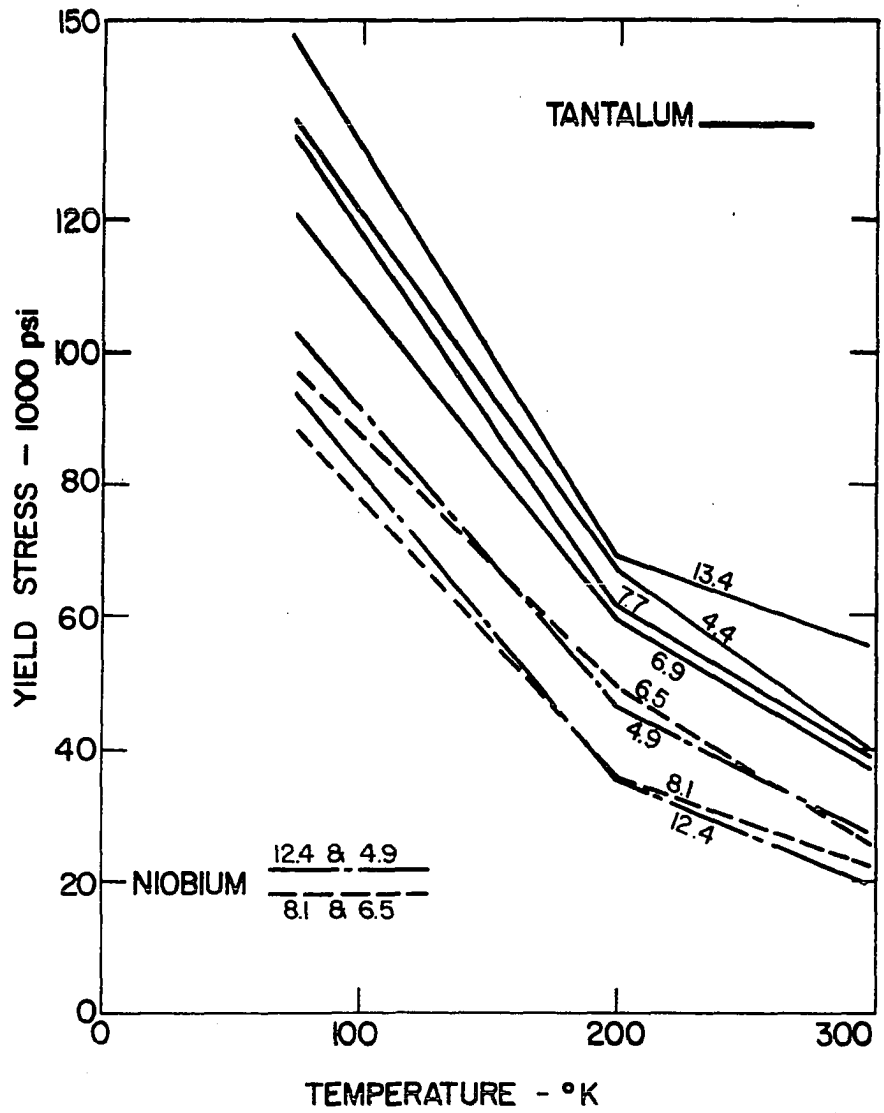

Figure 6. Low temperature yield strengths for niobium and tantalum of equivalent compositions

interpolations on Figure 6.

The reported effects of strain rate on yield properties of niobium and tantalum are summarized in Table 6. Near liquid nitrogen temperature the averages of the reported values for yield strength change with change in strain rate are twice as high for niobium as for tantalum. But both fall well within the variation in yield strengths observed for these metals at the same strain rate under the given testing conditions. Near room temperature the effect of strain rate on the strength of niobium is still very small but for tantalum amounts to a three per cent change in yield strength due to an increase in strain rate by a factor of ten. For fine-grained tantalum tested at room temperature, three per cent variation in yield strength is not unusual even for tests at one strain rate. Then for testing at nearly the same temperatures, differences in strain rate effects in niobium and tantalum are so small that equal strain rates may be considered equivalent strain rates.

The information available from the literature is insufficient to determine the absolute magnitudes of the yield strengths of niobium and tantalum for a given temperature and strain rate.

Determination of equivalent test conditions must, therefore, be a trial-and-error process in which either strain rate or temperature is held constant and the other

Table 6. Summary of effects of strain rate on yield stress in niobium and tantalum

Temp. °K	Niobium			Tantalum		
	Change in yield stress %	Change in strain rate x $\dot{e}_o$	$\frac{\Delta\sigma_y}{\Delta 10\dot{e}}$ [a]	Change in yield stress %	Change in strain rate x $\dot{e}_o$	$\frac{\Delta\sigma_y}{\Delta 10\dot{e}}$ [a]
77	20.4	300	0.68	1.6	90	0.18
	15.9	300	0.53	-0.8	90	-0.09
	17.6	300	0.65	-4.6	90	-0.52
				-6.2	90	-0.69
				0.8	90	0.09
				1.6	90	0.17
				3.2	90	0.36
				-0.8	90	-0.09
				-0.8	90	-0.09
				3.1	31	1.02
				18.6	1780	0.14
Averages			0.62			0.33
123	36.3	10	36.30			
148	5.3	2000	0.03			
173	7.3	10	7.90			
195				22.8	90	2.53
				22.3	90	2.59
				19.7	90	2.19
				26.2	90	2.91
				27.6	90	3.06
				14.1	90	2.43
				21.9	90	1.57
Average						2.49
223	0.0	10	0.00			
293	14.5	2000	0.07	44.4	90	4.00
				22.4	90	2.49
				26.3	90	2.92
				26.3	90	2.92
Average						3.08

[a]Per cent change in yield stress per increase in strain rate by a factor of 10.

adjusted to obtain essentially equal strengths in otherwise equivalent niobium and tantalum. The equivalent temperatures estimated from Figure 6 should serve as starting values.

Summary of Conditions to be Obtained

The tantalum and niobium to be used in this investigation shall be high purity, single phase material. The amount of substitutional alloying elements shall be as low as possible. The interstitial impurity levels should be low in order to assure solid solubility and should be in ratios to produce the same potential energy of interaction of dislocations and interstitials in both materials. The grain sizes and subgrain structures must be essentially equal.

The specimens shall be small, uniform, cylindrical tensile specimens, metallographically polished and etched to minimize contamination, roughness and surface strains. The testing temperatures and strain rates will be adjusted so as to produce the same values for yield stress in both materials.

ATTAINMENT OF CONDITIONS

The purpose of this investigation is to study deformation behavior of equivalent niobium and tantalum in the range where niobium undergoes a ductile-to-brittle transition in mechanical properties. The first requirement for the investigation was selection of conditions such that brittle behavior could be obtained. The accompanying requirements were that ductile behavior also be attained, and that both behaviors be observable and amenable to some sort of systematic analysis.

General conditions necessary to equivalence were discussed in the previous section, and the purpose of this section is to extend the discussions to determine specific conditions of equivalence. This section describes in detail the experimental procedures used in attaining the selected equivalent conditions.

Niobium was selected as the base material to be adjusted to desired conditions, because it is known to exhibit brittle behavior. Tantalum was then adjusted for equivalence with the previously prepared niobium.

The ductile-to-brittle transition in tension has been reported to occur in niobium at temperatures below 148°K, depending on the composition, grain size, strain rate, etc. Except for composition, grain size and strain rate, the conditions affecting ductile-to-brittle transition were fixed by considerations presented in the previous section. The

problem began, therefore, with attempts to control the remaining variables so as to induce brittle behavior under tensile stresses applied at experimentally convenient temperatures. Nitriding and annealing were used to adjust compositions. Grain size control was accomplished by annealing, and strain rate was used as the final adjustment during testing. Nitriding, annealing, sample preparation and tensile testing are described in this section, but detailed analyses of the tensile testing results are reserved for the following section.

Nitriding

Attempts to purchase niobium and tantalum of equivalent composition were unsuccessful. Materials of high enough purity to permit adjustment of composition within the limits imposed by the problem were then obtained from Fansteel Metallurgical Corporation.

Nitriding was selected as the principal means for adjustment and control of the alloys, first because confirmation of Hiltz's data (see Figure 4) was desired, second because some work was necessary to determine lattice strain of niobium caused by nitrogen, and third because the reaction of niobium and tantalum with nitrogen is slow enough to permit some control over the process (67, 82). Before describing the experiments performed for nitriding, the expression for compositional equivalence will be considered,

and the terms of the expression will be determined.

Preliminary development

Development of the expression for equivalence In developing the expression (Equations 3 and 5) for the energy of interaction of dislocations with solute atoms, Cottrell calculated the strain energy in the elastic region around an edge dislocation and the elastic strain energy of an individual solute atom inducing hydrostatic strain in a homogeneous elastic lattice. He then considered the difference in strain energy attained by placing the solute atom in the strain field of the dislocation and called this the interaction energy. He notes that this is a rough approximation since the greatest strain relief would be obtained by locating the solute atom in the core of the dislocation where the lattice distortion is greatest. But the amount of strain energy at the core of the dislocation is not amenable to evaluation, and the behavior of a foreign atom in that location is also unknown.

The second approximation in the expression comes from the fact that an interstitial atom in a body-centered cubic lattice may not produce hydrostatic strain but instead is expected to strain the lattice primarily along a [100] direction. Thus a shear strain may also be introduced and the interstitial solute atoms may interact with both edge and screw dislocations. The form of the interaction energy expression remains the same if the volume strain due to the

interacting solute atom is used in place of the linear strain in the expression for edge dislocation-atom interaction, but the most probable location of the interstitial atom is found to be in the slip plane of the dislocation (94).

At this point an additional problem arises. How may the volume strain (or for that matter, the linear strain) be evaluated? For carbon in iron, martensite is a supersaturated solid solution of carbon in body-centered tetragonal iron. The tetragonal lattice may be assumed to be the result of anisotropic distortion due to carbon in the body-centered cubic lattice, and the tetragonal lattice parameters may be determined for various amounts of dissolved carbon. The volume variation with carbon is then extrapolated to 33-1/3 atom per cent carbon - one carbon per unit cell - to evaluate the local lattice strain due to interstitial carbon. Since the maximum solubility of carbon in martensite is 2 weight per cent (about 10 atom per cent), the extrapolation to 33-1/3 atom per cent may be somewhat presumptuous.

The carbon in martensite evaluation also ignores the presence of defects such as vacancies and dislocations in martensite. The defects could interact with some of the carbon atoms and thereby reduce their strain contribution to the measured lattice parameters. If the number of defect-carbon interactions were the same throughout the range of composition considered, then the parameter measurements would

be valid over that range. The only way in which constant defect-carbon interaction could be assured would be by saturation of all defects present for all compositions considered. The number of defects available in the martensite lattice parameter determinations has not been determined. The saturation concentration is not certain either. Some authors (52, 117, 118) propose that precipitation must occur on dislocations as a limiting condition of interstitial-dislocation interaction, while others (19, 56, 62) suggest that some sort of equilibrium atmosphere concentration will be attained. Either way, we have no assurance that the measured strain with carbon content is really the value necessary for the Cottrell expression. The amount of carbon in martensite is large, however, and the error in strain measurement may be even less than the original approximations in the expression.

In other body-centered cubic metals, strain evaluation is not quite so convenient. First, no supersaturated tetragonal forms on which to make lattice strain measurements have been produced. Some tetragonal phases consisting of body-centered cubic refractory metals and elements which dissolve interstitially have been observed, but in other cases the phases in equilibrium with the solid solution are hexagonal or cubic. Any of the three types of structures may be analyzed for cell volume and compared with the solid

solutions, but the fact that they are distinct phases indicates that they are lower energy states than a solution at the same composition. Lower energy may be attained by metal-interstitial atom bonding to achieve a smaller volume per mole. If this were the case, the strain due to solid solution would be greater than that calculated from the tetragonal phase unit cell dimensions.

Lattice strain with solid solubility may be determined readily, and has been determined for many combinations of metal-interstitials as a method for determination of solubility limits. For the transition metals, however, the total solid solubility is somewhat less than one atom per cent, and information about conditions at 33-1/3 atom per cent are required. The low solubility of interstitials in them indicates that precipitation readily occurs at low concentrations so some of the atoms may be taken out of solution as dislocation precipitates which are not detectable by x-ray methods.

Information on dislocation densities in body-centered cubic metals is scarce, and information on dislocation precipitation is rare. Determination of solute concentration is difficult and for low concentrations values are imprecise. The fact that precision in composition determination improves at high concentrations coupled with the likelihood of dislocation saturation by solutes at higher concentrations

enhances confidence that variation in average lattice strain may actually be due to variation in interstitial solute concentration. Extrapolation from 0.3 to 33 atom per cent, however, remains a dubious procedure.

From the above it appears that evaluation of lattice strain with interstitial solution at concentrations near the solubility limit would give meaningful values if the dislocation density were the same for all measurements, and if the dislocations were saturated in all measurements. Approximately the same dislocation densities may be obtained by identical annealing procedures; and if the material were of the desired composition prior to annealing, identical annealing times would be expected to achieve consistent distribution of impurities in the materials.

If the ratios of interaction energies are considered, the inherent uncertainty in the expressions may be minimized; and the lattice strain with solid solubility will be a better comparative value than a value obtained by linearly extrapolating a possibly non-linear function over two orders of magnitude. When the interaction energy of a given solute with dislocations in tantalum is compared with the equivalent interaction energy in niobium, expressing the comparison as an energy ratio does not necessarily remove the ambiguities due to uncertainty as to the true state of the dislocation core. The dislocation dimensions are the same for both

metals, however; and if the core condition is related to the first power of the elastic shear modulus, the errors due to dislocation core approximations should be minimized by using the ratio.

Evaluation of terms of the equivalence expression

Table 7 summarizes values for lattice strain with interstitial solubility for the interstitials of interest in niobium and tantalum. The values reported in the literature are generally in good agreement except for nitrogen in niobium.

The values from Brauer and coworkers for nitrogen in niobium may have been influenced by other impurities. Cost and Wert (24) conclude from examination of the thermodynamic properties of the nitrogen-niobium solution that dissolution of nitrogen involves practically no entropy change due to lattice distortion. Their conclusion seems incongruous with the findings by Hiltz (Figure 4) that nitrogen was much more potent in raising the ductile-to-brittle transition temperature than oxygen or carbon.

A different approach was taken by A. Ferro (39). Ferro postulated that the mechanism of interstitial diffusion in body-centered cubic lattices was by jump from one interstitial site to another adjacent, and that the activation energy required for such a jump was just the elastic strain energy necessary to fit the interstitial atom into the new interstitial site. His calculations of activation energies

Table 7. Average lattice strains per atom per cent interstitial in niobium and tantalum

Interstitial element	Niobium lattice parameter change Å per a/o	Reference	Tantalum lattice parameter change Å per a/o	Reference
Carbon	0.0010	15	0.0010	51
Hydrogen	unknown		unknown	
Oxygen	0.0027	97, 12	0.0038	40, 41
Nitrogen	0.0060 0.0050 0.0062 0.0056	13, 95 14 --[a] 39[b]	0.0048	42, 16

[a]This work.

[b]Calculated.

for diffusion in several body-centered cubic metals agree very well with experimental values. For tantalum and niobium, his results are shown in Table 8.

The discrepancy for niobium may be due to use of the wrong model. However, agreement between calculated and experimental values for other body-centered cubic metals (including iron, tungsten, and molybdenum as well as tantalum) indicates that the model is generally good, but something about niobium does not conform to the model assumptions. The expression for activation energy from which he made the

Table 8. Ferro's theoretical and experimental activation energies and D_o values

Diffusion of	$\frac{d-h}{a}$[a]	Activation energy cal/mole		Diffusion coefficient	
		Theoretical	Experimental	Theoretical	Experimental
C in Ta	0.338	42,000	39,600	0.009	0.018
N in Ta	0.298	35,000	37,500	0.008	0.006
O in Ta	0.267	29,000	25,800	0.004	0.007
N in Nb	0.298	20,000	38,600	0.020	0.003
O in Nb	0.267	17,000	27,600	0.008	0.015

[a]Lattice strain for one atom in one unit cell.

calculations in Table 8 is

$$Q = 1.3\ N\ A\ G\ a_o\ (d-h)^2\ (1-\frac{\beta\ q}{RT_m}) \qquad (9)$$

where N = number of atoms involved

A = thermal equivalent of work

G = polycrystalline shear modulus

a_o = lattice parameter of solvent

d = diameter of interstitial

h = height of interstitial hole along [100]

R = gas constant

T_m = melting temperature of solvent

β = temperature coefficient of the shear modulus

referred to the melting temperature.

q = average atom energy at the temperature of diffusion.

The height of the interstitial hole is the same for both tantalum and niobium (0.44 Å) if calculated from the lattice parameters assuming spherical atoms. Ferro derived the energy expressions in terms of the elastic constants in the directions of local strain, but in the absence of experimental values for the directional elastic moduli he used polycrystalline shear moduli values (0.7 dynes per $cm^2 \times 10^{12}$ for tantalum, 0.4×10^{-2} dynes/cm^2 for niobium). He assumed $\beta = 0.40$ for niobium since that value was found experimentally for tantalum. The experimental value (107) for niobium is 0.31. The values 1.42 Å for nitrogen, 1.54 for carbon and 1.32 for oxygen were used for interstitial diameters.

The discrepancy between calculated and experimental activation energies for niobium diffusion cannot be accounted for by simply correcting β; therefore, either d or h or both must be incorrect. Using experimental values for Q, (d-h), the lattice strain in the unit cell for one atom in an interstitial hole may be solved for. Thus (d-h)/a is precisely the term used in Cottrell's expression.

Solving the equation above for niobium yields

$$\frac{(d-h)}{a} \text{ N in Nb} = 0.3565$$

$$\frac{(d-h)}{a} \text{ O in Nb} = 0.3275$$

versus 0.298 and 0.267 calculated by Ferro from the spherical atom model. These values are then effective interstitial strains.

These values may be compared with average lattice strain per atom per cent interstitial by comparing Ferro's values for tantalum with the previously cited average strain values. Then the niobium-nitrogen lattice strain was found to be 0.00563 Å per atom per cent. Similar comparison between Ferro and experimental results for oxygen diffusion in niobium shows that the calculated oxygen average strain would be much higher than that actually obtained experimentally.

In order to determine what niobium-nitrogen strain value should be used in equivalence calculations, the strain was experimentally determined using samples from the starting niobium. The niobium powder containing 50 ppm nitrogen and 50 ppm oxygen was annealed at 950°C under a vacuum of 10^{-5} mm Hg for two hours. The annealed powder was divided into two parts. One part was nitrided before the lattice parameter of the niobium was determined; the lattice parameter of the other part was determined in the annealed condition.

Lattice parameter determinations were made from x-ray powder patterns taken with a back-reflection focusing system. The lattice parameters determined for each pattern line were plotted against $(90-\theta) \tan (90-\theta)$, where θ was the diffraction

angle, and extrapolated to $\theta = 90°$. A least-squares method was used in the extrapolation.

Comparison of the annealed and nitrided patterns showed that lines ascribed to the mixed nitrogen-oxygen-niobium compound appeared in both patterns but were much more clearly defined in the pattern from nitrided powder. Vacuum fusion analyses indicated that the oxygen content after annealing was well above the room temperature solid solubility limit. Therefore, no contribution to lattice strain was expected from further change in oxygen content. The niobium lattice parameter changed by 0.0010 Å, and the nitrogen in solution changed by about 250 ppm (0.16 atom per cent). Assuming that all change was due to nitrogen,

$$e_{Nb-N} = 0.0062 \text{ Å per atom per cent.}$$

This is more than twice the value for oxygen in niobium - a result consistent with mechanical behavior (37, 68).

Comparison of room temperature yield strength for varying oxygen and varying nitrogen content showed that change in yield strength with nitrogen per ppm was 5.7 times as great as for oxygen. Comparisons of deformation energy - more nearly the proper comparison parameter - found nitrogen 10 times as effective as oxygen. The grain size of the nitrogen material was somewhat larger than that for the oxygen tests.

The conclusion is that nitrogen has a larger effect on

dislocations in niobium than does oxygen, and the values obtained by Brauer and coworkers and in this investigation are likely high but nearly correct. The average of these values is 0.0057 Å per atom per cent, which compares very closely with the 5.63×10^{-3} from Ferro based on diffusion activation energies. Therefore, despite Cost and Wert, the value for e_{Nb-N} will be taken as 0.0057 Å per atom per cent for calculation of equivalence.

Since the only variables in the equivalence expression for comparison of two metals are the composition terms, it is convenient to rearrange the expression and collect all the constant terms into one number.

For compositional equivalence we want the same energy of interaction between interstitials and impurity atoms for both materials. The energy expression, Equation 5, shows that the energy for an interstitial inducing a strain, e_I, varies inversely with the distance r of the interstitial from the dislocation. The same interaction energy will then be obtained for different interstitials at different distances depending on the amount of strain induced by the interacting atom. The distance between a dislocation segment and an atom is inversely proportional to the concentration of atoms if the atoms are randomly distributed, i.e. do not interact with each other, in the crystal. Powers and Doyle (88, 89, 90, 91) found by internal friction measurements that interactions

between interstitial oxygen and nitrogen atoms were not detectable in alloys with concentrations less than 700 ppm oxygen and 300 ppm nitrogen. Above those concentrations, oxygen interacted preferentially with nitrogen first then with other oxygens. No carbon interactions were observed.

Therefore, if our alloys are sufficiently dilute solutions that no interstitial-interstitial interaction occurs, the dislocation-interstitial interaction energy is proportional to the concentration, in atom per cent, of the interstitial considered. The effect of adding more interstitials would be to either force the atoms closer to the dislocation, thereby raising the interaction energy, or to supply atoms for interaction with initially free dislocation segments. Either way the effects of separate interstitials would be additive so long as the atoms did not interact. Then the length of dislocation with interstitial interaction energy, V_I, is,

$$l_D = V_I \times \text{a/o I}.$$

The condition desired is equal pinning of dislocations in both tantalum and niobium, i.e.

$$\frac{l_{DNb}}{l_{DTa}} = 1 = \frac{V_{INb} \times \text{a/o } I_{Nb}}{V_{ITa} \times \text{a/o } I_{Ta}} \qquad (10)$$

If the interstitials interact only with the dislocation and

not with each other, we may assume that the pinning effects are additive. Then,

$$\frac{l_{DNb}}{l_{DTa}} = 1 = \frac{V_{C-Nb}xa/oC_{Nb} + V_{O-Nb}xa/oO_{Nb} + V_{N-Nb}xa/oN_{Nb}}{V_{C-Ta}xa/oC_{Ta} + V_{O-Ta}xa/oO_{Ta} + V_{N-Ta}xa/oN_{Ta}} \quad (11)$$

or

$$\frac{l_{DNb}}{l} = \frac{\frac{4}{3} G_{Nb} r_{Nb}^3 \underline{b}_{Nb} \frac{(1+\nu_{Nb})}{(1-\nu_{Nb})} \frac{\sin \alpha}{r}}{\frac{4}{3} G_{Ta} r_{Ta}^3 \underline{b}_{Ta} \frac{(1+\nu_{Ta})}{(1-\nu_{Ta})} \frac{\sin \alpha}{r}} \quad (12)$$

$$\frac{e_{C-Nb} \times a/o\ C_{Nb} + e_{O-Nb} \times a/o\ O_{Nb} + e_{N-Nb} \times a/o\ N_{Nb}}{e_{C-Ta} \times a/o\ C_{Ta} + e_{O-Ta} \times a/o\ O_{Ta} + e_{N-Ta} \times a/o\ N_{Ta}}$$

Since for body-centered cubic lattices with spherical atoms $4r = \sqrt{2}\ a$, where a is the lattice parameter, and edge dislocations available for slip lie along [111] where the atom spacing is 2r,

$$\underline{b} = 2r = \frac{\sqrt{2}\ a}{2}$$

or some integral multiple of that value. Rewriting the coefficients of Equation 12 in terms of the lattice parameters, a, and using the following values:

	Niobium	Tantalum
shear modulus	5.44×10^6 psi	10×10^6 psi
lattice parameter	3.301 Å	3.303 Å
Poisson's Ratio	0.38	0.35

and the lattice strain values in Table 7, Equation 12 reduces to

$$\frac{l_{DNb}}{l_{DTa}} = \frac{(0.5675)(0.001a/oC_{Nb}+0.0027a/oO_{Nb}+0.0057a/oN_{Nb})}{(0.001a/oC_{Ta}+0.0038a/oO_{Ta}+0.0048a/oN_{Ta})} \quad (13)$$

Experimental operations

Starting materials Niobium and tantalum were purchased from Fansteel Metallurgical Corporation in the form of as-swaged 1/4 inch diameter rod. The material requested was to have equivalent compositions and specified maximum interstitial impurities. The material received met only the maximum impurity requirements, but was of high enough purity so that composition adjustments could be made. Table 9 summarizes the reported compositions of the as-received material. Subsequent analyses were all performed at the Ames Laboratory, and the original composition reported by Fansteel Metallurgical Corporation was used only in preliminary calculations.

Figure 7 shows, at 250 magnification, representative microstructures of the as-received rods. No second phases were observed. The as-received material satisfied the equivalence requirements for single phase alloys containing low levels of substitutional alloying elements.

Selection of nitriding method Nitrogen alloys of niobium and tantalum may be prepared by either direct

Table 9. Composition of starting niobium and tantalum in the as-received condition

Element	Analysis by	Composition - ppm 8-5 Nb	6-9 Ta
Carbon	Fansteel	10	10
	Conductimetric[a]	34	109
Hydrogen	Fansteel	-	-
	Vacuum fusion[a]	5	5
Nitrogen	Fansteel	40	10
	Vacuum fusion[a]	68	8
Oxygen	Fansteel	40	10
	Vacuum fusion[a]	70	29
Niobium	Fansteel	Bal.	100
Tantalum	Fansteel	600	Bal.
Iron	Fansteel	70	50
Molybdenum	Fansteel	-	50
Nickel	Fansteel	-	100
Silicon	Fansteel	100	100
Titanium	Fansteel	50	100
Tungsten	Fansteel	100	100
Zirconium	Fansteel	50	-

[a]Performed at Ames Laboratory.

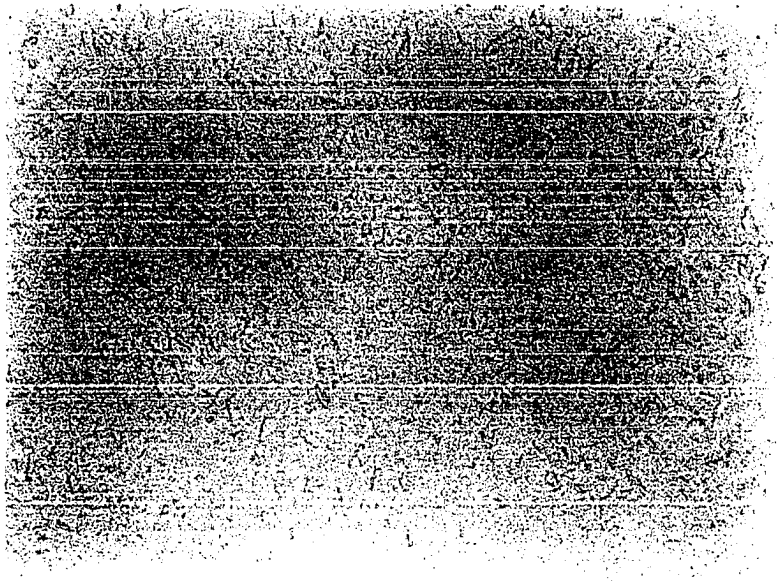

8-5 niobium

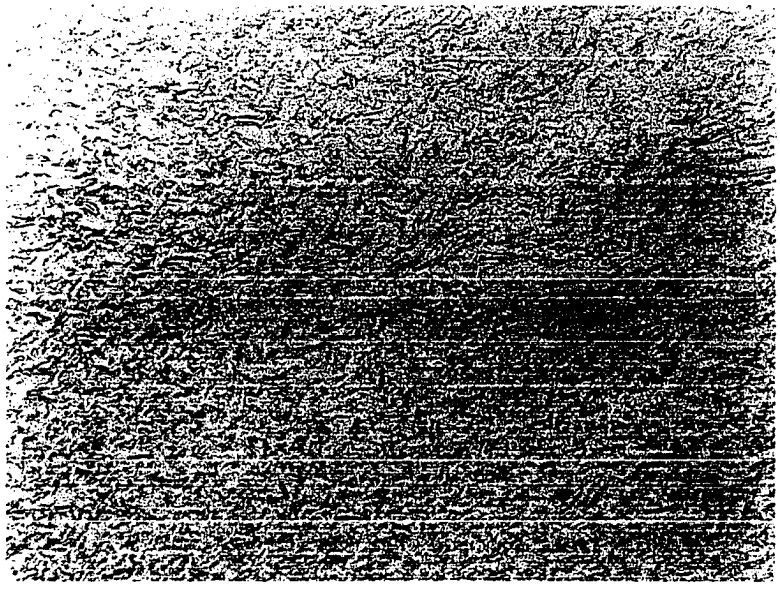

6-8 tantalum

Figure 7. Microstructures of niobium and tantalum starting materials at 250X

gas-metal reaction or by melting together pure metals with nitrides of the metals.

The starting material was obtained in rod form to eliminate processing operations such as melting and swaging in which uncontrolled contamination of the samples might occur; therefore, the method for preparing alloys by melting was not attempted.

Preparation of alloys by gas-metal reaction may be carried out by reaction with either pure nitrogen or nitrogen produced in the reaction chamber by cracking ammonia. The ammonia method for supplying nitrogen often results in hydrogen contamination of the alloys. Therefore, that method was avoided.

The amount of nitrogen added to metal samples by gas-metal reaction may be measured by pressure-drop or weight-gain methods. In either case, the reaction rate is a function of metal temperature. If hot metal is exposed to a known amount of nitrogen gas in a chamber of known volume, measurement of the reduction of chamber pressure with time provides adequate information to calculate the weight of nitrogen which had reacted with the metal during a given time. The alternative method consists of measurement of weight increase of a hot metal sample in contact with nitrogen gas.

Initial nitriding tests were made using the pressure measurement method. The equipment requirements for nitriding

included a chamber large enough to nitride enough 1/4 inch diameter rod tc provide 10 to 12 tensile specimens of the same composition, and uniform temperature to assure uniform reaction and composition over the full length of all specimens. A 3-3/4 inch diameter Vycor tube in a resistance wound tube furnace was found to meet size and temperature requirements, and a Vycor-glass charging system was constructed. The system was designed for either vacuum or nitrogen atmosphere and was arranged to permit measurement of the volume of gases used for chamber atmosphere. Pressure measurement was made by means of a mercury manometer. The best vacuum ever attained with the system was 50 microns, and the leak rate into the chamber was just sufficient to oxidize niobium before significant nitriding occurred.

Rather than abandon the system, it was converted to use with the weight-gain method for nitriding in nitrogen.

Equipment Figure 8 is a schematic diagram of the apparatus used in nitriding and a cross-sectional drawing of the nitriding chamber.

The top portion of Figure 8 shows the internal detail of the Vycor chamber with samples in the two holders in place in the chamber. Niobium shavings and wool were placed in the inlet tube and in the chamber proper to act as "getters" for oxygen in the chamber. Since the nitrogen pressure in the chamber was greater than atmospheric, it was supposed that

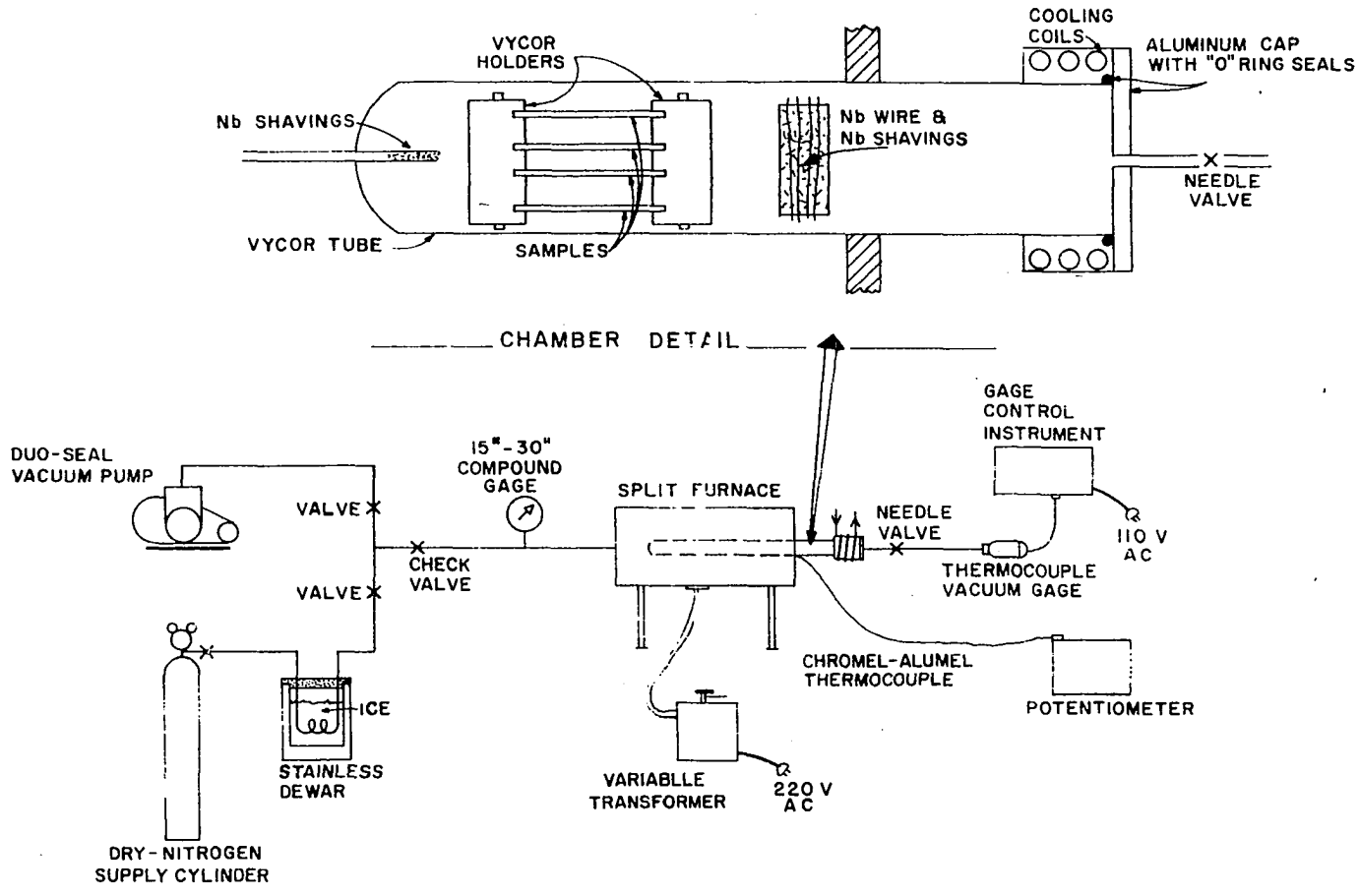

Figure 8. Schematic of nitriding apparatus with cross-section detail of the chamber

virtually no oxygen would leak into the chamber during the nitriding run, but that some oxygen would remain in the chamber after the flushing operations. The getter material was intended to react with most of the residual oxygen during the nitriding heating cycle. The niobium shavings in the inlet tube were intended to remove possible oxygen contamination from the nitrogen gas supplied to the chamber.

The charging end of the chamber was sealed by an O-ring between an aluminum head and brass collar. The brass collar was attached to the Vycor chamber tube with epoxy adhesive and was water cooled to protect the epoxy and O-ring from over-heating. A stainless steel needle valve to permit flushing the chamber was connected to an opening in the aluminum head. A thermocouple vacuum gauge was attached to the outlet valve during vacuum testing runs.

The furnace used in the system was a 220 volt split-tube resistance-wound furnace controlled by means of a Powerstat variable transformer. Manual control was found to be adequate for control within ± 5°C of the nitriding temperatures for the duration of most of the nitriding runs.

Two stainless steel sheets were formed into tubes 3-1/4 inches in diameter by 10 inches long and wrapped tightly around the Vycor chamber tube at the center of the tube furnace. The stainless sheets served to maintain uniform heat distribution over the section of the chamber in which

the samples were placed for treatment.

Temperature measurement during nitriding was made by means of a chromel-alumel thermocouple placed between the stainless steel heat distribution sheets. Thermocouple potential was measured to the nearest 0.01 mv with a Rubicon potentiometer. The external thermocouple was calibrated against a thermocouple located at the central axis of the chamber during heating cycles performed in the same manner as nitriding treatments. The temperatures determined by the external thermocouple during nitriding were recorded and corrected using the calibration curves.

The temperature variation in the chamber cross-section within the portion covered by the stainless steel sheets was found to be less than 2°C. With the chamber tube at nitriding temperature and open to the atmosphere, the temperature differed by 10°C from one end of the covered portion of the chamber to the other. With the tube closed, the variation at the same chamber temperature was about 5°C.

System pressure during nitriding was measured by means of a compound gauge calibrated in inches of mercury for vacuum and pounds per square inch for positive pressures. The compound gauge was located in the inlet line (see Figure 8) between the pressure relief valve and the chamber. System pressure during runs was measured in psig.

A thermocouple vacuum gauge was placed in the outlet side

of the chamber-heat needle valve during tests on the vacuum capabilities of the system. As noted previously, the best vacuum obtained in this system was about 50 microns and pressures of 100 to 200 microns were more common lower limits. Extensive testing of the original glass system revealed that leakage sometimes occurred around the stopcocks. When the glass was replaced by copper, the vacuum tests were repeated, but the source of leakage was not identified. The Vycor chamber tube was replaced just prior to final nitriding to assure that the chamber would not fail during the final treatments. The replacement tube was also vacuum tested with the same result as for the original tube.

The system vacuum was obtained by means of a mechanical vacuum pump. During vacuum testing several pumps or combinations of pumps were used without sufficient improvement in system vacuum to warrant a more complex arrangement than shown in Figure 8. The vacuum system was used for flushing the system of air prior to the weight-gain nitriding tests and final treatments.

Nitrogen for the reaction was supplied from a "dry" nitrogen cylinder with a standard regulator for supply of nitrogen at practically constant pressure. The inherent system leakage obviated attempts (other than the getters mentioned above) to remove any oxygen impurity from the nitrogen. The cold trap shown as part of the nitrogen

supply line in Figure 8 was intended to remove any moisture present in the "dry" nitrogen. Nitriding tests with the trap deWar filled with ice, dry ice or liquid nitrogen gave the same final results; therefore, ice was used during final nitriding as a precaution. The use of liquid nitrogen in the deWar caused violent pressure surges in the gas supply. The surges were reduced by the relief valve, but were still violent enough to scatter some niobium shavings out of the inlet tube into the chamber.

Preliminary nitriding. Both niobium and tantalum were subjected to nitriding treatments at 900°C and 950°C in order to establish rates of weight gain with temperature so that some estimate could be made of the treatments required to obtain desired compositions. The weight changes, system pressures and thermal treatments for the preliminary tests are presented in the appendix. The results of the preliminary tests were plotted along with final nitriding results as weight gain per unit area versus time at temperature in Figure 9.

Log-log scales were used in Figure 9 in order to illustrate the fit of the data to the curves representing the calculated rate equations and to encompass the full range of nitriding times used in final nitriding tests. The figure shows that the weight gain per unit area for tantalum was greater than for niobium after the same times at temperature,

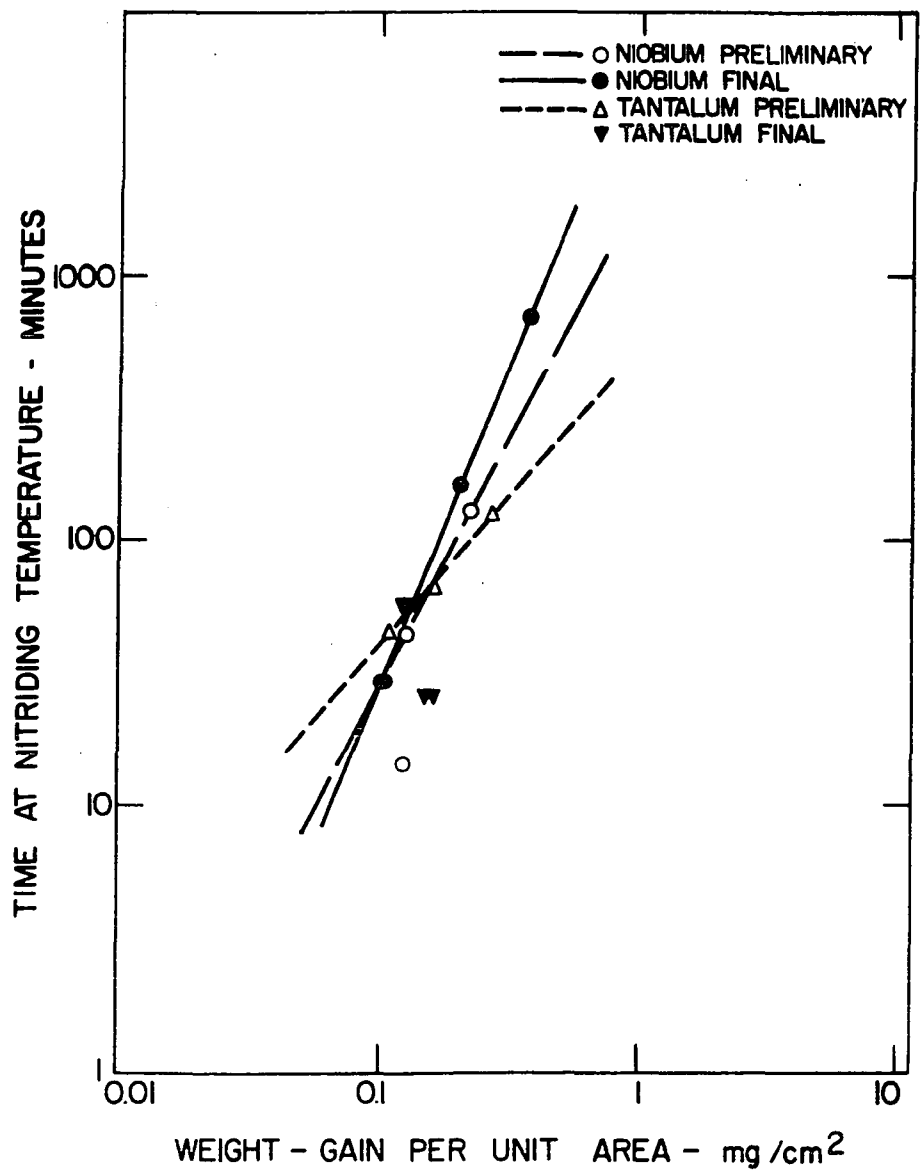

Figure 9. Weight gain per unit area with nitriding time at 950°C for preliminary and final nitriding

but the composition change in ppm was twice as great for niobium as for tantalum. The points representing 14 minutes at temperature do not agree well with the longer time results at least partly because determination of the starting time while heating was imprecise.

Since a reasonable vacuum could not be maintained in the system, it was necessary to fill the chamber with nitrogen prior to heating. Nitrogen was certainly reacting with the metals at some rate at all temperatures above 800°C (60, 72) and possibly at temperatures as low as 400°C. The weight gain value for "14 minute hold" therefore represents some sort of cumulative weight gain for a wide range of reaction rates and times. In order to minimize variations in weight gain during the heating period, the furnace power was set at the same voltage for each of the final nitriding treatments. The original setting was maintained for each run until the chamber temperature was above 935°C and then adjusted to hold the temperature steady at 950°C. Even after subtracting the weight gain for 14 minutes hold from each of the longer time results, the weight gain with time plot was not linear. Subsequent chemical analyses of the preliminary nitriding samples revealed that both oxygen and nitrogen contributed to the weight gain and at different rates.

Table 10 summarizes the weight-gain results for both preliminary and final nitriding treatments at 950°C and the

Table 10. Summary of results of preliminary and final nitriding of niobium and tantalum at 950°C

Material	Nitriding		Composition - ppm		
	Time min.	Weight gain ppm	Carbon C	Nitrogen N	Oxygen O
		Preliminary niobium treatments			
Cb 14	0	-	65	51	56
Cb 8	128	166	65	84	138
Cb 9	68	112	65	148	112
Cb 10	44	96	65	97	145
Cb 12	14	94	65	113	87
		Final niobium treatments			
Cb 15	0	-	34	68	107
Cb 18	29	79	34	127	130
Cb 19	29	81	34	105	94
Cb 20	29	74			
Cb 21	29	79			
Cb 22	161	155			
Cb 23	161	157			
Cb 24	161	151	34	178	93
Cb 25	161	155			
Cb 27	680	273	34	245	153
Cb 28	680	274			
Cb 29	680	279			
Cb 30	680	274			
		Preliminary tantalum treatments			
Ta 11	0	-	58	8	46
Ta 6	128	106	58	59	55
Ta 7	68	60	58	44	44
Ta 8	44	43	58	24	55
		Final tantalum treatments			
Ta 10	0	-	109	8	29
Ta 15	46	61	109	25	30
Ta 16	46	63		30	34
Ta 17	46	60		29	33
Ta 19	58	50		100	170
Ta 20	58	48		22	35
Ta 22	58	51		22	28

resultant compositions of some of the materials after annealing. Comparison of weight changes in preliminary nitriding and annealing with the reported analyses revealed that if all weight change in annealing were attributed to oxygen, the remaining increase in nitrogen and oxygen over the starting composition was approximately equal to the weight gain in nitriding. The assumption of only oxygen change during annealing appeared to be more nearly correct for niobium than tantalum.

The analytically determined increases in nitrogen and the calculated increases in oxygen during preliminary nitriding were fitted by least squares methods to an expression of the form

$$\Delta m = A\ t^b \tag{14}$$

where Δm was the change in weight of the nitrogen or oxygen per unit area; t was the time of hold in the temperature range $935 < t < 960$°C; and A and b were constants to be determined by the analysis. The resulting equations describing weight gain during preliminary nitriding were: for nitrogen in niobium

$$\log \Delta N = 0.7579 \log t - 1.7153; \tag{15}$$

for oxygen in niobium

$$\log \Delta O = 0.2510 \log t - 0.7652; \tag{16}$$

for nitrogen in tantalum

$$\log \Delta N = 1.1098 \log t - 3.1542; \text{ and} \qquad (17)$$

for oxygen in tantalum

$$\log \Delta O = 0.8369 \log t - 2.3365. \qquad (18)$$

These equations were then used to predict nitriding times for specific compositions.

Based on the behavior of the system and results obtained during preliminary nitriding, the following procedure was established as the standard procedure for final nitriding with the equipment described above and in Figure 8.

1. The specimen rods (6-5/8 inches long and 1/4 inch in diameter), holders and the Vycor chamber were washed, degreased and dried.

2. The specimens were placed in Vycor holders and the assembly was placed in the Vycor chamber tube at the center of the section covered by the stainless steel sheets. Niobium shavings were placed in the inlet tube and at both ends of the specimen assembly.

3. The system was sealed, then evacuated by means of the mechanical vacuum pump.

4. While under dynamic vacuum the chamber was dried by heating to approximately 100°C for two hours and then permitted to cool to room temperature.

5. The system was isolated then refilled with dry nitrogen to two psig pressure.

6. The system was flushed by releasing the nitrogen through the valve at the end of the Vycor chamber most remote from the inlet end. Steady flow through the system was maintained by the nitrogen cylinder regulator.

7. Evacuation and flushing were repeated five times to minimize the amount of oxygen remaining in the chamber.

8. When the chamber was filled after final flushing, the furnace voltage was set at 58 per cent of full scale.

9. When the desired temperature was attained the power was manually adjusted to compensate for variations in room conditions and line voltage during the holding period.

10. Cooling after the prescribed holding time was accomplished by turning the furnace power to zero and permitting the system to furnace cool. The cooling rate was about 10°C per minute at 900°C and 1°C per minute at 300°C.

11. The chamber was opened after the temperature dropped below 50°C, and the samples were transferred to a desiccator for cooling before final weighing.

Nitriding niobium The equivalent values for the starting niobium and tantalum were calculated using Equation 13 and the values in Table 7. The niobium was found to be of higher equivalent purity than the tantalum, and calculations determined that the addition of 50 ppm nitrogen would increase

the equivalent niobium composition to that of tantalum.

Equation 15 was used to calculate the nitriding time to increase the niobium content by 50 ppm, the minimum for equivalence; 100 ppm, twice the amount necessary for equivalence; and 250 ppm, solubility limit for nitrogen in niobium.

Final nitriding was performed in accordance with the above standard procedure. The resulting weight gain for each treatment was included in Table 10 and plotted as indicated on Figure 9. The close agreement between experimental and predicted weight increases confirmed that Equations 15 and 16 closely described the nitriding of niobium in this system at 950°C. The agreement also indicated some validity for the assumption that all annealing weight changes were caused by oxygen.

Nitriding tantalum The equivalent purity of the nitrided niobium was calculated from the weight gain results shown in Table 10, and the necessary increases in nitrogen and oxygen for equivalent tantalum were calculated.

The times for nitriding tantalum for equivalence with the previously nitrided niobium were calculated from Equations 17 and 18 by successive approximations. Final tantalum nitriding was performed in accordance with the procedure described above, and the results in terms of weight gain and compositions are shown in Table 10. The first nitriding set (Ta 15,

16, 17) was intended to correspond with the intermediate niobium composition but resulted in weight gain radically higher than calculated from preliminary tests. The calculation was repeated and the second set (Ta 19, 20, 22) was also nitrided so as to correspond with the intermediate niobium alloys. The resultant weight gains from the second nitriding were consistent with predictions but slightly low.

The consistent behavior of one tantalum nitriding treatment indicated that the calculation techniques were valid for at least that nitriding time, but the extremely high weight gain of the short-time nitriding treatment indicated that either the calculations were invalid or, more likely, the system failed at some point in the treatment.

Subsequent final annealing of nitrided tantalum was also plagued by inconsistent weight change so that final compositions of the tantalum specimens could not be calculated with confidence. In order to group the tantalum specimens into two groups for testing under conditions equivalent to those used for the two higher nitrogen niobium compositions, microhardness tests were made at each end of each tantalum tensile specimen. An average microhardness difference of 10 points DPH was found between the specimens nitrided in the two treatments discussed above with the first set the harder.

After tensile testing, one end of each tensile specimen of niobium and tantalum was submitted for analysis for

nitrogen, oxygen and carbon. The results of the analyses are discussed in the final chapter of this report, where evaluation of equivalence is discussed.

Annealing

All the niobium and tantalum materials were annealed as a last operation prior to machine into tensile specimens. Since the as-received material was in the cold-worked state, annealing was necessary for recrystallization and grain growth in those samples which received no nitriding treatment. Nitrided samples were annealed in order to homogenize the alloys and to induce grain growth to the same extent as induced by annealing of unnitrided samples.

Preliminary annealing treatments were performed to determine the response of the starting and nitrided materials to various annealing temperatures and times.

Based on preliminary results, the temperatures selected for final annealing treatments of niobium and tantalum were higher than those employed during annealing tests in order to assure large grain size and to minimize grain size gradients in the reduced sections of final tensile specimens. Final niobium annealing was at 1700°C for four hours. Final tantalum annealing was at 2090°C for four hours.

This section presents details of preliminary and final annealing procedures and equipment. The grain sizes and compositions resulting from annealing treatments are also

described and discussed.

Equipment

The equipment used in annealing treatments was selected to provide high temperatures for long periods of time with minimum contamination of the samples. The possibility of annealing more than one tensile specimen under exactly the same conditions also influenced the equipment selection.

A self-resistance heating arrangement in a chamber capable of better than 10^{-5} mm Hg vacuum was available and appeared to satisfy the requirements listed above. Figure 10 illustrates schematically the vacuum system and the power supply system for the annealing apparatus. The power supply was found to be quite stable so that once the desired temperature was attained, further adjustment was unnecessary for periods of up to four hours of annealing at temperatures from 1300°C to 2100°C. During the holding period of the treatments, the input amperage at constant setting was found to vary as necessary to maintain essentially constant temperatures. That self-compensating behavior was very efficient so long as the electrode contact surfaces were clean but became erratic when samples were clamped to dirty surfaces.

During annealing runs, pressure was maintained continuously below 5×10^{-6} mm Hg except for occasional pressure surges accompanying increases in specimen temperature. The pressure surges never exceeded 10×10^{-6} mm Hg and lasted

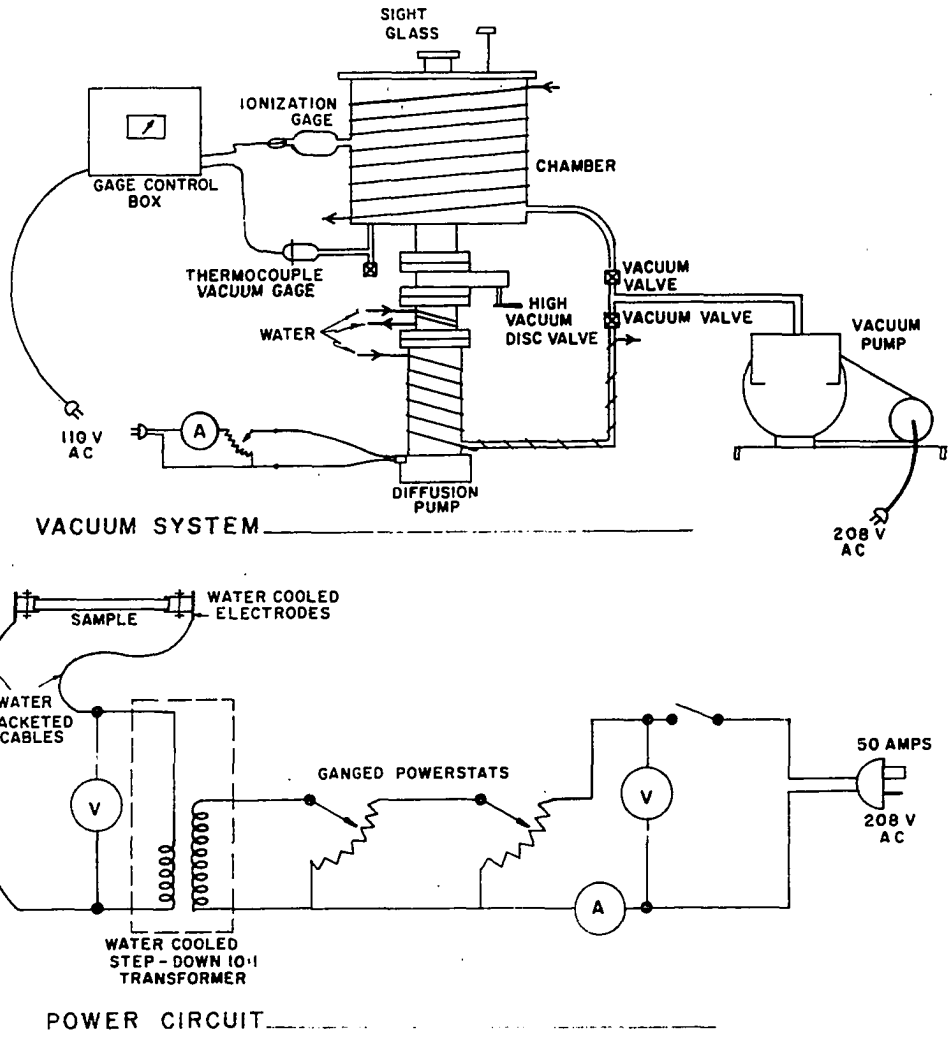

Figure 10. Schematics of vacuum and power supply systems for the annealing apparatus

for periods not over one to two minutes. Pressure was measured during annealing by means of an ion gauge located in the chamber wall at the same height as the annealing sample and about six inches from the sample. The gauge was routinely calibrated before and after each heating and cooling cycle and occasionally during the hold period. Location of the annealing chamber directly over the high capacity vacuum diffusion pump permitted rapid evacuation of the chamber and aided maintenance of low pressures during annealing. The chamber pressure could be reduced from atmospheric to 10^{-5} mm Hg in 20 minutes. A steam supply was arranged for convenient conversion of the chamber cooling coils to heating coils. The chamber walls were steam heated before opening the chamber, while the chamber was open for sample installation, and during initial evacuation in order to minimize moisture condensation in the system and to speed outgassing during evacuation.

Figure 11 is a cut-away view of the annealing chamber showing the large diameter coils of 1/4 inch copper tubing which permitted adjustment of the electrode clamps to accommodate variations in specimen lengths. The electrodes were also individually reversible so that specimen lengths from 2-1/8 inches to 6-5/8 inches were conveniently mounted under slight tension to prevent buckling during heating. The small electrode coils shown in Figure 11 connected the two

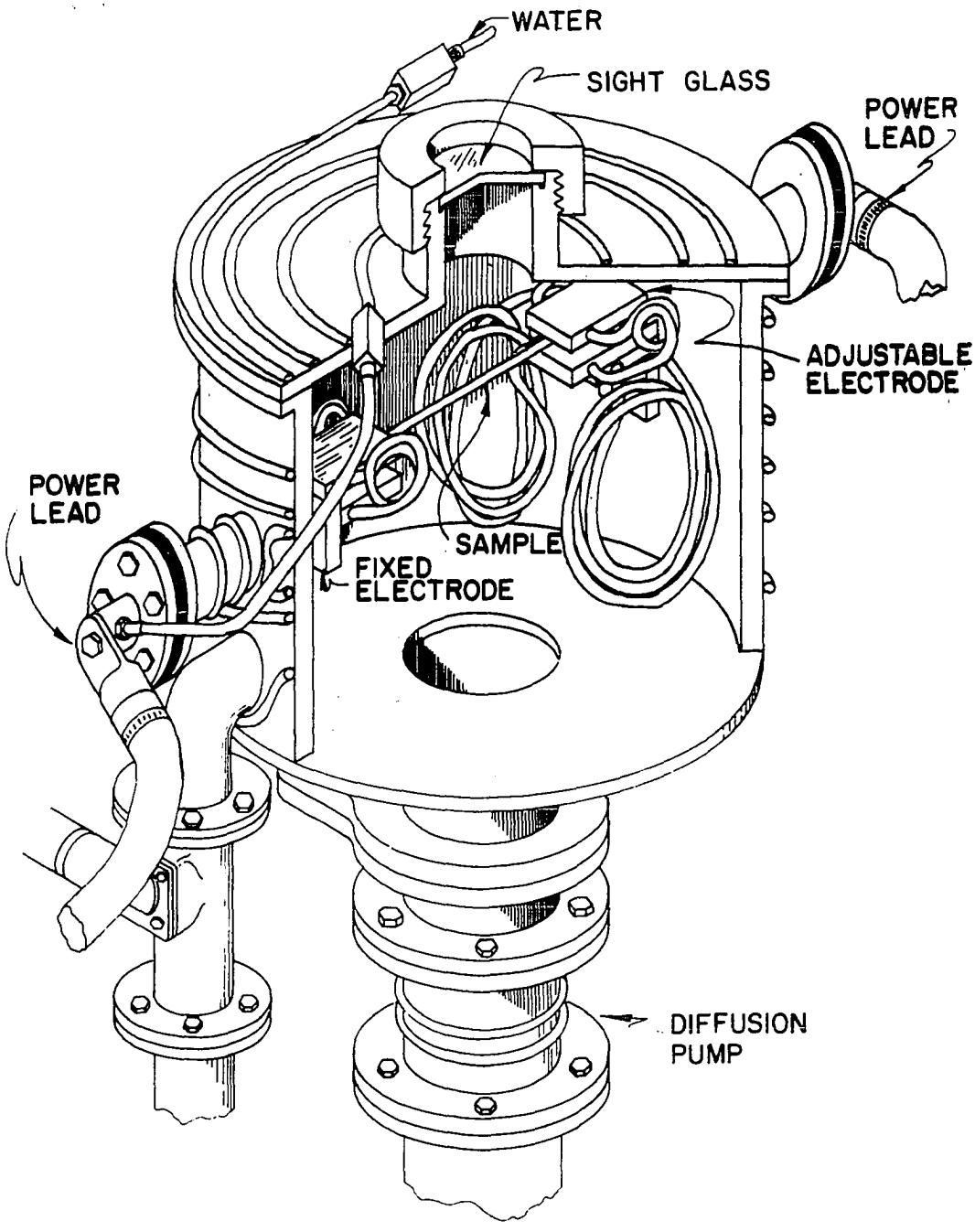

Figure 11. Cut-away view of the annealing chamber

flat copper electrode plates and provided water cooling and adjustment of clamp spacing.

The figure shows the sight glass through which temperature measurements were made by means of an optical pyrometer. The sight glass to specimen distance was about 6 inches. The illustration also shows that the electrodes and power supply cables were cooled by separate water supply systems to permit interchangeability of power supply parts if necessary. The ion gauge part is not visible in Figure 11 but was located in the chamber wall away from the viewer.

Two disadvantages of this system should be noted. First, the existence of a thermal gradient during annealing resulted in grain size variation in the final product. This disadvantage was less harmful than first supposed, since it insured that the ends of the specimen, away from the center of the tensile reduced section, had smaller grain size than the reduced section and were, therefore, stronger. The second disadvantage was the undetermined effect of the thermal gradient and electrical current on the distribution of the interstitial elements in solution in the metals. The nitriding products were deposited largely as a surface layer with only limited diffusion into the interior of the specimens during nitriding. In order to minimize loss of the nitriding products during heating and to maintain low pressures during heating, the annealing temperature was increased in steps so

that temperature was reached in an hour and a half after start-up. The final 4 or 5 increments were steps of perhaps 100°C with holding times of 10 to 15 minutes at each step. Since calculation of the effects of heating rate, thermal gradient and electrical current on interstitials are presently impossible, each specimen was submitted for analysis after tensile testing. Uniformity in the amounts of the weight losses or gains during annealing at various temperatures indicated that at least consistent if not precisely predictable compositions were obtained.

Preliminary annealing

Preliminary annealing was carried out on rods 6-5/8 inches long by 1/4 inch in diameter. It was expected that specimens of that size would provide three tensile specimens from each annealing run. Figures 12, 13, 14 and 15 illustrate the abortion of that expectation. Figures 12 and 14 show the microstructures of the entire cross-sections of 1/8 inch diameter samples taken from preliminary annealed rods at the locations indicated. The figures show that the ends of the rod differed very little in grain size from the starting material, and that the center of the annealed rod consisted of very few grains. Locations 1-2, 4-5 and 7-8 represent the reduced sections which would have been obtained by machining the annealed rods into three equal tensile specimens. Locations A-B and C-D represent locations of reduced sections

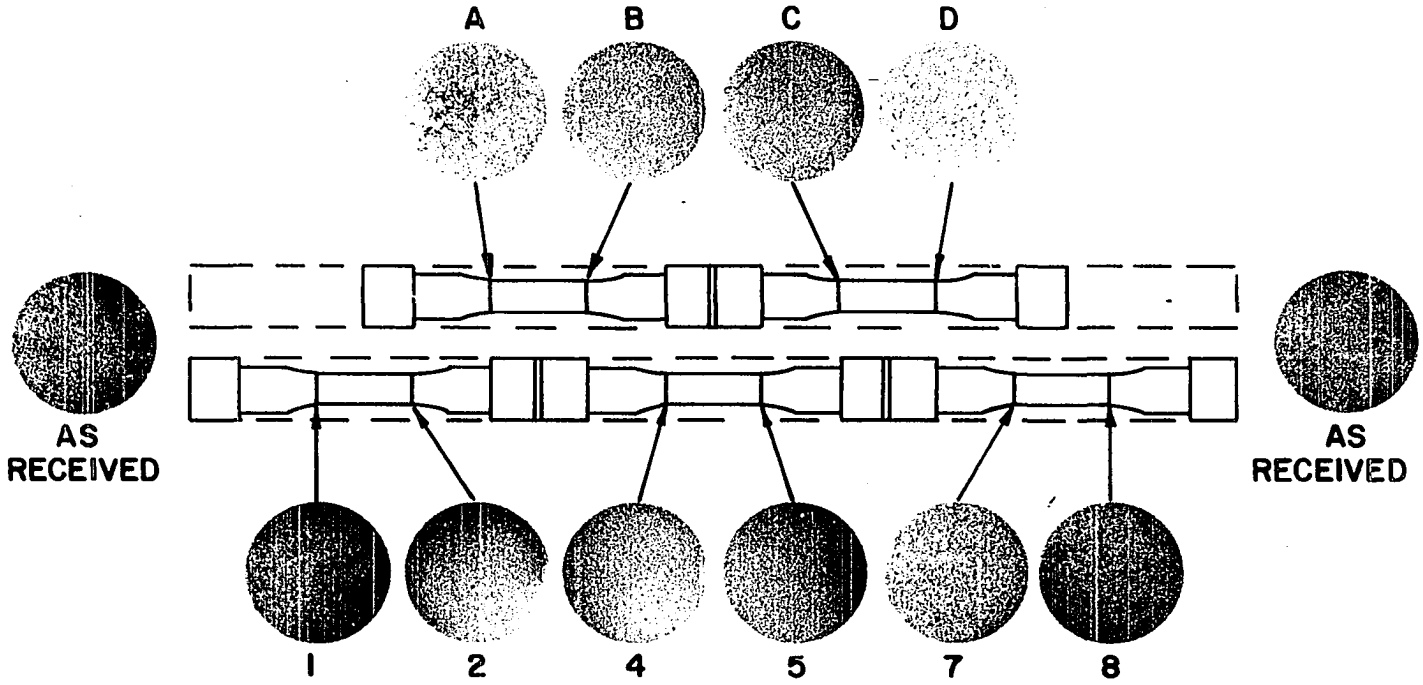

Figure 12. Microstructures from niobium preliminary annealing rod

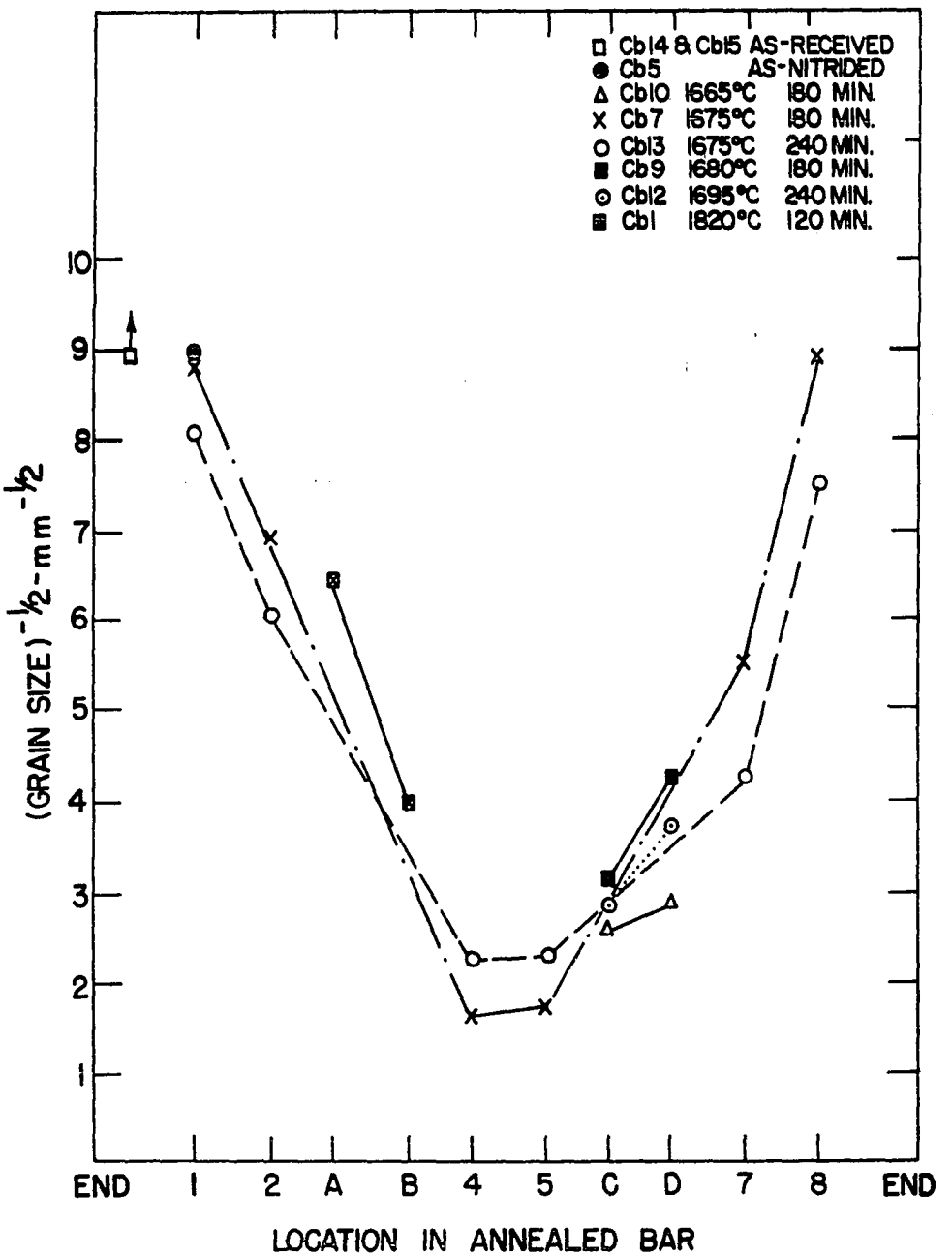

Figure 13. Variation of grain size of annealed niobium with location in annealing rods

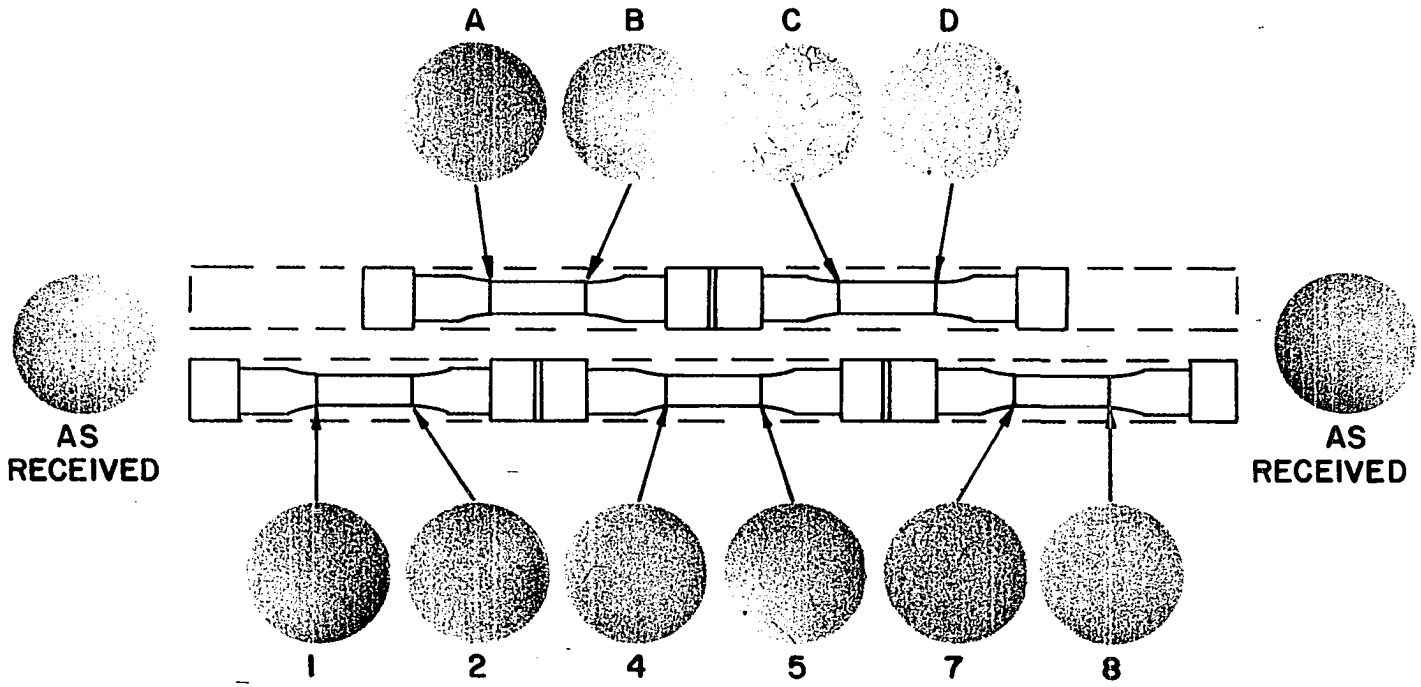

Figure 14. Microstructures from tantalum preliminary annealing rod

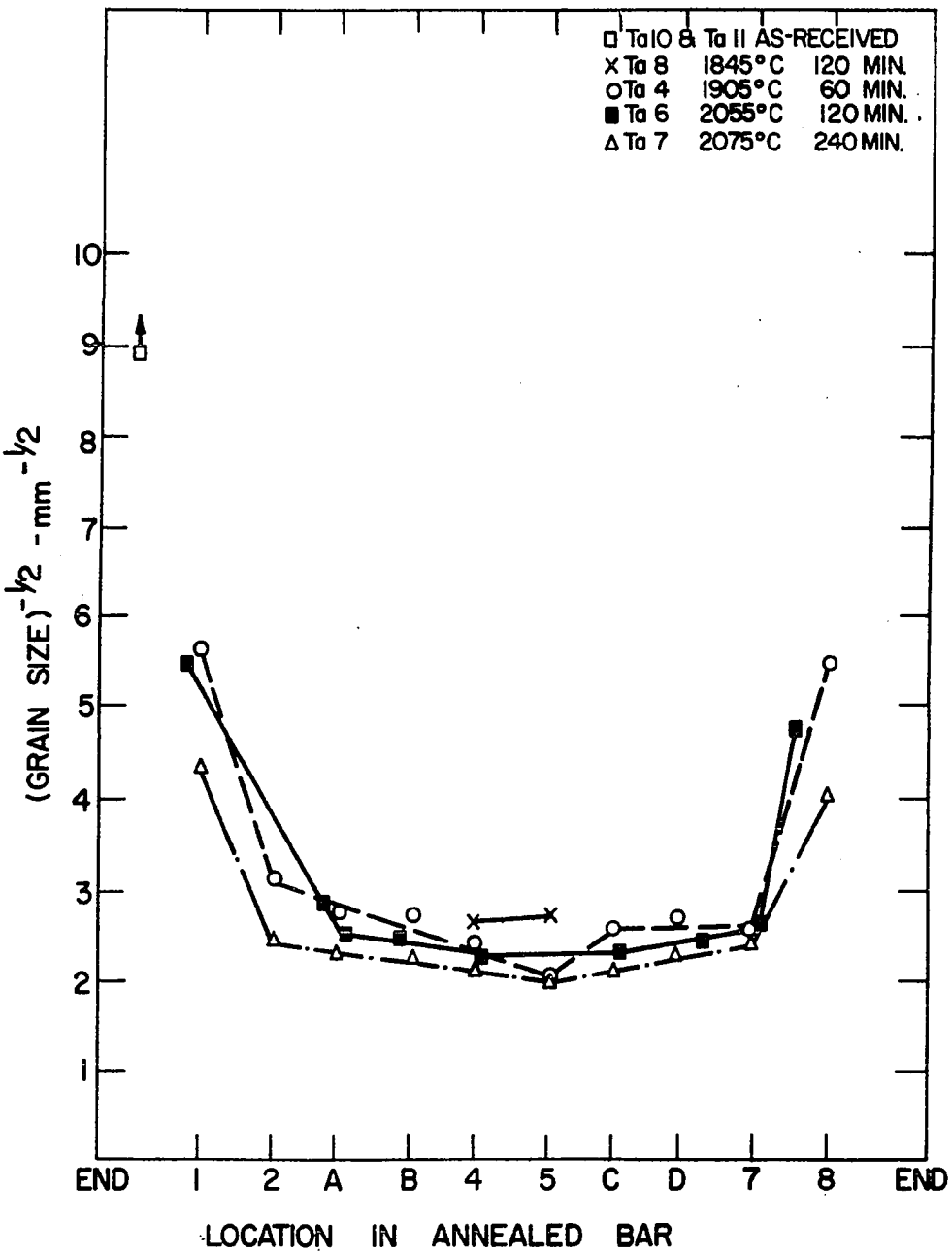

Figure 15. Variation of grain size of annealed tantalum with location in annealing rods

of tensile specimens, had two specimens been taken from the center of the annealed rod.

From these photographs and the accompanying graphs, Figures 13 and 15, of grain size versus location, it was clear the uniform average grain size could be obtained from annealed niobium rods only for a single tensile specimen machined from the center of the annealed rod. The figures also showed that for tantalum, two tensile specimens with approximately uniform average grain size over the length of the reduced section could have been taken from the center of the rod. However, the supply of tantalum was insufficient to afford wasting 1/3 of the material.

Figures 12 and 14 show that grain size at any individual cross-section is far from uniform, but attainment of uniform grain size requires strain-annealing techniques which require repeated operations. Each operation affects the sample composition. Approximate control of composition was preferred to complete uniformity of grain size. The conditions for and results of preliminary annealing tests on niobium and tantalum are summarized in the Appendix.

No consistent relationship between weight change and temperature, time, pressure or input amperage was observed for preliminary annealing treatments. Analysis of the annealed materials revealed that all weight change in niobium could be accounted for as oxygen content change within the

precision of weight change determinations and vacuum fusion analyses. The analytical results for tantalum were not as consistent, and it appeared that more than just oxygen was involved in weight change; but no consistent variation in other conditions was found to augment the oxygen variations.

The temperatures reported for annealing treatments were corrected from optical pyrometer observations by accounting for the emissivity of specimen surfaces and for the sight glass absorption. The pressures reported were those indicated by the ion gauge system. Weight change was determined by weighing the annealing specimens to the nearest 0.0001 gram before and after annealing, taking appropriate precautions to keep the rods clean and dry.

The following procedure, based on observations during preliminary annealing, was established for final annealing treatments.

1. The specimens were cleaned in trichloroethylene, acetone and distilled water then dried and weighed to the nearest 0.0001 gram.

2. Niobium or tantalum wires were attached to the ends of the specimens and the wires clamped between the water-cooled copper electrode plates so that only the wires were in contact with the copper. The electrodes were adjusted to exert a slight tension on the specimen to prevent buckling during heating.

3. The furnace chamber was sealed and evacuated by means of the oil diffusion pumping system shown in Figure 10.

4. The chamber wall was steam heated for 30 minutes.

5. When the chamber pressure was less than 10^{-5} mm Hg, cooling water for the electrodes, chamber head, chamber walls, power transformer and power leads was turned on.

6. The specimen heating was begun after the chamber pressure was less than 3×10^{-6} mm Hg. The heating current was increased by steps, with 15 minutes hold between each increase to permit thermal equilibrium and to maintain low pressure.

7. Holding for periods up to 4 hours with temperature variation of $\pm$ 10°C was accomplished without adjustment of the power supply after temperature was reached.

8. The specimens were cooled by stepwise decreases in current with 10 minute hold periods to permit the system to equilibrate.

9. Ten minutes after the current was decreased to zero, the chamber was isolated, cooling water shut off, chamber wall steam heated, and the chamber opened. The specimens were weighed immediately after removal from the clamps and bands, then recleaned and dried for check weighing later.

Final annealing

The temperatures selected for final annealing of niobium and tantalum were higher than those used during preliminary

annealing tests in order to minimize grain size variations. The specimens used for final annealing were of individual tensile test size, that is 2-1/8 inches long by 1/4 inch in diameter. The use of short specimens and higher temperatures appeared to achieve the desired large grain size within the reduced section of both niobium and tantalum specimens, but resultant grain size was not uniform in the final annealed specimens. The temperature, time and pressure conditions for each final specimen, and the weight gain or loss incurred during annealing are presented in detail in the Appendix. The only significant difference observed between preliminary and final annealing behavior was that tantalum weight losses were much higher during final annealing.

Vacuum fusion analysis of final annealed tantalum samples revealed that increases in oxygen, and perhaps nitrogen, composition accompanied the overall weight losses in the specimens. Perkins' (85) report on outgassing and annealing tantalum shows that temperatures near 2200°C and pressures less than 10^{-5} mm Hg were required to remove oxygen and nitrogen. The reported results were based on weight change and microhardness determinations rather than analyses after "degassing". Hamilton and Wilhelm (50) attributed weight loss from tantalum at 2250°C to TaO vaporization. Small amounts of TaO vaporization would result in weight losses which could easily mask the weight increases associated

with significant oxygen absorption.

Specimen Preparation

Once the compositions of niobium and tantalum were adjusted by nitriding and annealing, the final steps in this study consisted of tensile testing and analysis of results of tensile testing. In order to minimize effects of testing peculiarities on the specimens during tensile testing, specimen preparation was uniform and careful.

Figure 16 shows the dimensions chosen for the tensile test specimens to be used in this investigation and a photograph of a finished sample ready for testing. The configuration is a miniature of specimen configuration recommended for testing of brittle materials. The configuration is advantageous for testing brittle materials because threads introduce stress concentrations which may cause failure in the threaded ends rather than in the reduced section of the tensile specimen. Specimens of this configuration are clamped by split couplings around the 3/16 inch barrels against the butt ends. The fillet radii between the barrels and the reduced section are large in order to minimize stress concentration in that region. A further advantage of this configuration is the relative ease of machining as compared to threaded-end specimens, since niobium and tantalum are difficult materials to machine.

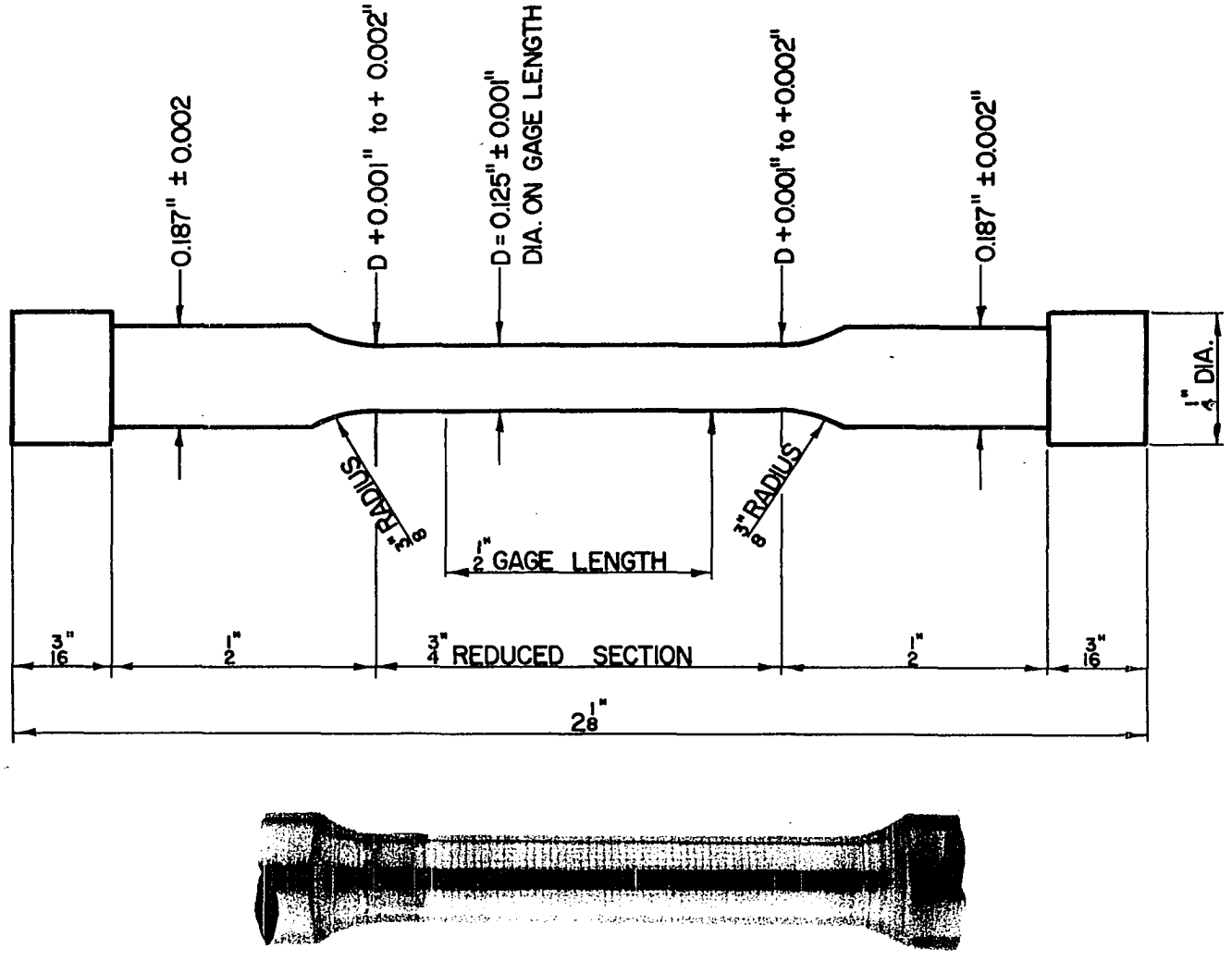

Figure 16. Tensile specimen configuration and photograph of finished specimen with photo-grid

Machining

The specimens were machined on a Hardinge lathe to assure that dimensional tolerances and straightness were maintained. Contrary to recommendations (76) carbide tools were used for machining, because they were found to maintain sharpness for a much longer period of time. High speed steels recommended for cutting tantalum and niobium required resharpening after each tensile specimen and showed no compensating advantages when used under the same conditions as the carbide tools. Lubrication and machine set-up were much the same as for machining other gummy materials such as stainless steel.

The principal difficulties encountered in machining these materials occurred during cutting of the barrel-to-reduced-section radius. The radius cut involved the full thickness of the material between the reduced section and barrel and applied a bending stress to the thin, weak reduced section. About one sample in five was damaged during machining.

Polishing

Each of the machined specimens was polished using 600 grit silicon carbide abrasive in a direction perpendicular to the machining marks in the reduced section of the specimen. After all machining marks were removed, the reduced section was polished with Linde A abrasive on Microcloth using a

stirring motor to rotate the specimen during polishing. The Linde A polishing was followed by etching. After etching, Linde A polishing was repeated and followed by Linde B polishing. After re-etching, the specimen was given a final buffing with Linde B on Microcloth.

This polishing procedure was designed to produce a strain free surface of high enough polish to permit observation of slip bands after tensile testing. No tests were conducted to determine the effect on polishing on tensile strength, but examination of specimens after testing indicated that the technique was adequate to permit delineation of both fine and coarse slip.

Etching

The etchant used to delineate grain boundaries and to remove strained material from the polished specimens consisted of 5 parts sulfuric acid, 2 parts hydrofluoric acid, 2 parts nitric acid and either 9 parts water for niobium etching or 4 parts water for tantalum etching. Initial etching consisted of immersion for 3 minutes while stirring the solution. A one minute immersion was used for final etching. Longer etching times or immersion without stirring resulted in severe pitting of the surfaces.

Several recommended solutions (18, 66, 69, 106) were evaluated for electrolytic polishing and etching in place of the mechanical-chemical system employed. All systems

evaluated were found to be excellent for producing adherent oxide layers on either niobium or tantalum. In some unreproducible cases, excellent electropolishing results were obtained; however, reproducibility was of utmost importance in this testing program.

Photo-grid

As will be discussed in later sections, the orientation of individual grains can readily be determined by means of Laue back-reflection x-ray techniques. Determination of the orientation of slip bands in the same grains is somewhat more ambiguous. The most commonly used method for single crystal orientation determinations is the two-surface method in which the angles of slip traces on two flat surfaces at approximately 90 degrees to each other are measured and the angle between the surfaces defined by the slip traces and the deformation axis is calculated. Cylindrical tensile specimens, however, do not normally have two flat surfaces at 90 degrees apart on which traces can be measured. A coordinate system was, therefore, attached to each specimen prior to tensile testing. The coordinate system was attached by means of photo-grid technique (23, 79).

The photo-grid on the reduced sections of a tensile specimen shown in Figure 16 consisted of dark lines spaced 1/100 of an inch apart in a square grid pattern. From the intersections of slip traces with the grid lines on an

individual grain in the specimen, the equation describing the plane in cylindrical coordinates was determined. The equation of the plane in the cylindrical coordinate system was then transformed into orthogonal coordinates, and the direction cosines of the normal to the plane (which are in the same ratio as the coefficients of the orthogonal terms) were related to the coordinate system used in interpretation of the Laue x-ray photograph. In this way, the slip planes were plotted (as represented by their normals) on the diagrams representing the crystallographic orientations of the grains.

The photo-grids consisted of a mixture of polyvinyl alcohol in water with potassium dichromate and Nigrosine dye. The mixture is soluble in water even after drying, but after exposure to bright light for a given period of time, the mixture is no longer water soluble. The application of photo-grid is accomplished by applying a thin layer of the mixture to a surface, permitting the layer to dry, then covering the dry emulsion with a negative of the pattern desired. When the specimen is exposed to bright light for a given period of time, the unexposed portion of the emulsion may be washed off with warm water, leaving behind the exposed pattern.

Application of a grid of lines spaced at 1/100 of an inch to 1/8 inch diameter cylinders 3/4 inch long is an artistic operation. The procedure found to be most effective

at accomplishing a desirable artistic result is as follows:

1. The photosensitive emulsion consisted of 35 grams of water-soluble polyvinyl alcohol, 1.75 grams of potassium dichromate, 15 grams of 0.6 per cent aqueous Nigrosine (black) dye and 1.5 grams of glycerine mixed into 330 ml of water to obtain a uniform black mixture. The mixture was filtered through cloth to remove lumps.

2. The tensile test specimen surface was cleaned to remove dirt and grease. Surface roughness was not a significant factor in grid preparation, though it was a factor for other reasons.

3. The photosensitive emulsion was flowed over the surface to obtain uniform coverage and to eliminate all bubbles from the area of interest. The coated sample was then rotated to speed up drying and to form a uniform film thickness. The drying process may be speeded further by blowing hot air over the rotating sample after the film flow has stopped. The desired film thickness of approximately 0.0005 inch was obtained by varying either the emulsion viscosity (higher viscosity gives a thicker film) or the speed of rotation (higher speed gives a thinner film) during drying.

4. After the photosensitive film was thoroughly dry, a negative of the desired pattern was placed on the specimen in contact with the film. Transparent cellophane tape is

useful for attachment of negatives and has no detectable effect on the resultant image. The film was sensitized through the negative by light from a flood lamp at a suitable distance for a suitable time. For 100 lines-to-the-inch negative grids on 1/8 inch diameter tensile specimens, the exposure time was 15 minutes with a new No. 2 flood lamp in a 10 inch diameter reflector at 18 inches from the sample. The photosensitive emulsion may be stored for weeks in a dark area without loss of sensitivity, but the emulsion viscosity increases noticeably during such storage periods.

5. The grid pattern was developed from the exposed photosensitive film by washing off the unexposed film with warm water. The exposed film was not soluble in water. The sample was washed under a warm water spray until first, the grid image appeared, then the film peeled off. The washed specimen was rinsed with acetone and held in a vertical position to dry.

When thoroughly dry the grid pattern was strong enough to withstand moderate handling but was distorted by rough handling, scratching, etc.

Figure 17 illustrates the variation in photo-grid which may be obtained by variations in exposure time and intensity. The white grid pattern in the upper right corner of the top photo was due to severe over-exposure of the film. Under-exposure produced a pattern with insufficient contrast. In

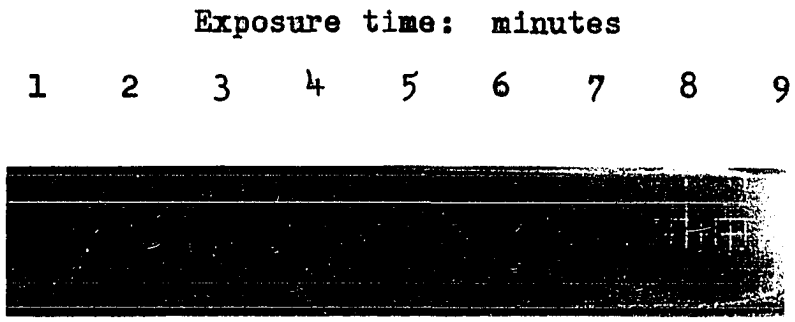

Figure 17. Photo-grid lamp-distance and exposure time study

cases where the film layer was too thick, the grid peeled off leaving a white grid pattern with the same appearance as the over-exposed grid in Figure 17. When the emulsion was too thin, the resultant grid was too faint for consistent measurements. The other difficulty often encountered in photo-gridding was the presence of bubbles either in the emulsion or under the tape holding the negative on the sample. In either case, the result was a shadow on the resulting image. The bubbles in the emulsion were far more serious than the bubbles in the tape.

The photo-grid was tested in use over the temperature range from liquid nitrogen to room temperature. However, additional studies were made at elevated temperatures up to 500°C. When subjected to elevated temperatures, the photo-grid eventually evaporated leaving the dye residue. The grid image was actually improved by heating at 200°C, because the residual emulsion between the grid lines evaporated leaving the clean metal surface exposed without noticeably reducing grid line intensity. The photo-grid was clearly visible and useable for periods up to 1/2 hour in air at 450°C.

The photo-grid remained intact on all specimens tested as low as -196°C. At the lowest temperatures and at strain rates up to 10 in/in/sec, the photo-grid remained intact on individual grains which strained up to 70 per cent. In the regions of necking, the photo-grid often became indistinct due

to spreading of individual lines over large areas of the deformed grains. In one instance, the line appeared to have spread approximately 1/100 of an inch over a region where slip bands had considerably roughened the surface.

Two difficulties were encountered in using the photo-grid for slip band orientation determinations. First, some areas were not properly printed due to local failures in the artistic process. In this case, a positive of a grid printed on photographic film was wrapped around the sample, and slip orientations were determined from points read as intersections of slip bands with the film grid. The second difficulty encountered was deformation of individual grains into non-cylindrical forms. Even though the grid remained on these grains, the non-cylindrical shape of the surface invalidated the use of cylindrical coordinates to determine slip band orientations. In some cases of this type, a tube of film of positive grid was placed over the distorted grain and estimations made of the intersection of projected slip lines with the overlying grid.

In summary, the photo-grid technique was useful both as a coordinate system for determination of surface marking orientation and for measurement of local strain. In strain measurement, the photo-grid method should prove useful for determination of the local strain in necking or other inhomogeneous plastic deformation, even in fine grained

specimens. The technique appears to have some applicability over a rather large range of temperature.

Tensile Testing

Tension testing was selected for the deformation method in this investigation to assure initial uniformity of stress and to facilitate specimen preparation. Both niobium and tantalum were to be tested under equivalent conditions such that niobium was ductile in some tests and brittle in others.

The ductile-to-brittle transition was found between -155 and -196°C for the three classes of niobium described in Table 11. Equivalent testing temperatures for the equivalent tantalum alloys were found to be the same as the niobium testing temperatures.

This section discusses the apparatus used for tensile testing and presents the resultant test data. The information concerning deformation behaviors and discussion of testing equivalence will be covered in the next chapter.

Equipment

The initial requirements for the testing apparatus were that it be capable of attaining and maintaining any temperature between liquid nitrogen and room temperature, permit observation of the specimen during deformation, and provide for relatively easy change of tensile specimens of the previously described configurations. Subsequent testing

Table 11. Classification of niobium and tantalum alloys for tensile testing

Material	Nitriding identification	Tensile specimen number	Composition ppm N	Composition ppm O	Equivalent energy factor
		Class I			
Niobium	Cb 18A	30	24	34	1.0
	18B	32	98	140	3.5
	19B	34	104	150	3.7
	19C	35	107	100	3.3
	20A	36	100	94	3.1
	20B	37	264	183	7.4
	20C	38	80	42	2.2
Tantalum	Ta 18B	43	5	75	4.2
	18C	44	10	32	3.8
	21A	45	18	57	4.1
	21B	46	14	42	4.6
	21C	47	17	88	6.4
		Class II			
Niobium	Cb 22A	50	165	126	4.8
	22B	51	154	148	4.8
	22C	52	166	140	4.9
	23A	53	145	140	4.5
	23B	54	167	128	3.9
	23C	55	180	111	5.0
Tantalum	Ta 19B	93	100	170	14.1
	20A	85	21	43	4.8
	20B	86	20	31	4.2
	20C	87	26	31	4.6
	22B	89	22	28	4.2
		Class III			
Niobium	Cb 27A	70	190	92	5.0
	27B	71	254	112	6.6
	28A	73	2.3	132	5.9
	28B	74	224	106	5.9
	28C	75	258	104	6.6
	29A	76	216	83	5.5

Table 11. (Continued)

Material	Nitriding identification	Tensile specimen number	Composition ppm N	Composition ppm O	Equivalent energy factor
		Class III			
Tantalum	Ta 15B	63	25	30	4.6
	16B	66	35	34	5.4
	16C	67	26	34	4.9
	17B	69	31	32	5.1
	17C	170	27	34	4.9

and evaluation showed that the first and last of these requirements were met by an apparatus described by Anders, et al. (3) in which the cooling system is operated by conduction. Figure 18 is a schematic diagram of the temperature control system used. Figure 19 shows the chamber in detail.

The cooling system consists of two copper cans to which the ends of the sample are connected and which are maintained full of liquid nitrogen throughout the testing period. These copper cans do not support the load but are merely attached to a stainless steel pull rod. The extension sleeves of the copper cans are connected to the samples by beryllium copper split couplings held in place by beryllium copper taper lock rings. This system provides very high cooling rates by conduction through the beryllium copper and copper sleeve

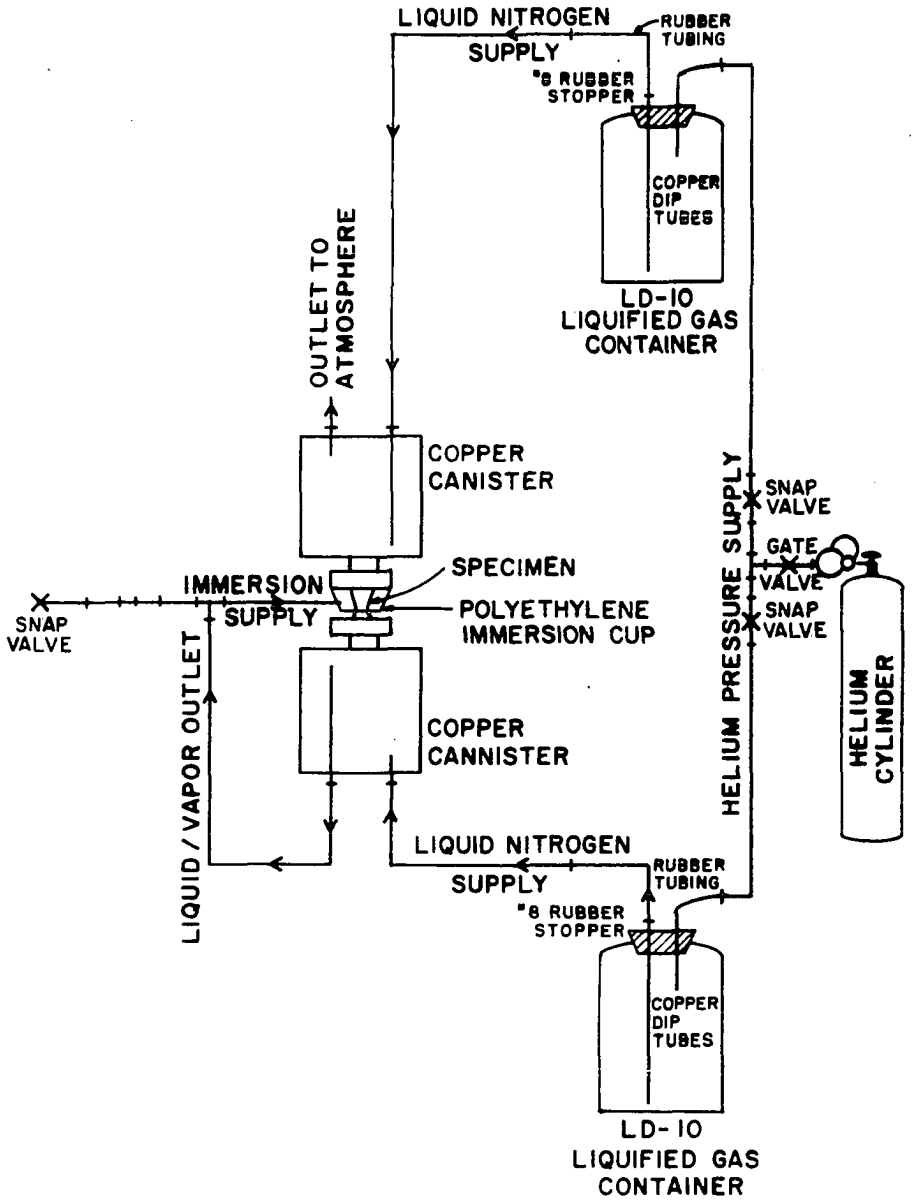

Figure 18. Schematic of cooling system for the low temperature tensile testing chamber

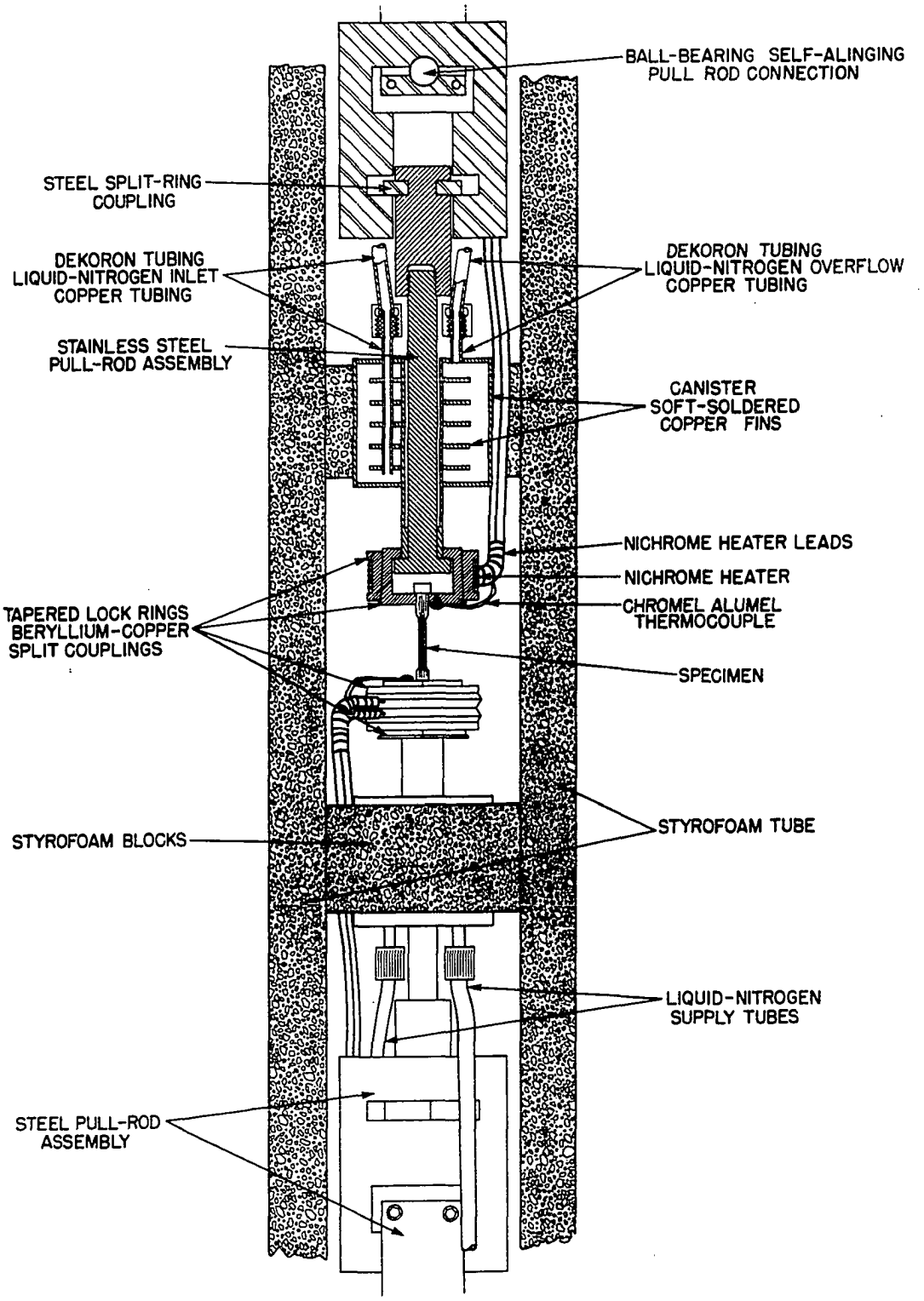

Figure 19. Cross-section view of low temperature tensile testing chamber

to the cold sinks at each end while providing adequate strength with the beryllium copper-stainless steel load transmission system. With insulation in place, the elapsed time between start of nitrogen flow to the cans and attainment of temperatures of approximately -196°C at the sample shoulders was about 10 minutes under good conditions. Specimen temperatures above -196°C (77°K) were obtained by altering the conduction rate provided by the cold sinks. The conduction rate was reduced by means of heaters wrapped around the beryllium copper taper lock rings.

Despite careful control during fabrication, the lock ring heaters on each end were not quite identical, and different current was required in each to maintain equal temperatures at both ends of the specimen. Once equilibrium was achieved, temperatures measured at the specimen shoulders could be maintained to $\pm$ 1°C for periods limited only by the nitrogen supply to the cold sinks. For the short periods of testing used here, manual control of the nitrogen flow and heater currents was found to be adequate.

Chamber insulation consisted of a styrofoam tube with one inch thick walls. The cold sink copper cans were also covered with about one-half inch styrofoam, and the outer insulating tube was constructed to fit around the can insulation so that the tube could be raised or lowered without interferring with the load application or temperature

control equipment. The actual chamber dimensions were approximately 4 inches by 4 inches by 5 inches long, with the specimen mounted approximately in the center of that space. In order to minimize temperature gradients within the chamber, both copper cans were vented into the chamber along the side walls so that any nitrogen overflow from the cans flowed into the chamber but not onto the specimen. For immersion tests in nitrogen, one of the overflow lines was connected to a polyethylene cup punched so as to fit snugly around the tensile specimen shoulder.

Temperatures of the specimens were recorded by means of chromel-alumel thermocouples clamped so as to contact the shoulders of the specimens at the split ring couplings. Preliminary tests of the equipment indicated that the temperature of the center of the specimen was only 1°C to 2°C higher once the specimen reached the same temperature at both ends. In all final testing, therefore, balanced temperatures were attained and held prior to actual testing. The change in load measured by the tensile machine was found to be a sensitive indicator of thermal fluctuations within the chamber.

The stainless steel pull rods around which the copper cans were mounted were attached by split steel couplings to pull rods mounted on the tensile machine through ball joints. The elastic behavior of this system of steel, stainless steel,

and beryllium copper in a temperature gradient from that of the chamber to room temperature altered the stress-strain diagrams so that the elastic moduli of niobium and tantalum were not determined at low temperatures. The amount of elastic deformation of the system depended not only on the load applied, but also on the temperature of each of the components and connections.

The ball joints were found to be satisfactory for maintenance of alignment during testing. Alignment was checked by means of a steel tensile specimen to which SR-4 strain gauges were attached on opposite sides. When loaded to approximately 60,000 psi, the misalignment was found to cause a stress differential across the sample of less than one per cent with the insulation, etc., in place. No attempts were made to check alignment on low temperatures.

The tensile machine was a Tinius-Olsen screw driven tensile machine equipped with a load-strain/time recorder system. Load was measured by a lever torsion bar system. Elongation of the specimens was calculated from the cross-head speed and the travel of the constant speed chart paper on which the load was recorded. During some preliminary tests, cross-head motion was measured by means of a deflectometer which actuated the chart drive of the machine recorder, but the additional complications in setting up the deflectometer were not found to provide any compensating

advantages in strain measurement. Extensometers and bonded strain gauges were avoided, because polished specimen surfaces were necessary to subsequent analyses.

The photo-grids attached to the specimens were intended to provide strain measurement during testing by sequential photographs of the specimens during testing. Preliminary tests using the open system revealed that the specimens frosted, and photographic strain measurements were impossible. Several systems were designed to eliminate frosting during testing, but none of the systems was adequate to permit photographic strain measurement. It appears that a vacuum chamber would be necessary to achieve frost-free testing conditions.

Strain rate was selected by means of an electronic system of the tensile machine. Unfortunately the control was tenuous, and calibrations to determine actual cross-head speed for a given setting of the strain rate control were required before each series of tests. Variations of less than 5 per cent in strain rate were observed in calibrations made immediately before and after a sequence of tests conducted over a two-day period with the electronic controls on at all times. Strain rates varied by as much as 100 per cent when determined immediately after start-up of the electronic systems and again several hours later. The strain rate was also found to differ for a given control

setting from one time to the next, even after equal warm-up times.

Preliminary testing

Series of preliminary tests were run to determine the system behavior during actual testing of specimens, to establish the amounts of deformation necessary to permit observation of slip traces and to establish the probable temperatures and strain rates necessary to obtain cleavage fracture in niobium.

Scrap tantalum and niobium were used in system testing to determine the temperature gradients to be expected at various temperature levels during final testing. During the preliminary testing, it was found that temperatures could be maintained only if the cold sink cans were vented directly to the atmosphere. Back-pressure drastically increased the minimum temperature obtainable, and the original plumbing system was gradually simplified to eliminate vapor locks, etc. During these tests it was also noted that after the cold sink cans were once filled, self pressure of the nitrogen supply containers was more than adequate to keep the cans full. These tests also revealed that the conduction surfaces required careful cleaning before each test sequence, since the frost which collected during testing deposited dirt on conduction surfaces. Icing presented difficulties only when the system was permitted to warm up between low temperature

tests.

Cox, et al. (27), and Hull (54), in tests on silicon iron alloys, found that strains of 2 to 3 per cent were required to produce observable slip traces on electrolytically polished surfaces; therefore, highest purity niobium was strained at room temperature to various amounts of total elongation to determine the amount of deformation necessary to produce observable slip traces. Slip traces were observed on samples deformed greater than 2 per cent, i.e. beyond yield elongation in the material tested. On specimens of niobium loaded to fracture, some grains in the fractured specimens displayed slip traces but had undergone small enough overall deformation that x-ray analysis of grain orientation was still practical. Since both slip and fracture behavior were observable from each preliminary specimen, final testing was carried to fracture.

In order to determine the effects of strain rate on the fracture behavior of the materials available, a series of high purity annealed niobium and tantalum specimens was tested at selected strain rates while immersed in liquid nitrogen. One niobium specimen was consecutively loaded from zero load to yielding at strain rates of 10^{-4}, 10^{-3}, 10^{-2} and 10^{-1} in/in/sec. The yield stress was found to increase slightly with increasing strain rate, but cleavage fracture was not obtained. In the final test at 10^{-1}

in/in/sec, the sample necked down immediately after yielding and fractured after approximately 70 per cent reduction in area. Even at liquid nitrogen temperatures, none of the highest purity (annealed starting material) niobium specimens showed any evidence of brittle fracture. The tantalum specimens all necked to approximately 95 per cent reduction in area at fracture at all strain rates. Tensile specimens taken from rods used in preliminary nitriding tests exhibited partial cleavage fracture at temperatures up to -175°C (98°K) at a strain rate of 10^{-2} in/in/sec.

The preliminary tests showed that strain rate had little effect on the tensile behavior of high purity niobium and that increase in nitrogen and oxygen contents due to nitriding would induce brittle behavior in a convenient temperature range.

Final testing

Table 12 summarizes the values of tensile properties obtained in testing of niobium and tantalum. The results of analyses of deformation behaviors will be covered in the next chapter.

The niobium specimens were tested first, starting with the highest purity material (Class I) at the lowest temperature attainable by the apparatus (77°K). The first specimen tested fractured by cleavage. The second specimen was then tested at the same temperature but at a slower, more readily

Table 12. Summary of niobium and tantalum tensile testing results

Material	Specimen number	Test temp. °C	Nominal stress 1000 psi Lower yield	Nominal stress 1000 psi Maximum	Fracture appearance
		Class I			
Niobium	32	-196	111.0	112.0	cleavage
Tantalum	47	-187	97.1	100.4	shear
Niobium	35	-184	--	108.8	cleavage
Niobium	37	-180	102.8[a]	102.8	shear
Niobium	36	-175	100.0	106.7	shear
Tantalum	44	-172	100.0	102.8	shear
Niobium	34	-155	85.5	88.1	shear
Tantalum	45	-154	93.2	96.6	shear
Tantalum	43	23.5	25.6	27.9	shear
Niobium	38	23.5	19.9	22.3	shear
		Class II			
Tantalum	85	-175	99.4	107.2	shear
Niobium	50	-175	107.3	114.2	cleavage
Tantalum	89	-169	--	104.6	shear
Niobium	51	-169	103.0	108.8	mixed
Niobium	55	-170	97.5	100.8	mixed
Tantalum	86	-165	--	98.2	shear
Niobium	52	-165	100.1	106.2	mixed
Niobium	53	-160	97.4	103.0	shear
Tantalum	83	-121	71.0	74.3	shear
Tantalum	87	23.5	28.6	30.0	shear
Niobium	54	27.5	27.9	30.8	shear

[a]Yield stress taken as 0.2 per cent offset.

Table 12. (Continued)

Material	Specimen number	Test temp. °C	Nominal stress 1000 psi Lower yield	Nominal stress 1000 psi Maximum	Fracture appearance
		Class III			
Niobium	70	-185	113.2	121.8	cleavage
Tantalum	63	-180	--	114.2	shear
Niobium	71	-170	110.4	118.7	mixed
Tantalum	170	-170	--	101.0	shear
Niobium	73	-165	106.9	114.0	cleavage
Tantalum	66	-165	--	103.3	shear
Niobium	75	-160	98.2	106.1	mixed
Tantalum	67	-160	--	96.7	shear
Niobium	74	-155	93.5	101.4	shear
Tantalum	69	23.5	29.7	31.5	shear
Niobium	76	26.5	24.0	26.2	shear

controlled strain rate and at higher strain magnification on the recorder. The second specimen also failed completely by cleavage, and ability to obtain ductile-to-brittle transitions in all classes of niobium was assured.

Location of the transition temperature (-180 to -185°C) for Class I niobium required six specimens and for Class III (-160 to -165°C) required four specimens. From these results the Class II transition was expected to be around -170°C and only three specimens were required to locate the transition

at -165 to -170°C.

The same strain rate (about 5×10^{-3} in/in/sec) was used in testing the tantalum specimens. Equivalent tantalum temperatures were estimated by interpolations on Figure 6 using equivalent composition values calculated from nitriding weight gain and preliminary chemical analyses. It was found that tantalum specimens tested at the same temperature as their equivalent niobium specimens had nearly the same yield strengths as the niobium specimens.

Specimens of niobium and tantalum from each composition class were also tested at room temperature to provide a base comparison for strength and deformation changes. The room temperature tests were continued only to maximum loads than unloaded before extensive necking could occur.

Detailed information on test conditions and load and elongation results is presented in the Appendix.

EVALUATION OF RESULTS

With testing completed, the last step in the investigation consisted of evaluation of the significance of the results and comparison of the results in detail. The first thing to be considered was how well equivalence was achieved in the testing. The evaluation of equivalence leads to consideration of the tensile properties including strength, ductility and other characteristics of the stress-strain diagrams. The external fracture and slip appearances were compared, and finally the crystallographic aspects of slip and cleavage were compared for niobium and tantalum.

Equivalence

The tensile testing was carried out in three parts. The materials were divided into three classes, all samples within a class having approximately equal composition as calculated or estimated from nitriding and annealing weight change information. After tensile testing, each individual specimen was submitted for chemical analysis to determine the composition of the material at the location of fracture. The column of equivalent energy factors in Table 12 shows that the compositions were not uniform within any one class for either niobium or tantalum. Therefore, some variation in tensile behavior was to be expected within each testing class. The arbitrary assignment of materials for Class II and Class III

tantalum was correct in order of increasing impurity concentration, but the interaction energies for Class III tantalum were somewhat lower than those for Class III niobium.

More distinct correlations were recognized when the tensile testing results were arranged according to interaction energy factors determined from final analyses of individual specimens. Table 13 shows that for equivalent materials testing at equal temperatures and strain rates resulted in virtually the same yield strengths in both niobium and tantalum.

Tensile Properties

Two requirements were set for tensile testing: first that a ductile-to-brittle transition be produced in niobium, and second that equal yield strengths be obtained in equivalent tantalum. Both objectives were met.

Figures 20, 21 and 22 consist of photographs of the fracture surfaces of Class I, Class III and Class II niobium arranged on a plot of per cent reduction in area versus testing temperature. The ductile-to-brittle transition in Class I niobium was found to lie between 89 and 93°K. Class III niobium was then tested, and the ductile-to-brittle transition was found to lie between 108 and 118°K. From these two results, it was predicted that the transition temperature of Class II niobium would be about 103°K. Figure 22 shows that the transition temperature did lie

Table 13. Yield strengths and interaction energy factors for niobium and tantalum tensile tested at equal temperatures

Temperature °K	Interaction[a] energy factor	Yield stress 1000 psi	Testing class	Material
300 (Room T)	5.5	24		Nb
	5.1	30		Ta
	4.6	29		Ta
	4.2	26		Nb
	3.9	28		Ta
	2.2	20		Nb
118	5.9	94	III	Nb
	4.1	93	I	Ta
	3.7	86	I	Nb
113	6.6	98	III	Nb
	4.9	97	II	Ta
	4.5	97	II	Nb
108	5.9	107	III	Nb
	5.4	103	III	Ta
	4.9	100	II	Nb
	4.6	98	I	Ta
	4.2	98	II	Ta
103	6.6	110	III	Nb
	5.0	98	II	Nb
	4.9	102	III	Ta
	4.8	103	II	Nb
	4.2	105	II	Ta
98	4.8	107	II	Nb
	4.8	99	II	Ta
	3.8	100	I	Ta
	3.1	100	I	Nb
93	7.4	111	I	Nb
	4.6	111	III	Ta

[a]Due to inherent precision of the analysis method energy factors may vary ± 0.3 for Class I niobium, ± 0.4 for Class II niobium, ± 0.6 for Class II niobium and ± 0.2 for all tantalums.

Table 13. (Continued)

Temperature °K	Interaction[a] energy factor	Yield stress 1000 psi	Testing class	Material
88	6.4	97	I	Ta
	5.0	113	III	Nb
	3.3	105	I	Nb
77	3.5	111	I	Nb

between 98 and 113°K. It should be noted that the most brittle material in terms of reduction in area still exhibited more than 20 per cent reduction in area, which for many materials is not considered brittle behavior. The criterion used here was that cleavage fractures were designated as brittle, and shear fractures were designated as ductile. Several specimens were tested which fractured by some combination of shear and cleavage, and their ductility, expressed as reduction in area, was found to be intermediate between those samples which fractured entirely by cleavage and those which fractured entirely by shear. The sharpness of the transition from shear to cleavage behavior was unexpected, but the range of values of reduction in area for specimens exhibiting mixed fracture behavior was not surprising. A large number of tests would be required to more precisely define the ductile-to-brittle transition.

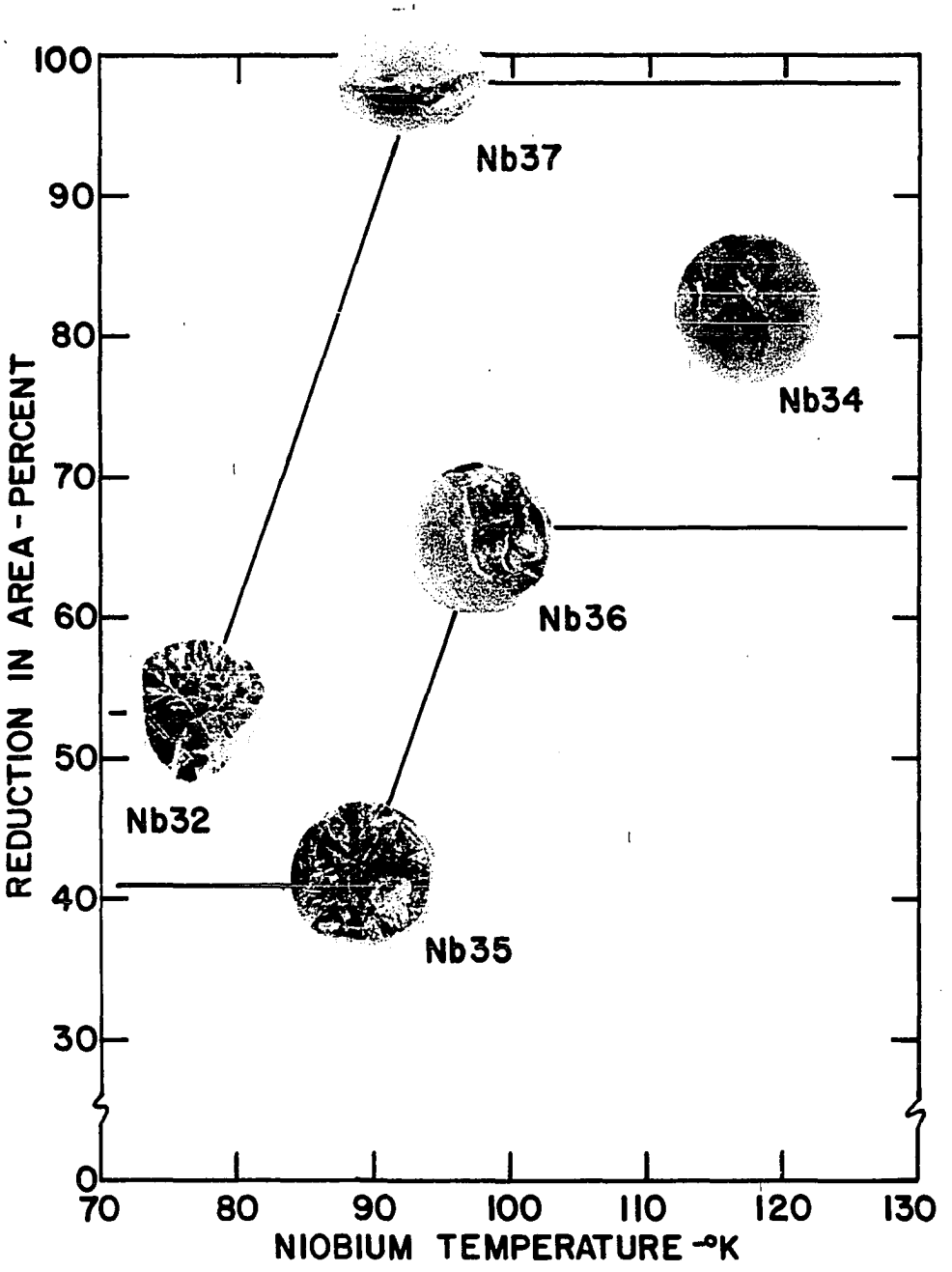

Figure 20. Ductile-to-brittle transition in Class I niobium

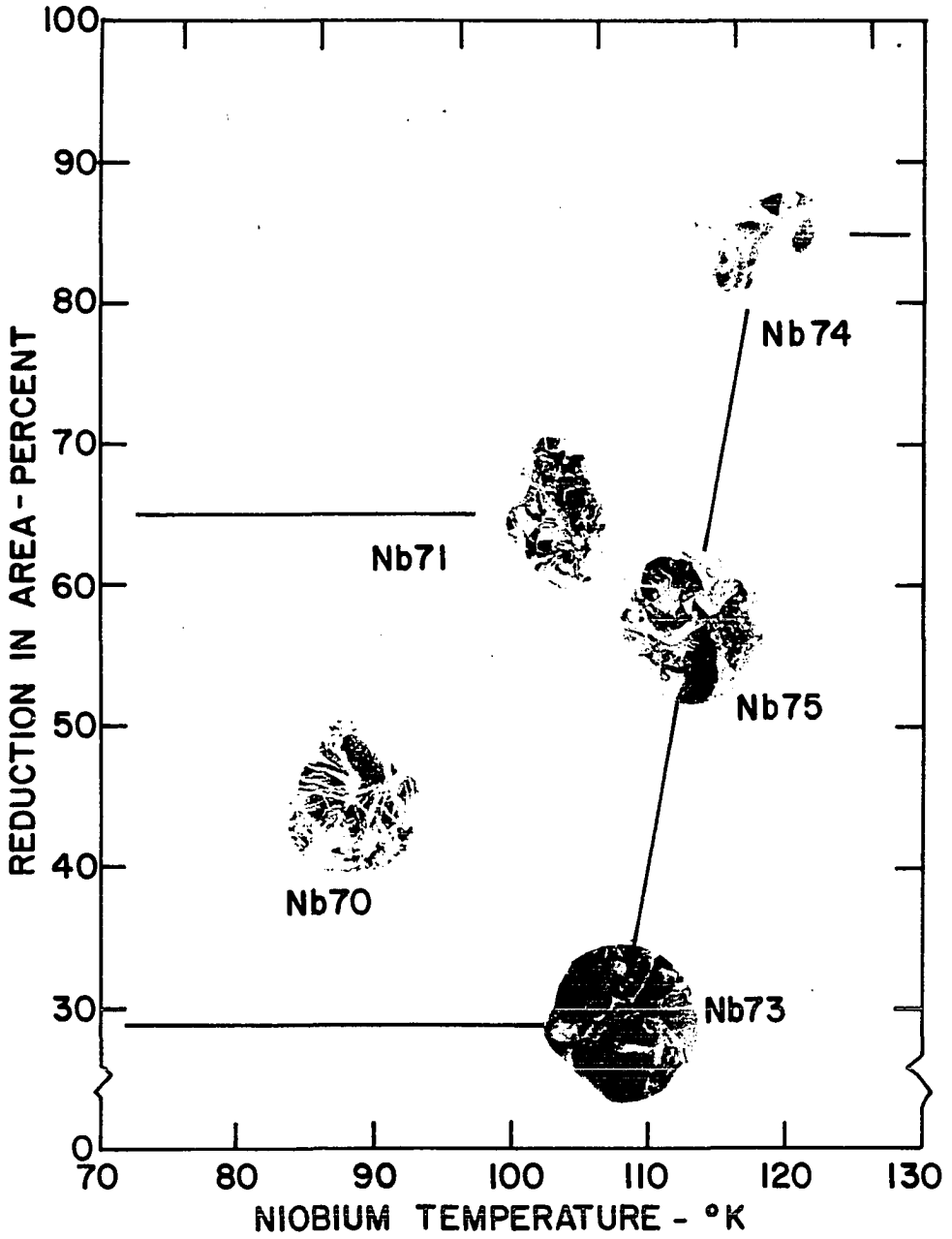

Figure 21. Ductile-to-brittle transition in Class III niobium

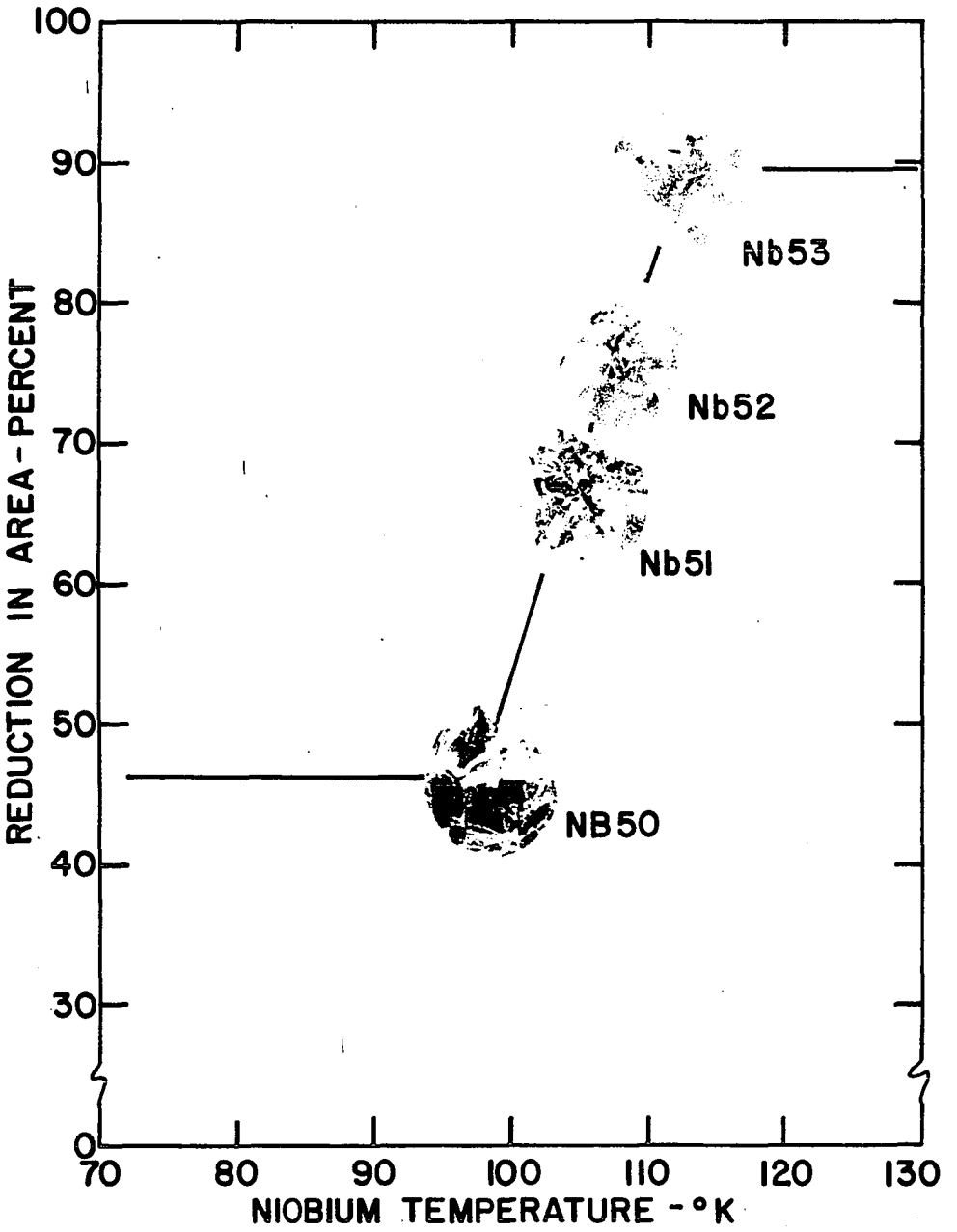

Figure 22. Ductile-to-brittle transition in Class II niobium

The brittle behavior of the niobium specimens was also reflected in the stress-strain diagrams obtained during testing. Specimens which failed completely by cleavage showed sharply higher maximum strengths and yield strengths than the materials which failed by shear. Several Class II niobium specimens failed by mixed shear, and the differences in stress-strain diagrams were less distinct than for the other two classes.

The stress-strain diagrams for Classes I, II and III niobium and tantalum are presented to the same scale in Figures 23, 24 and 25. It was not evident in the Class I niobium stress-strain diagrams, but clicking noises associated with twinning and a drop in load accompanying twinning were observed for every niobium specimen which failed completely by cleavage. Specimens which exhibited mixed shear and cleavage occasionally made twinning-type noises but were not entirely consistent in this respect. Since none of the niobium specimens which failed completely by shear exhibited any traces of twinning, we must conclude that twinning is associated in some way with the cleavage fracture of niobium.

Whereas twinning in niobium was confined to samples in which cleavage was observed, twinning was observed in all tantalum specimens tested at temperatures below 119°K and even the specimen tested at that temperature may have twinned. Table 14 summarizes the twinning stresses and load drops

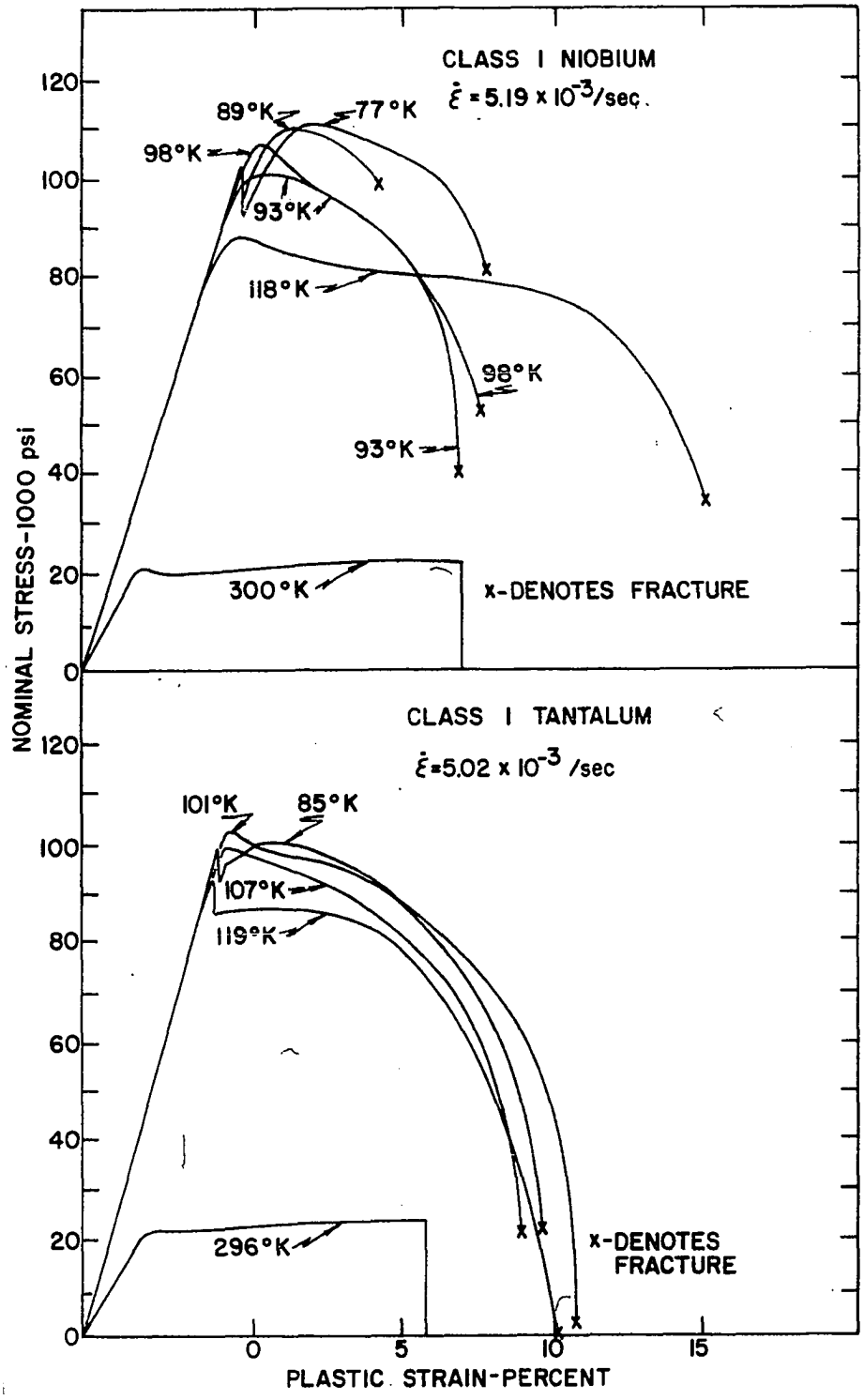

Figure 23. Stress-strain diagrams from tensile tests of Class I niobium and tantalum

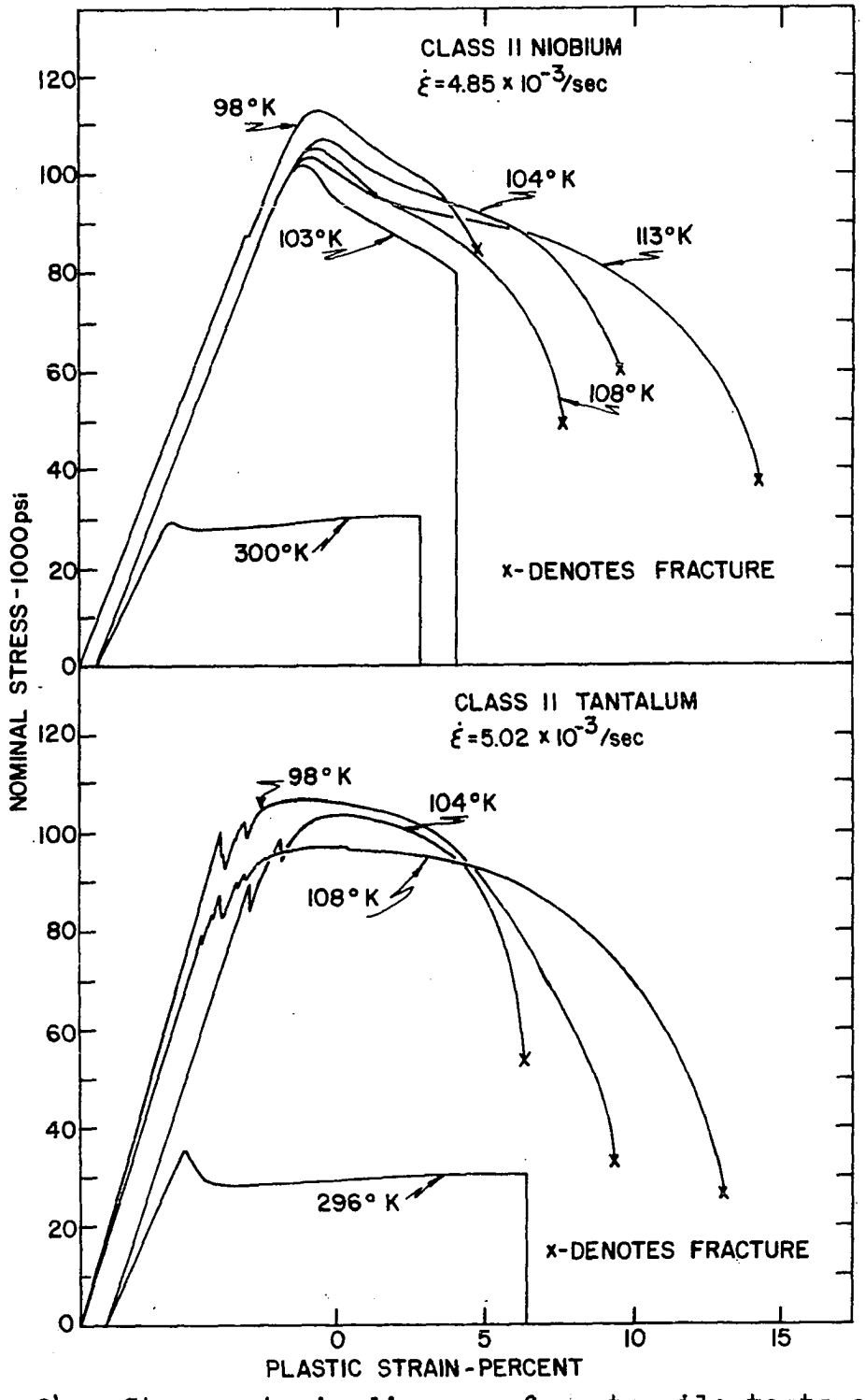

Figure 24. Stress-strain diagrams from tensile tests of Class II niobium and tantalum

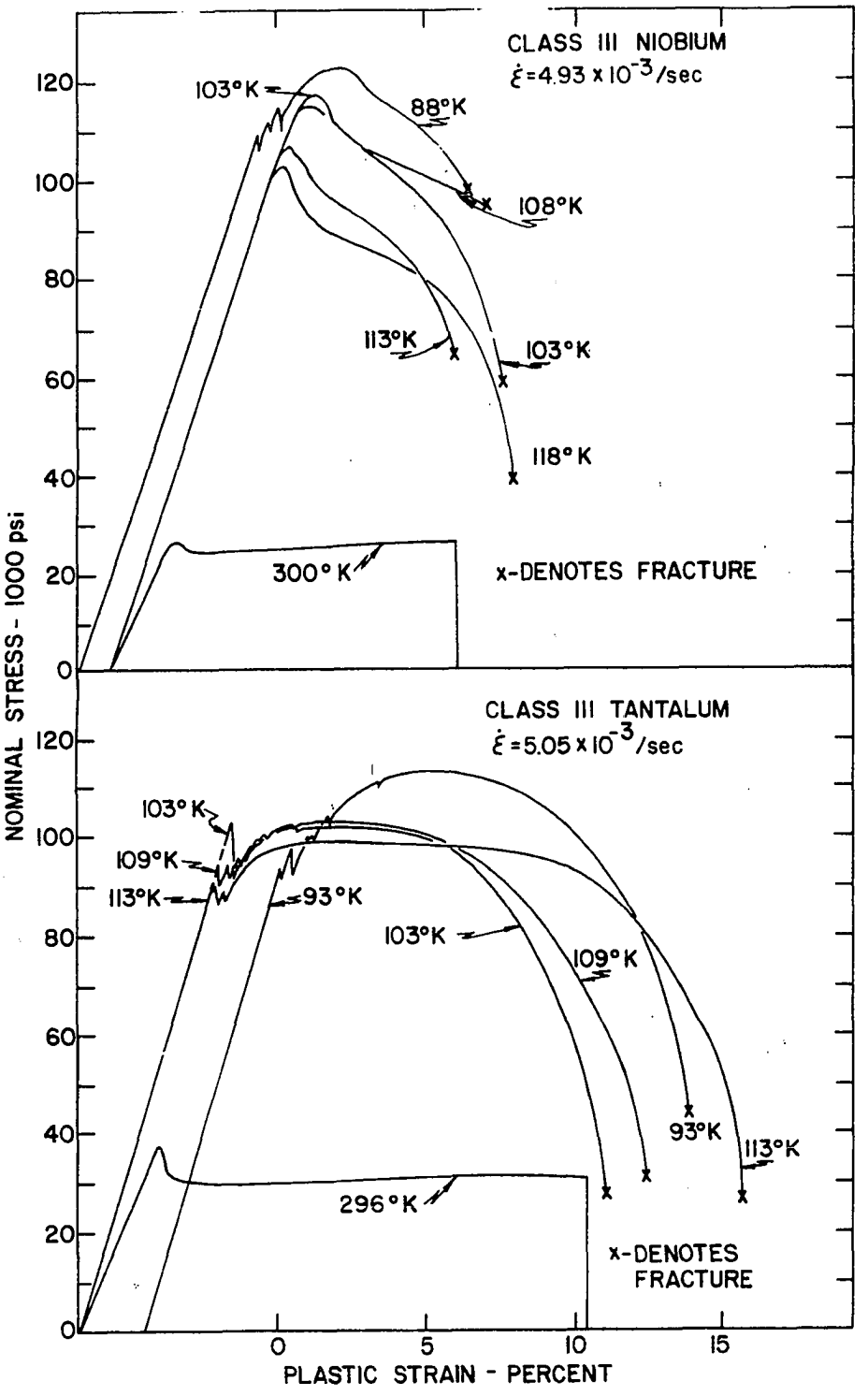

Figure 25. Stress-strain diagrams from tensile tests of Class III niobium and tantalum

Table 14. Twinning behaviors of niobium and tantalum

Specimen number	Stresses - 1000 psi			Test temp. °K
	Upper	Lower	Drop	
30	95.9	93.2	2.7	77
	91.0	89.4	1.6	
32	101.8	93.0	8.8	77
35	100.2	94.0	6.2	89
44	--[a]	--	--	101
46	98.2	96.0	2.2	109
47	100.4	93.4	7.0	86
50	89.0	88.5	0.5	98
51	97.9	96.6	1.3	104
53	58.6	57.4	1.2	113
63	94.9	92.2	2.7	93
	98.9	93.0	5.9	
	100.9	100.0	0.9	
	103.2	101.5	1.7	
	105.2	103.6	1.6	
66	94.7	90.3	4.4	108
	94.6	91.7	2.9	
	96.0	94.3	1.7	
	100.7	99.5	1.2	
	101.9	100.8	1.1	
67	86.7	85.0	1.7	113
	87.9	84.1	3.8	
	89.4	86.5	1.9	
170	101.8	90.6	11.2	103
	95.7	75.6	0.1	
	101.7	100.8	0.9	
70	108.5	104.7	3.8	88
	110.9	108.5	2.4	
	114.0	108.5	5.5	
73	--[a]	--	--	108
75	--[a]	--	--	113
83	70.9	66.1	4.8	152
85	100.8	92.4	8.4	98
	102.7	99.2	3.5	
86	80.1	78.3	1.8	108
	84.6	83.8	0.8	
	88.4	86.7	1.7	
	90.9	89.9	1.0	
	92.9	91.5	1.4	

[a]Clicking noises associated with twinning were heard, but no change in the stress-strain diagram was detected.

Table 14. (Continued)

Specimen number	Stresses - 1000 psi			Test temp. °K
	Upper	Lower	Drop	
89	90.1	84.3	5.8	104
	99.3	87.0	12.3	

observed in niobium and tantalum. The Class I tantalum specimens exhibited a single twinning load drop and their stress-strain diagrams are very similar to the equivalent Class I niobium diagrams. The severity and frequency of the twinning load drops increased in tantalum with increasing impurity concentrations.

One other characteristic of the stress-strain diagrams for niobium and tantalum should be noted. That is, the fracture stresses for niobium were considerably higher than those for tantalum. Some of the Class I tantalum specimens fractured at virtually zero loads. The total elongations for the two materials were similar except that tantalum showed slightly greater elongation. From the stress-strain diagrams and the sounds associated with tensile testing, it appears that twinning in niobium is associated only with cleavage behavior; whereas in tantalum, twinning occurs in specimens of all compositions.

Deformation Appearances

Figures 20, 21 and 22 presented the appearances of fractured niobium specimens for the three classes of material. Figure 26 consists of four photographs at slightly larger magnification of the characteristic fracture appearances of tantalum and niobium. Part a of Figure 26 shows the severe distortion accompanying shear fracture in tantalum. The very sharp black spots seen on the end are holes and were characteristic of all shear fractures in tantalum. Shear fractures in niobium exhibited the same behavior, as can be seen in Part b of Figure 26. No specific differences could be identified between the tantalum and niobium shear fractures.

Part c of Figure 26 illustrates mixed shear and cleavage fractures. In this instance, the fracture is primarily cleavage; but in other specimens, shear was the dominant fracture mode. Part d of Figure 26 illustrates complete cleavage fracture observed in niobium. The fine white lines called "river markings" (108) were observed on each cleavage facet. The point from which the river markings radiate is the location from which fracture propagated across the grain, and that location was observed to be at interior grain boundaries. The river markings themselves consist of steps on the cleavage face where the cleavage changed atomic planes as the crack grew. On some cleavage faces, fine, straight, parallel traces were observed crossing the river markings. Since all such

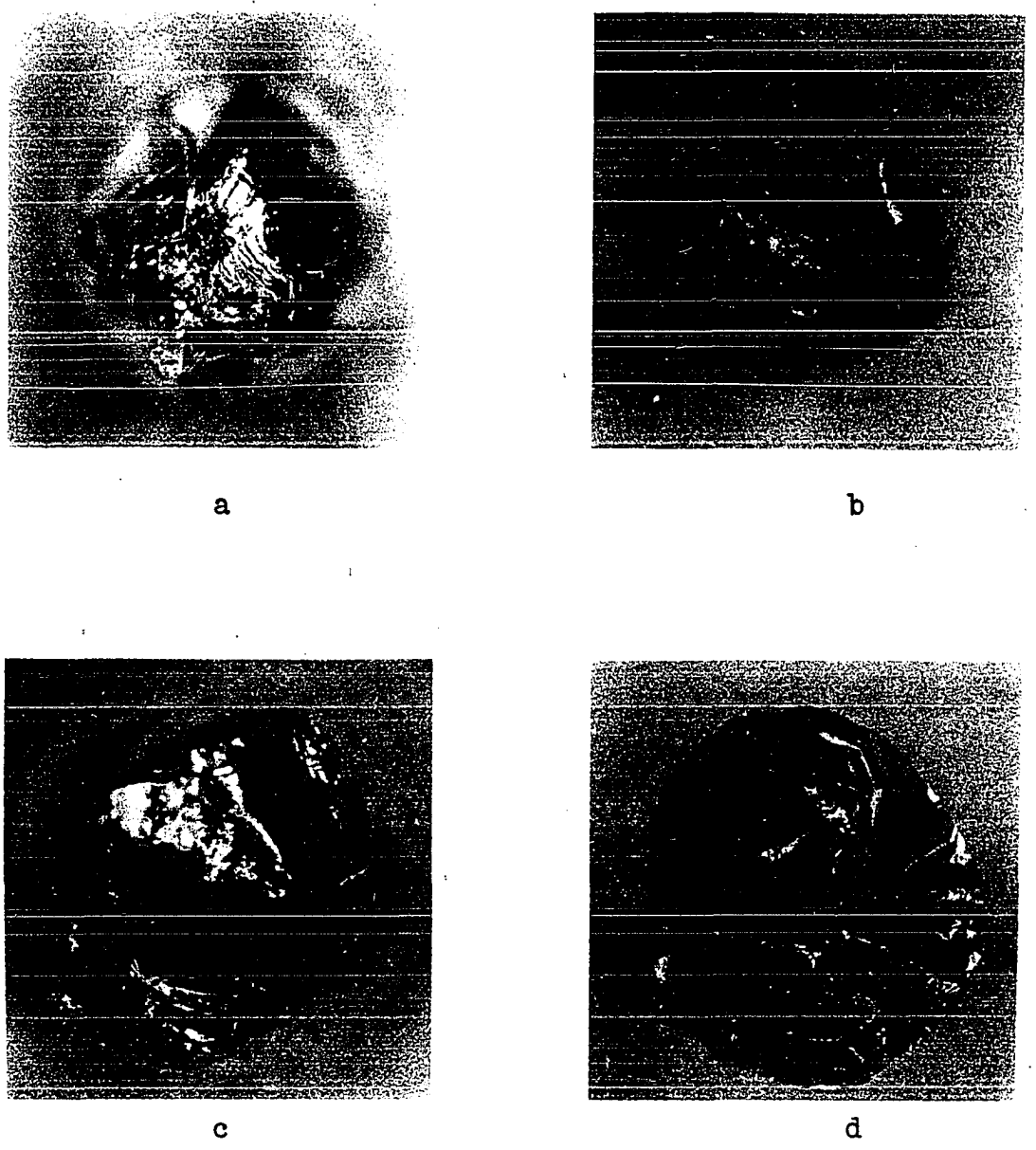

a b

c d

Figure 26. Typical fracture surfaces

a. Shear fracture in tantalum
b. Shear fracture in niobium
c. Mixed shear and cleavage fractures in niobium
d. Pure cleavage fracture in niobium

lines on a given cleavage face were parallel and straight, they were assumed to be traces of twinning or perhaps slip.

Some of the niobium specimens which exhibited mixed shear and cleavage also fractured along lines parallel to the tensile axis. These longitudinal fracture lines were fairly straight but not smooth, and appeared to be cleavage fractures.

Figure 27 illustrates the severe local deformation associated with both shear and cleavage fractures. Part a is a photograph of a tantalum tensile specimen which necked down to a fine point before finally separating. The distortion of individual grains can be seen in Part a, and the extreme deformation of grains at the fracture surface is emphasized by the distortion of the photo-grid on the grain at the center at the fracture end. The photo-grid farther away from the fracture is virtually the same size as originally applied; whereas, the grid spacing at the fracture surface is somewhat more than double the original spacing. Note too that the the deformation within the individual grains is not uniform.

Part b of Figure 27 shows a niobium specimen which failed primarily by cleavage. The bright area at the top consists of cleavage facets. The distortion of the photo-grid on the grain at the center was characteristic of all specimens which failed by cleavage. In this particular case, the grain had elongated about 100 per cent at the point on the surface at which cleavage occurred. Note that some

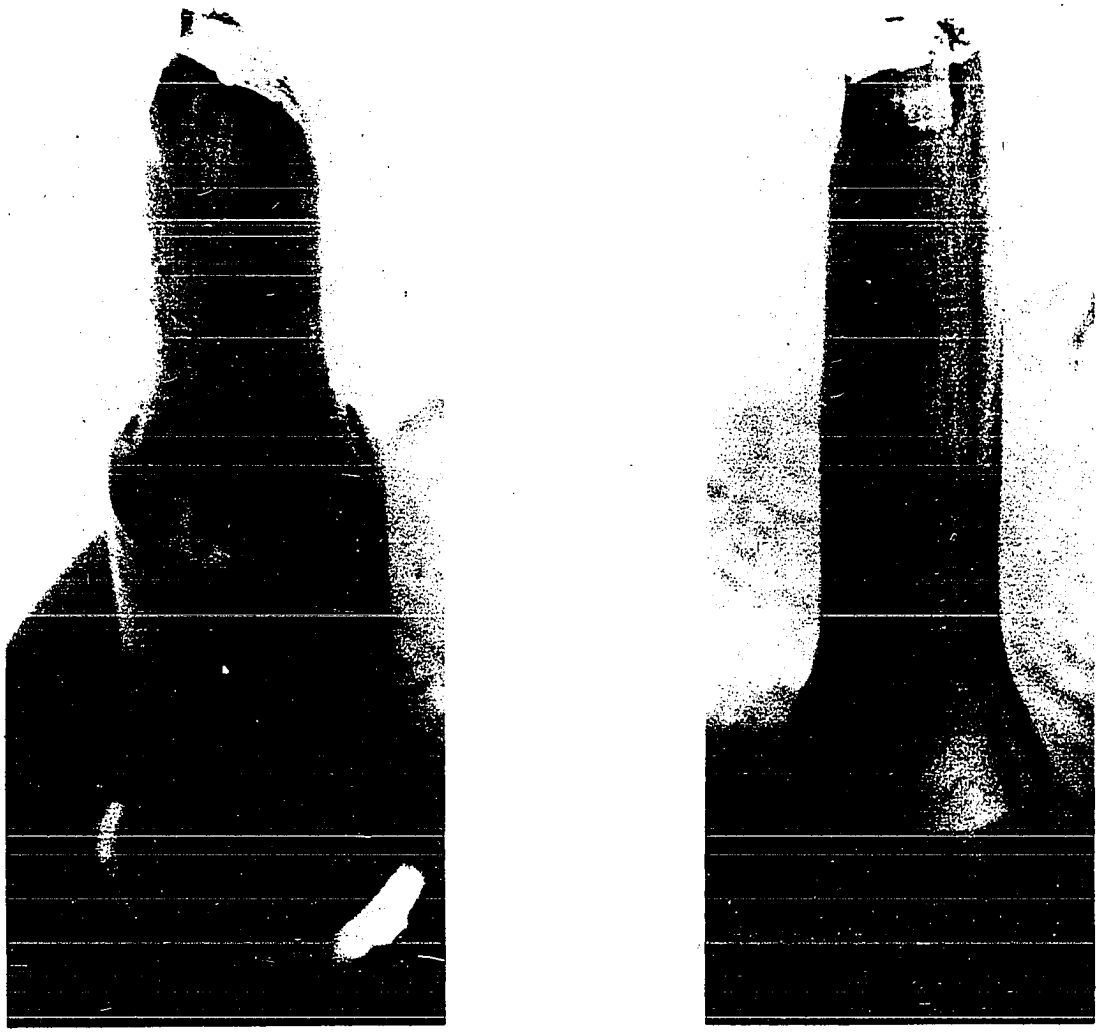

a b

Figure 27. Examples of localized deformation emphasized by distortion of photo-grid

a. Shear fracture in tantalum T-170 tested at 103°K
b. Distortion in cleaved grain in niobium T-75 tested at 113°K

twisting of the grid has occurred as the individual grains twisted and elongated.

The deformation which led to fracture was extremely inhomogeneous as was illustrated by Figure 27. In some cases more than one portion of the reduced section exhibited initial necking. In every case, the location of grain boundaries was made more clear by deformation within the individual grains which resulted in formation of ridges or grooves between the grains. In the preceding chapter, we found from examination of tensile data that grain size had little effect on the strength of niobium or tantalum at low temperatures. In this investigation it was observed that fracture, whether shear or cleavage, occurred where the original specimen diameter had been smallest (differences in specimen diameter amounted to $\pm$ 0.0005 inch maximum) rather than in the largest grains or in the regions of larger grain size. In at least one instance, cleavage occurred in a section made up of at least ten grains, while another section of the same specimen composed of two grains did not even exhibit slip. These results indicate that the deformation behavior was much more sensitive to very small differences in applied stress than to very large differences in grain size.

Figure 28 illustrates characteristic markings found on the tensile specimens away from the fracture region. Part a of Figure 28 illustrates the fine, closely spaced, irregular

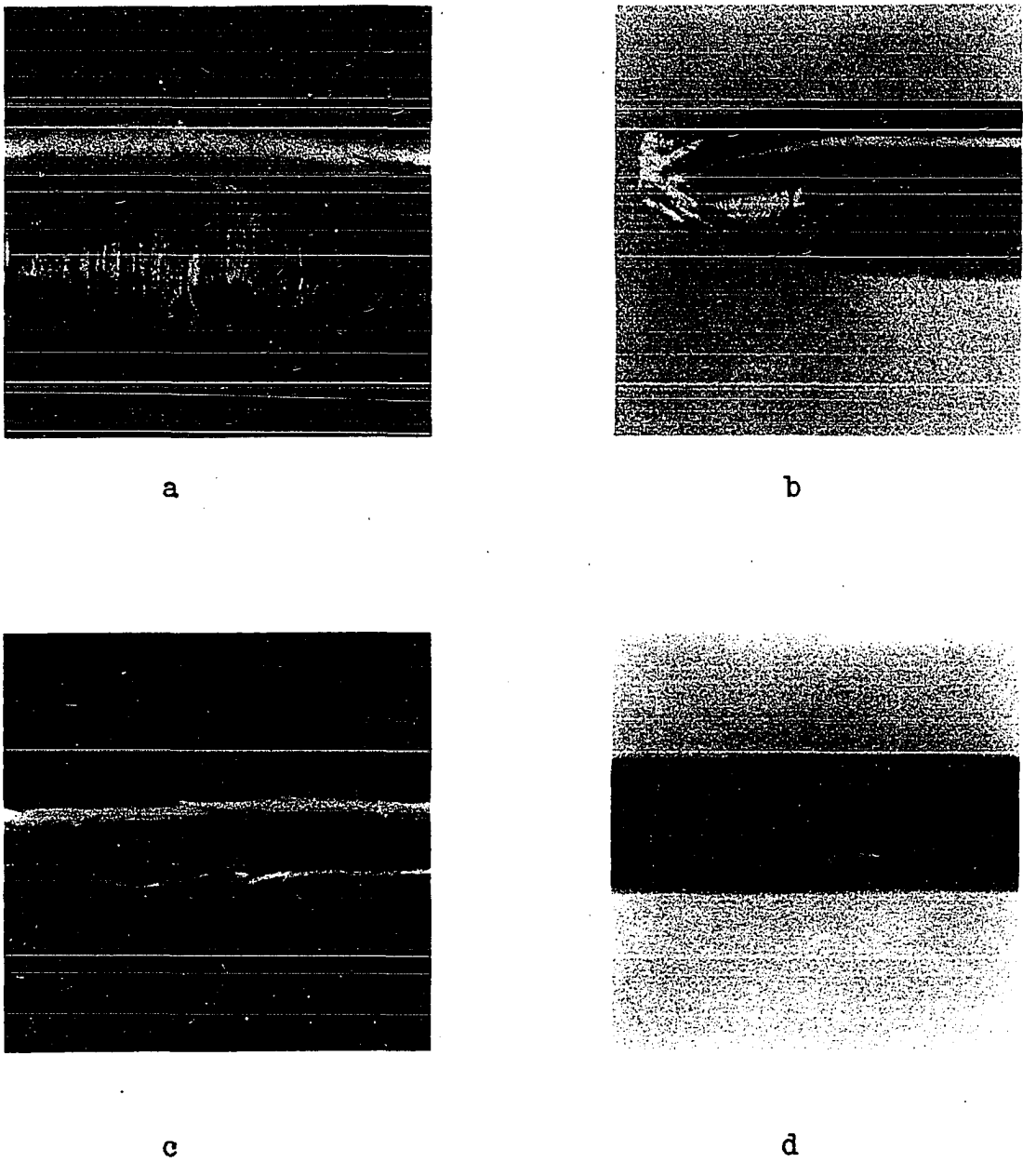

Figure 28. Characteristic deformation markings

a. Fine slip in niobium tested at room temperature
b. Coarse slip and fine slip (arrow) in tantalum at low temperatures
c. Coarse slip in niobium at low temperatures
d. Twinning and coarse slip in tantalum at low temperatures

slip traces found in both niobium and tantalum tested at room temperature. Close examination of these fine markings reveals that the traces consist of intersecting segments of lines which are not parallel. These slip traces correspond to the ones described by Elam (31, 32) which she accounted for by postulating that slip was occurring on several non-parallel slip planes at the same time. This fine slip was never observed in niobium specimens tested at low temperatures, but it was occasionally observed in tantalum specimens tested at low temperatures. Part c of Figure 28 illustrates the coarse slip traces more commonly observed on tantalum specimens tested at low temperatures. The grain to the right and slightly below the one which illustrates coarse slip exhibited fine slip.

Part b of Figure 28 illustrates the coarse slip traces characteristic of niobium tested at low temperatures. Traces of this type more often occurred in grains located near the fracture region, but occasionally were observed in grains away from the fracture. There was no detectable difference between coarse slip in niobium and in tantalum.

Part c of Figure 28 illustrates the twinning markings found on most tantalum specimens tested at low temperatures. Similar markings were occasionally observed in single grains from niobium specimens, but were not observed to have spread over the entire surface.

Aside from the differences in occurrence of twinning in niobium and tantalum, and the occurrence of cleavage of niobium, there do not exist distinct differences in deformation behavior. The complex fine slip characteristic of deformations in both materials at room temperature was not observed on niobium specimens tested at low temperatures. Some complex slip was observed in low temperature tantalum tensile specimens. Careful examination of coarse slip traces at high magnifications revealed that the traces were not uniform lines but contained many fine, short branches in both metals. Cleavage, whether caused by twinning or not, occurred in niobium specimens which exhibited twinning, but only after extensive plastic deformation.

Crystallography of Deformation

Some information concerning the crystallographic characteristics of deformation is necessary to complete our comparison of the behaviors of niobium and tantalum at low temperatures. The determination of the planes on which slip or cleavage occurred was accomplished by x-ray diffraction techniques combined with analysis of traces or surface markings. The success of the method depends on the existence of well-defined surface markings plus relatively clear x-ray patterns. Complications which interfere with analysis of surface markings include distortion of the grains and damage to the photo-grid measuring system. The x-ray diagrams

become difficult or impossible to interpret when more than one grain contributes to the pattern or when excessive deformation has occurred and the diagram spots representing particular crystal planes become extensively smeared. Partial success was achieved in determination of crystallographic characteristics of deformation.

Method

The Laue back-reflection x-ray method produces an x-ray photograph by diffraction of white x-radiation from a single crystal. Each class of planes, e.g. {h00}, produces one diffracted beam which is recorded as a spot on a film located between the sample and the x-ray source. For a given crystal system, the angles between particular crystallographic planes are fixed. The angles between the spots produced by the diffracted x-rays then provide a means for identification of these spots with particular crystallographic planes. The interpretation of a Laue back-reflection photograph is accomplished by measuring the location of the diffraction spots and transferring this information to a stereographic projection. On the stereographic projection, the angles between the spots may be determined and, by a trial and error process, the various spots may be indexed. After indexing the orientation of the crystal from which the pattern was made is known with respect to the incident x-ray beam and the plane of the recording film.

The slip traces which appear on the surface of individual grains in the tensile specimens intersect the photo-grid pattern at particular locations, depending on the inclination of the slip plane with the tensile specimen axis. If the slip actually occurs on a single set of planes in the crystal, then any three non-colinear points on the slip trace at the surface will define the spacial orientation of the slip plane. The photo-grid provides a convenient method of measuring or locating three or more such points on a given slip trace. If a cylindrical coordinate system is used with the specimen axis corresponding to Z, then the r coordinate is the same for all points on the surface so long as it remains cylindrical. Then the equation of the slip plane can be determined by three sets of Θ and Z values. Once the equation of the plane is determined, the equation of the normal to the plane can be calculated since the direction cosines of the normal are in the same ratios as the coefficients of the equation of the plane. If the direction of the plane normal is transformed into the coordinate system of the x-ray arrangement, the normal may be represented by another spot on the stereographic projection. Once the x-ray pattern is indexed, the slip plane may be identified.

The x-ray camera used was arranged so that the tensile specimens were mounted horizontally, parallel to the recording film and parallel to the edges of the film. Precise location

and orientation of individual grains selected for analysis was accomplished by means of a metallurgical microscope adapted so as to fit in place of the x-ray collimator and film holder. The optical axis of the microscope coincided with the axis of the x-ray beam. The photo-grid provided a reference system by which particular grains were located for x-ray analysis, and ink spots on the photo-grid served to fix the system axes. Satisfactory x-ray patterns were obtained by variation of x-ray beam diameter so that only one grain of a specimen contributed to the diffraction pattern. The minimum grain size which could be analyzed by this technique was more often limited by the ability to measure slip traces than by x-ray limitations.

Cleavage

Determination of the planes on which cleavage occurred was accomplished by orienting the fracture surfaces so that cleavage facets were parallel to the incident x-ray beam. The cleavage plane is that plane perpendicular to the crystal axis coinciding with the incident beam axis. The principal complication arising in cleavage plane determinations was excessive plastic deformation. This caused the pattern spots to be smeared. The large majority of patterns, while indicating that some plastic deformation had occurred, were not clear enough to permit determination of crystal orientations. The extreme deformation of grains which failed by cleavage was

was discussed above, and the clarity of the majority of the x-ray patterns was surprising.

A total of eight satisfactory patterns was obtained from cleavage facets from niobium specimens. In four the cleavage planes were identified as having been (110). In the other four cases, the cleavage plane was identified as (100). This result is in agreement with the observations reported by Churchman (21) for cleavage in niobium. These results are illustrated in Figures 29, 30 and 31 in which a unit triangle from the stereographic projection is used to represent crystal orientations. As can be seen from the three figures, the cleavage orientations for all three classes of materials lie near the [110] and [100] directions.

Slip

Suitable grains for measurement of slip traces were located in nearly every tensile specimen. X-ray analysis of many of these grains, however, revealed that excessive deformation or twinning had occurred in the grains and thus the crystal orientation of such grains was not determinable. The excessive deformation smeared the spots into rings, making it impossible to measure the angles between the spots. Twinning essentially doubles the number of spots appearing in the diagram, and even though all of the spots are related by specific angles, the selection of spots which belong to one part of the twin orientation is quite difficult. In many of

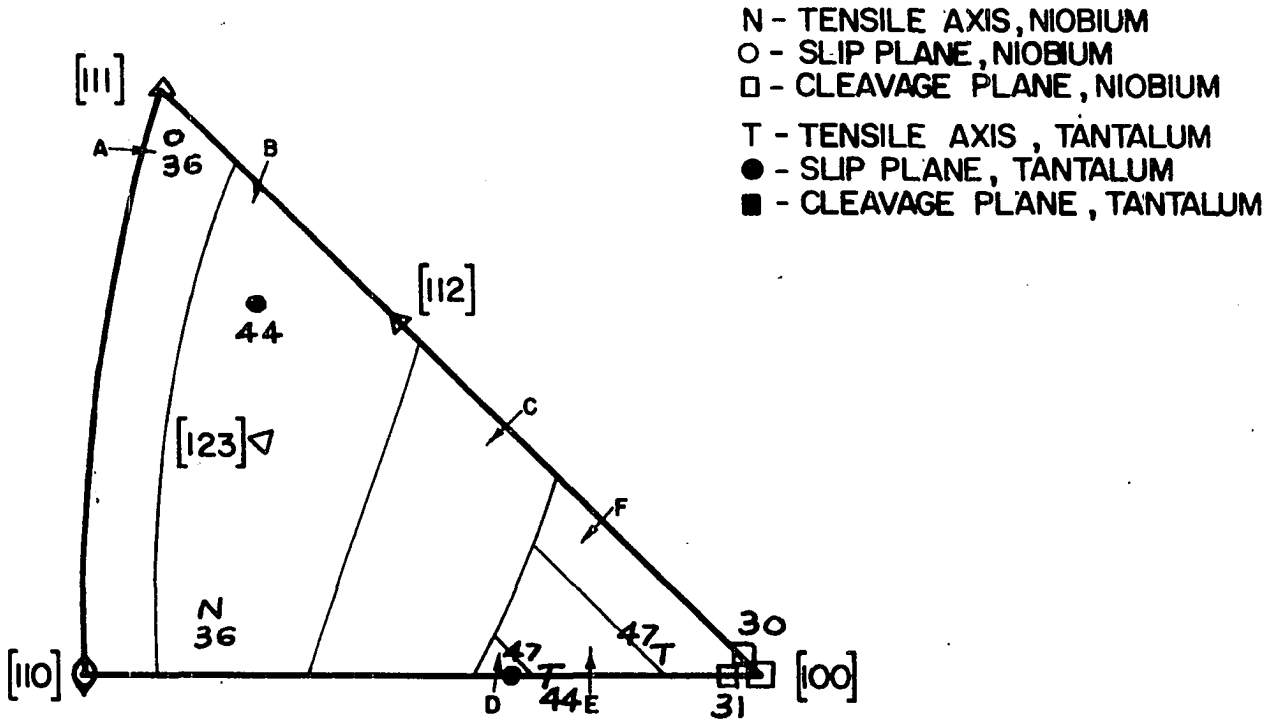

Figure 29. Unit stereographic triangle illustrating orientations of tensile axes, slip planes and cleavage planes in Class I niobium and tantalum

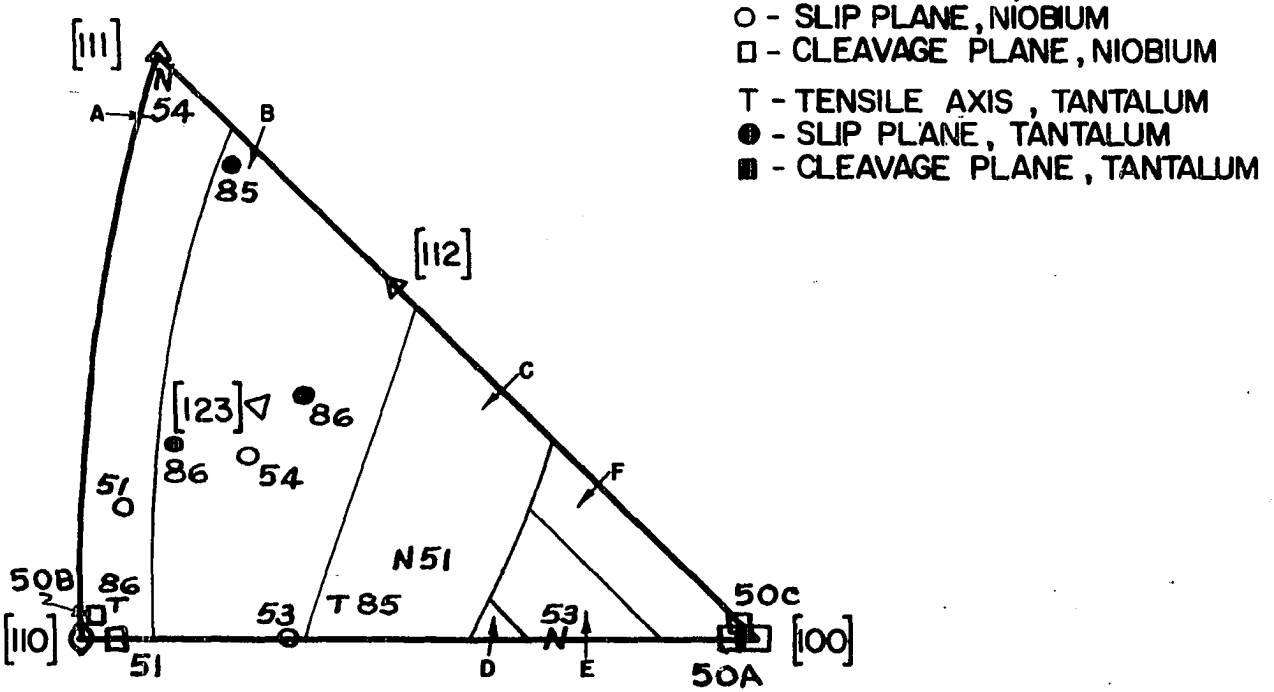

Figure 30. Unit stereographic triangle illustrating orientations of tensile axes, slip planes and cleavage planes in Class II niobium and tantalum

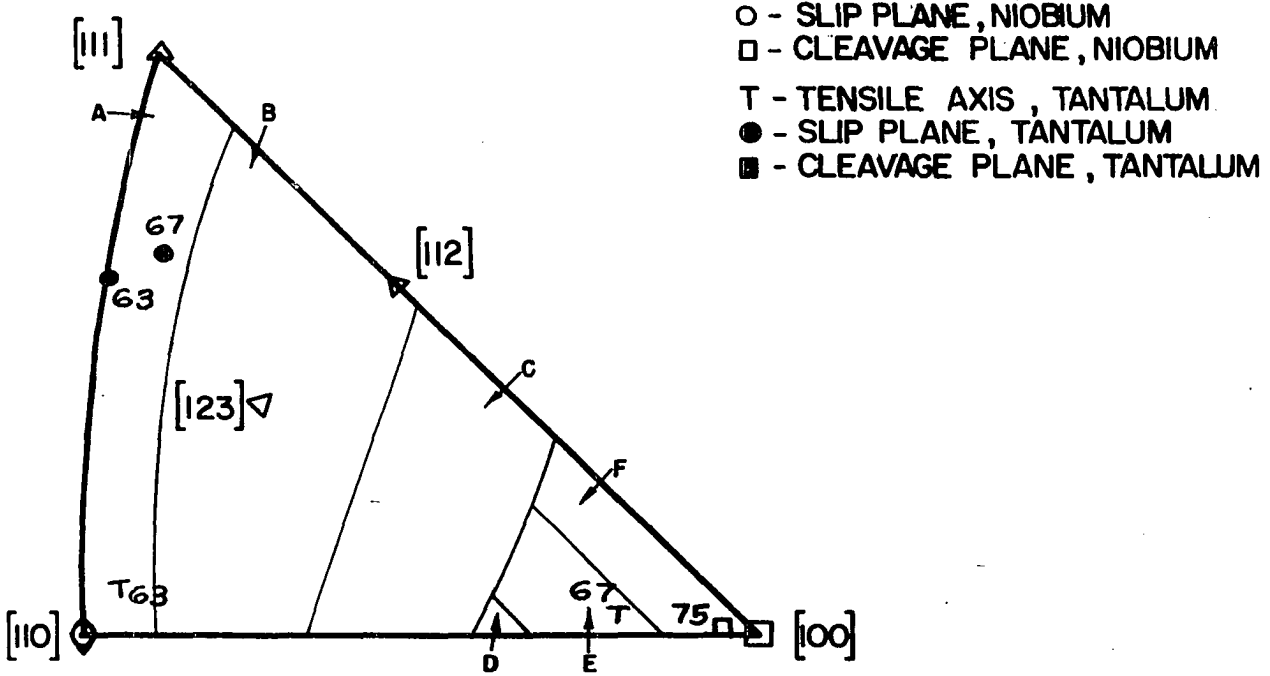

Figure 31. Unit stereographic triangle illustrating orientations of tensile axes, slip planes and cleavage planes in Class III niobium and tantalum

the patterns of grains selected for slip determinations, extraneous spots were found in the diagrams due to diffraction from other grains adjacent to the grain of interest. Again, separation of the spots belonging to individual grains is difficult.

The orientations of the individual grains are plotted in Figures 29, 30 and 31 along with the poles representing slip planes in these grains. The crystal orientation is defined as the direction parallel to the tensile axis. In the three figures, the unit triangles are divided into six zones lettered A through F, for which a particular slip plane has the greatest resolved shear stress. Opinsky and Smoluchowski (80, 81) determined the zones included in the figures by calculation of the resolved shear stress on {112}, {123} and {110} planes for crystals whose tensile axes lay in each zone. It was found that if a tensile axis of a given crystal were in Zone A, maximum resolved shear would be in the $(\bar{2}11)$ plane, for Zone B in the $(\bar{3}12)$ plane, for Zone C in the $(\bar{1}01)$ plane, for Zone D in the $(2\bar{1}3)$ plane, for Zone E in the $(21\bar{3})$ plane, and for Zone F in the $(11\bar{2})$ plane.

The slip orientations plotted in Figures 29, 30 and 31 exhibited no particular pattern except that slip near {110}, the planes expected to be dominant, was not observed. Slip traces which represent planes near both the other expected slip planes {112} and {113} were observed as well as traces

which represent planes near {111}. No particular pattern of change due to decreasing temperature could be determined.

It appears that unless slip occurs on crystallographic planes other than those having low indices, it must occur by some complex mechanisms such as those postulated by Elam. In the case of tantalum, complex slip was observed in low temperature specimens in some grains which were not included in this analysis. The results of x-ray analysis indicated that complex slip does occur in both niobium and tantalum at low temperatures.

In summary, cleavage was found to occur in niobium at both {110} and {100} planes. No cleavage was observed in any of the tantalum specimens. The slip traces observed in both tantalum and niobium were not systematically associated with any particular crystallographic plane. It was noted, however, that slip traces were not associated with {110} planes in these metals.

CONCLUSIONS

The deformation behaviors of equivalent niobium and tantalum were examined by means of tensile specimens tested in the temperature ranges in which the niobium materials exhibited a ductile-to-brittle transition. Twinning was found to be associated with cleavage or brittle fracture in niobium. Twinning was found to occur in all tantalum specimens. Complex slip in both niobium and tantalum was observed in room temperature test specimens as sets of fine, continuous traces with uniform angles of intersection. In low temperature niobium specimens, complex slip was indicated by irregularities in the traces observed at fairly high magnifications within coarse slip bands. The low temperature tantalum specimens exhibited both well-defined fine complex slip and irregularities in the coarse slip bands. X-ray determination of active slip planes in both niobium and tantalum deformed at low temperatures revealed no systematic behavior. The observed slip traces were not associated with particular crystallographic planes of low indices, indicating that complex slip occurred in both niobium and tantalum at the testing temperatures. Cleavage was observed to have occurred in niobium on {100} and {110} planes, but was not observed in any tantalum test specimens.

It was demonstrated that equal strengths for tantalum and niobium were obtained when equivalent composition structures

and testing conditions were maintained. Under these equivalent conditions the only observed difference in deformation behavior was that niobium fractured by cleavage at temperatures and compositions for which twinning deformation was obtained, and tantalum exhibited large amounts of twinning deformation without cleavage fracture. The factors specifically considered and controlled in this investigation appear to be those which determine the yielding behavior of niobium and tantalum, but twinning and cleavage appear to be influenced by other or additional factors. Precise knowledge of composition and structure of niobium and tantalum should be sufficient to predict their yielding behavior at particular temperatures and strain rates once the specific effects of compositional and structural variations have been isolated.

Considerable plastic deformation preceded cleavage fracture in the niobium materials used in this investigation. The conditions which produced cleavage therefore must have been attained after the yielding since the yield behavior of material which failed by cleavage was the same as that of material which did not fail by cleavage. Twinning, even though it accompanied yielding, appears to be influenced by the same factors which induce cleavage, and therefore better knowledge of the causes of twinning should improve understanding of the phenomena of cleavage fracture in niobium.

BIBLIOGRAPHY

1. Adams, M. A. and A. Iannucci. The mechanical properties of tantalum with special reference to the ductile-brittle transition. U. S. Air Force Systems Command (Aeronautical Systems Division, Wright-Patterson Air Force Base, Ohio) ASD Technical Report 61-203. 1961.

2. Adams, M. A., A. C. Roberts and R. E. Smallman. Yield and fracture in polycrystalline niobium. Acta Metallurgica 8: 328-337. 1960.

3. Anders, F. J., M. W. Toaz and E. J. Ripling. An apparatus for conducting tensile tests at moderately elevated and sub-zero temperatures. Proceedings of the Society for Experimental Stress Analysis 16: 127-137. 1959.

4. Anderson, R. W. and S. E. Bronisz. Twinning in tantalum. Acta Metallurgica 1: 123-125. 1953.

5. Ang, C. Y. Activation energies and diffusion coefficients of oxygen and nitrogen in niobium and tantalum. Acta Metallurgica 1: 123-125. 1953.

6. Barrett, C. S. Metallurgy at low temperatures. Transactions of the American Society for Metals 49: 53-117. 1957.

7. Barrett, C. S. and R. Bakish. Twinning and cleavage in tantalum. Transactions of the American Institute of Mining, Metallurgical and Petroleum Engineers 212: 122-123. 1958.

8. Bechtold, J. H. Tensile properties of annealed tantalum at low temperatures. Acta Metallurgica 3: 249-254. 1955.

9. Begley, R. T. Development of niobium-base alloys. U. S. Air Force Air Research and Development Command (Wright Air Development Center, Wright-Patterson Air Force Base, Ohio) WADC Technical Report 57-344, part 2. 1958.

10. Begley, R. T. and J. H. Bechtold. Effect of alloying on the mechanical properties of niobium. Journal of the Less-Common Metals 3: 1-12. 1961.

11. Begley, R. T. and W. N. Platte. Development of niobium-base alloys. U. S. Air Force Air Research and Development Command (Wright Air Development Center, Wright-Patterson Air Force Base, Ohio) WADC TR-57-344, part 4. 1960.

12. Brauer, G. Die oxyde des niobs. Zeitschrift für Anorganische und Allgemeine Chemie 248: 1-31. 1941.

13. Brauer, G. and J. Jander. Die nitride des niobs. Zeitschrift für Anorganische und Allgemeine Chemie 270: 160-178. 1952.

14. Brauer, G. and R. Lesser. Karbonitride des niobs. Zeitschrift für Metallkunde 50: 487-492. 1959.

15. Brauer, G., H. Renner and C. J. Wernet. Die carbide des niobs. Zeitschrift für Anorganische und Allgemeine Chemie 277: 249-257. 1954.

16. Brauer, G. and K. H. Zapp. Die nitride des tantals. Zeitschrift für Anorganische und Allgemeine Chemie 277: 129-139. 1954.

17. Bryant, R. T. The solubility of oxygen in transition metal alloys. Journal of the Less-Common Metals 4: 62-68. 1962.

18. Buchheit, R. D., C. H. Brady and G. A. Wheeler. Procedures for the metallographic preparation of beryllium, titanium and refractory metals. Defense Metals Information Center (Battelle Memorial Institute, Columbus, Ohio) DMIC Memo 37. 1959.

19. Bullough, R. and R. C. Newman. The flow of impurities to an edge dislocation. Proceedings of the Royal Society of London 249A: 427-440. 1959.

20. Campbell, J. E. Review of current data on the tensile properties of metals at very low temperatures. Defense Metals Information Center (Battelle Memorial Institute, Columbus, Ohio) DMIC Report 148. 1961.

21. Churchman, A. T. Cleavage fracture in niobium. The Journal of the Institute of Metals 88: 221-222. 1960.

22. Conrad, H. and W. Hayes. Thermally-activated deformation of the bcc metals at low temperatures. Transactions Quarterly, The American Society for Metals 56: 249-262. 1963.

23. Cornell, K. Photo-grid printing. American Photography 36: 16-17. 1942.

24. Cost, J. R. and C. A. Wert. Metal gas equilibrium in the niobium-nitrogen terminal solid solution. Acta Metallurgica 11: 231-242. 1963.

25. Cottrell, A. H. Theory of brittle fracture in steel and similar metals. Transactions of the American Institute of Mining, Metallurgical and Petroleum Engineers 212: 192-203. 1958.

26. Cottrell, A. H. and B. A. Bilby. Dislocation theory of yielding and strain aging of iron. Proceedings of the Physical Society (London) 62A: 49-62. 1949.

27. Cox, J. J., G. T. Horne and R. F. Mehl. Slip, twinning and fracture in single crystals of iron. Transactions of the American Society for Metals 49: 118-131. 1957.

28. Cracknell, A. and N. J. Petch. Frictional forces on dislocation arrays at the lower yield point in iron. Acta Metallurgica 3: 186-189. 1955.

29. Dyson, B. F., R. B. Jones and W. J. McG. Tegart. The tensile properties of high purity niobium at low temperatures. The Journal of the Institute of Metals 87: 240-242. 1959.

30. Edwards, C. A. and L. P. Pfeil. The production of large crystals by annealing strained iron. Journal of the Iron and Steel Institute 109: 129-158. 1924.

31. Elam, C. F. (Mrs. G. H. Tipper). Distortion of metal crystals. Oxford University Press, Oxford, England. 1935.

32. Elam, C. F. (Mrs. G. H. Tipper). The distortion of β-brass and iron crystals. Proceedings of the Royal Society of London 153A: 273-301. 1936.

33. Elliott, R. P. Columbium-oxygen system. Transactions of the American Society for Metals 52: 990-1014. 1960.

34. Elliott, R. P. Columbium-carbon system. Transactions of the American Society for Metals 53: 13-28. 1961.

35. English, J. J. Binary and ternary phase diagrams of columbium, molybdenum, tantalum and tungsten. Defense Metals Information Center (Battelle Memorial Institute, Columbus, Ohio) DMIC Report 152. 1961.

36. Evans, P. R. V. The dependence of the lower yield stress on grain size in niobium. Journal of the Institute of Metals 92: 57-58. 1963.

37. Evans, P. R. V. Effect of nitrogen on yield strength of niobium. Journal of the Less-Common Metals 4: 78-91. 1962.

38. Ferriss, D. P., R. M. Rose and J. Wulff. Deformation of tantalum single crystals. Transactions of the Metallurgical Society of the American Institute of Mining, Metallurgical and Petroleum Engineers 224: 975-981. 1962.

39. Ferro, A. Theory of diffusion constants in interstitial solid solutions of bcc metals. Journal of Applied Physics 28: 895-900. 1957.

40. Gebhardt, E. and H. Preisendanz. Uber die loslichkeit von sauerstoff in tantal und die damit verbundenen eigenschaftsanderungen. Zeitschrift für Metallkunde 46: 560-568. 1955.

41. Gebhardt, E. and H-D. Seghezzi. Untersuchungen in system tantal-saurstoff. II. Reaktionen und gleichgewichte zwishen mischkristall und oxydphasen. Zeitschrift für Metallkunde 50: 521-527. 1959.

42. Gebhardt, E., H-D. Seghezzi and W. Durrschnabel. Untersuchungen im system tantal-stickstoff. Zeitschrift für Metallkunde 40: 577-583. 1958.

43. Gilbert, A., D. Hull, W. S. Owen and C. N. Reid. The yield of polycrystalline tantalum. Journal of the Less-Common Metals 4: 399-408. 1962.

44. Gregory, D. P. Temperature variation of flow stress in body centered cubic metals. Acta Metallurgica 11: 455-462. 1963.

45. Gregory, D. P., G. H. Rowe and A. N. Stroh. Work hardening mechanisms in body centered cubic metals. U. S. Air Force Systems Command (Aeronautical Systems Division, Wright-Patterson Air Force Base, Ohio) ASD Report ASD-TDR-62-354. 1962.

46. Griffith, A. A. The phenomena of rupture and flow in solids. Philosophical Transactions of the Royal Society of London 221A: 163-198. 1920.

47. Hahn, G. T. A model for yielding with special reference to the yield-point phenomena of iron and related bcc metals. Acta Metallurgica 10: 727-738. 1962.

48. Hahn, G. T., A. Gilbert and R. I. Jaffee. The effects of solutes on the ductile-to-brittle transition in refractory metals. Defense Metals Information Center (Battelle Memorial Institute, Columbus, Ohio) DMIC Memo 155. 1962.

49. Hahn, G. T., A. Gilbert and C. N. Reid. Dislocation dynamics of yielding. Battelle Memorial Institute Columbus, Ohio, Technical Review 12, no. 6: 3-8. 1963.

50. Hamilton, C. B. and H. A. Wilhelm. The preparation of tantalum metal by the carbon reduction of tantalum pentoxide. Proceedings of the Iowa Academy of Sciences 68: 189-201. 1961.

51. Hansen, M. Constitution of binary alloys. 2nd ed. Metallurgy and Metallurgical Engineering Series. McGraw-Hill Book Company, New York, N. Y. 1958.

52. Harper, S. Precipitation of carbon and nitrogen in cold-worked α-iron. Physical Review 83: 709-712. 1951.

53. Heslop, J. and N. J. Petch. The stress to move a free dislocation in alpha iron. Philosophical Magazine, Series 8, 1: 866-783. 1956.

54. Hull, D. Effect of grain size and temperature on slip, twinning and fracture in 3% silicon iron. Acta Metallurgica 9: 191-204. 1961.

55. Hull, D., I. D. McIvor and W. S. Owen. The distribution of dislocations in annealed tantalum. Journal of the Less-Common Metals 4: 409-418. 1962.

56. Hundy, B. B. The strain-age hardening of mild steel. Metallurgia 53: 203-211. 1956.

57. Imgram, A. G., E. S. Bartlett and H. R. Ogden. Effect of O_2 and H_2 on the mechanical properties of tantalum and columbium at low temperatures. Transactions of the Metallurgical Society of the American Institute of Mining, Metallurgical and Petroleum Engineers 227: 131-136. 1963.

58. Imgram, A. G., F. C. Holden, H. R. Ogden and R. I. Jaffee. Notch sensitivity of refractory metals. Transactions of the Metallurgical Society of the American Institute of Mining, Metallurgical and Petroleum Engineers 221: 517-525. 1961.

59. Johnson, A. A. The low temperature tensile properties of niobium. Acta Metallurgica 8: 737-740. 1960.

60. Johnson, A. A. On the determination of the yield stress parameters σ_I and Ky from a single stress strain curve. Acta Metallurgica 10: 975-977. 1962.

61. Johnston, W. G. and J. J. Gilman. Dislocation velocities, dislocation densities, and plastic flow in lithium fluoride crystals. Journal of Applied Physics 30: 129-144. 1959.

62. Kamber, K., D. Keefer and C. Wert. Interactions of interstitials with dislocations in iron. Acta Metallurgica 9: 403-414. 1961.

63. Ke, T. S. Internal friction in the interstitial solid solutions of C and O in tantalum. Physical Review 74: 9-15. 1948.

64. Kocks, U. F. and R. Maddin. Observations on deformation of niobium. Acta Metallurgica 4: 91-92. 1956.

65. Koo, R. C. Grain-size effects on the deformation of tantalum at low temperatures. Journal of the Less-Common Metals 4: 138-144. 1962.

66. Krudtaa, O. J. and K. Stokland. Electropolishing of columbium and tantalum. Metals Progress 77: 101-103. 1960.

67. Kubaschewski, O. and B. E. Hopkins. Oxidation of metals and alloys. 2nd ed. Butterworths, London. 1962.

68. Leadbetter, M. J. and B. B. Argent. The effect of oxygen on the mechanical properties of zone-refined niobium. Journal of the Less-Common Metals 3: 19-28. 1961.

69. Lement, B. S., D. A. Thomas, S. Weissmann, W. S. Owen and P. B. Hirsch. Substructure and mechanical properties of refractory metals. U. S. Air Force Systems Command (Aeronautical Systems Division, Wright-Patterson Air Force Base, Ohio) WADD Technical Report 61-181. 1961.

70. Ludwik, P. Die bedeutung des gleit und reisswiderstandes fur die werkstoff prufung. Zeitschrift Verein Deutscher Ingenieure 71: 1532-1538. 1927.

71. McHargue, C. J. and H. E. McCoy. Effect of interstitial elements on twinning in columbium. Transactions of the Metallurgical Society of the American Institute of Mining, Metallurgical and Petroleum Engineers 227: 1170-1174. 1963.

72. Maddin, R. and N. K. Chen. Plasticity of columbium single crystals. Transactions of the Metallurgical Society of the American Institute of Mining, Metallurgical and Petroleum Engineers 197: 1131-1136. 1953.

73. Maddin, R. and N. K. Chen. Geometrical aspects of the plastic deformation of metal single crystals. Progress in Metal Physics 5: 53-95. 1954.

74. Magnusson, A. W. and M. W. Baldwin, Jr. Low temperature brittleness. Journal of the Mechanics and Physics of Solids 5: 172-181. 1957.

75. Maitland, E. The treatment of gun-steel. Proceedings of the Institution of Civil Engineers 89: 114-240. 1886.

76. Miller, G. L. Metallurgy of the rarer metals. Volume 6. Tantalum and niobium. Academic Press, Inc., New York, N. Y. 1959.

77. Mincher, A. L. and W. F. Sheely. Effect of structure and purity on the mechanical properties of columbium. Transactions of the Metallurgical Society of the American Institute of Mining, Metallurgical and Petroleum Engineers 221: 19-25. 1961.

78. Ogden, H. R. Physical and mechanical properties of tantalum. Defense Metals Information Center (Battelle Memorial Institute, Columbus, Ohio) DMIC Memo 32. 1959.

79. O'Haven, C. P. and J. F. Harding. Studies of plastic flow problems by photo grid methods. Proceedings of the Society for Experimental Stress Analysis 2: 59-70. 1945.

80. Opinsky, A. J. and R. Smoluchowski. The crystallographic aspect of slip in body-centered cubic single crystals. I. Theoretical considerations. Journal of Applied Physics 22: 1380-1384. 1951.

81. Opinsky, A. J. and R. Smoluchowski. The crystallographic aspect of slip in body-centered cubic single crystals. II. Interpretation of experiments. Journal of Applied Physics 22: 1488-1492. 1951.

82. Osthagen, K. and P. Kofstad. The reaction between tantalum and nitrogen at 800-1300°C. Journal of the Less-Common Metals 5: 7-25. 1963.

83. Page, J. P. The annealing behavior of cold-rolled niobium. U. S. Atomic Energy Commission (Oak Ridge National Laboratory, Oak Ridge, Tenn.) Report ORNL-2372. 1957.

84. Parker, E. R. Brittle behavior of engineering structures. John Wiley and Sons, Inc., New York, N. Y. 1957.

85. Perkins, R. H., S. H. Cox, R. K. Waits and H. M. Busey. Tantalum annealing and degassing and hardness effects of dissolved gases. U. S. Atomic Energy Commission (Los Alamos Scientific Laboratory, Los Alamos, N. M.) Report LA-2136. 1957.

86. Petch, N. J. The ductile-brittle transition in the fracture of α-iron. Philosophical Magazine, Series 8, 3: 1089-1097. 1958.

87. Petch, N. J. The fracture of metals. Progress in Metal Physics 5: 1-52. 1954.

88. Powers, R. W. Internal friction in solid solutions of oxygen-tantalum. Acta Metallurgica 3: 135-139. 1955.

89. Powers, R. W. and M. V. Doyle. The associations of oxygen atoms in interstitial solid solution in tantalum. Transactions of the Metallurgical Society of the American Institute of Mining, Metallurgical and Petroleum Engineers 215: 655-665. 1959.

90. Powers, R. W. and M. V. Doyle. Internal friction in solid solutions of tantalum. Acta Metallurgica 4: 233-242. 1956.

91. Powers, R. W. and M. V. Doyle. Some internal friction studies in columbium. Transactions of the Metallurgical Society of the American Institute of Mining, Metallurgical and Petroleum Engineers 209: 1285-1288. 1957.

92. Pugh, J. W. Temperature dependence of the tensile properties of tantalum. Transactions of the American Society for Metals 48: 677-688. 1956.

93. Schmidt, F. F. Tantalum and tantalum alloys. Defense Metals Information Center (Battelle Memorial Institute, Columbus, Ohio) DMIC Report 133. 1960.

94. Schoeck, G. and A. Seeger. The flow stress of iron and its dependence on impurities. Acta Metallurgica 7: 469-477. 1959.

95. Schonberg, N. Some features of the Nb-N and Nb-N-O systems. Acta Chemica Scandanavica 8: 208-212. 1954.

96. Schwartzberg, F. R., H. R. Ogden and R. I. Jaffee. Ductile-brittle transition in the refractory metals. Defense Metals Information Center (Battelle Memorial Institute, Columbus, Ohio) DMIC Report 114. 1959.

97. Seybolt, A. U. Solid solubility of oxygen in columbium. Transactions of the American Institute of Mining, Metallurgical and Petroleum Engineers 200: 774-776. 1954.

98. Shank, M. E. A critical survey of brittle failure in carbon plate steel structures other than ships. National Academy of Sciences (Division of Engineering and Industrial Research, Washington, D. C.) Serial No. SSC-65. 1953.

99. Stiegler, J. O., C. K. H. Dubose, R. E. Reed, Sr. and C. J. McHargue. Dislocations in deformed and annealed niobium single crystals. Acta Metallurgica 11: 851-860. 1963.

100. Stiegler, J. O. and C. J. McHargue. The effect of impurities on mechanical twinning and dislocation behavior in body centered cubic metals. U. S. Atomic Energy Commission (Oak Ridge National Laboratory, Oak Ridge, Tenn.) Report ORNL-TM-542. 1963.

101. Stroh, A. N. Brittle fracture and yielding. Philosophical Magazine, Series 7, 46: 968-972. 1955.

102. Stroh, A. N. The cleavage of metal single crystals. Philosophical Magazine, Series 8, 3: 597-606. 1958.

103. Stroh, A. N. The formation of cracks as a result of plastic flow. Proceedings of the Royal Society of London 223A: 404-414. 1954.

104. Stroh, A. N. A theory on the fracture of metals. Advances in Physics 6: 418-465. 1957.

105. Taylor, G. I. and C. F. Elam. The distortion of iron crystals. Proceedings of the Royal Society of London 112A: 337-361. 1926.

106. Tegart, W. J. McG. The electrolytic and chemical polishing of metals in research and industry. 2nd ed. Pergamon Press, New York, N. Y. 1959.

107. Tietz, T. E., B. A. Wilcox and J. W. Wilson Mechanical properties and oxidation resistance of certain refractory metals. Stanford Research Institute (Menlo Park, California) AD 214829. 1959.

108. Tipper, C. F. The brittle fracture story. Cambridge University Press, Cambridge, England. 1962.

109. Todhunter, I. A history of the theory of elasticity and of the strength of materials from Galilei to the present time. Completed by Karl Pearson, ed. University Press, Cambridge, England. 1893.

110. United Kingdom Atomic Energy Authority Industrial Group. Brittleness in metals - a conference held at R&D Branch Culcheth Laboratories on 1st November, 1957. U. S. Atomic Energy Commission (Information Service Extension, Oak Ridge, Tenn.) Report TIS-347. 1960.

111. Van Torne, L. I. and G. Thomas. Yielding and plastic flow in niobium. Acta Metallurgica 11: 881-898. 1963.

112. Wellings, J. F. and R. Maddin. Low temperature tensile properties of zone-refined niobium (columbium). U. S. Atomic Energy Commission (University of Pennsylvania, Philadelphia, Pa.) Report NP 11795. 1962.

113. Wessel, E. T. Abrupt yielding and the ductile-to-brittle transition in body-centered cubic metals. Transactions of the Metallurgical Society of the American Institute of Mining, Metallurgical and Petroleum Engineers 209: 930-935. 1957.

114. Wessel, E. T. and D. D. Lawthers. The ductile-to-brittle transition in niobium. Westinghouse Research Laboratories, Pittsburgh, Pennsylvania. Scientific paper 6-94701-5-P1. 1957.

115. Wilcox, B. A., A. W. Brisbane and R. F. Klinger. The effects of strain rate and hydrogen content on the low-temperature deformation behavior of columbium. Transactions Quarterly of the American Society for Metals 55: 179-192. 1962.

116. Wilcox, B. A. and R. A. Huggins. The effect of interstitial atom-dislocation interactions on the deformation behavior of columbium, tantalum and 1020 steel. U. S. Air Force Systems Command (Aeronautical Systems Division, Wright-Patterson Air Force Base, Ohio Technical Report ASD-TR-61-351. 1962.

117. Wilson, D. V. and B. Russell. The contribution of atmosphere locking to the strain-ageing of low carbon steels. Acta Metallurgica 8: 36-45. 1960.

118. Wilson, D. V. and B. Russell. The contribution of precipitation to strain-ageing in low carbon steels. Acta Metallurgica 8: 468-479. 1960.

ACKNOWLEDGMENTS

I wish to thank my graduate committee, Steven Chamberlin, T.& A.M.; John Greene, History; William Larsen, Metallurgy; Sam Legvold, Physics; Harold Sharlin, History and Harley Wilhelm, Metallurgy, for their cooperation and encouragement in pursuing an independent and diverse program of study. Special thanks are due Dr. Wilhelm for his patience and assistance in conducting the research reported here and Dr. Larsen for his aid in preparing the dissertation.

The research was made possible by the Ames Laboratory which provided the materials, equipment and services necessary for the project. Most notable contributors of their services were Bob Howe, Keith Wolf, George Carter and Fred Lichte of Metallurgy Group I, who generously provided all-round assistance; Clifton Hill, who always performed vacuum fusion analyses ahead of schedule despite me and the materials; Harlan Baker and Earl Hopkins, whose metallographic and photographic skills are illustrated throughout the thesis; Dick Seliger, who fashioned the unseen equipment; and finally the patient souls Mary Lou Cowgill, "Jake" Jacobsen, Denny Sailsbury and Gary Wirtz who made it look pretty.

The driving force which sustained me through these years was fueled by my family and my stimulating friends in Metallurgy and the Mechanical Engineering Department. To all of these my grateful thanks.

APPENDIX

Table 15. Preliminary and final nitriding results for niobium

Material	Holding temperature °C	Holding time minutes	Weight g	Weight change mg	Weight change per unit surface area mg/cm^2	Weight change ppm
Cb4	836	0	45.3937	5.3	0.1557	117.0
	880	270	45.3990	4.2	0.1233	92.5
Cb5	836	0	45.4341	5.5	0.1614	121.0
Cb6	900	0	44.8010	1.8	0.0536	40.2
	900	0	44.8028	0.4	0.0119	8.9
	900	0	44.8032	0.0	0.0	0
	899	60	44.8033	0.1	0.0030	2.2
Cb7	900	0	45.3367	2.0	0.0588	44.0
	900	0	45.3387	0.1	0.0029	2.2
Cb8	947	120	45.7159	7.6	0.2217	166.2
Cb9	960	60	45.7118	5.5	0.1604	112.0
Cb10	960	30	45.7564	4.4	0.1282	96.2
Cb12	948	5	41.4743	3.9	0.1252	94.0
Cb18	951	15	45.6919	3.6	0.1051	78.8
Cb19	951	15	45.8358	3.5	0.1019	80.7
Cb20	951	15	45.7201	3.5	0.1021	74.4
Cb21	951	15	45.7341	3.6	0.1050	78.7
Cb22	955	150	45.7047	7.1	0.2071	155.3
Cb23	955	150	45.7366	7.2	0.2099	157.4
Cb24	955	150	45.7902	6.9	0.2009	150.7
Cb25	955	150	45.7048	7.1	0.2071	155.3
Cb27	960	660	45.7583	12.5	0.3643	273.2
Cb28	950	660	45.6448	12.5	0.3652	273.8
Cb29	960	660	45.8144	12.8	0.3725	279.4
Cb30	960	660	45.7024	12.8	0.3647	273.5

Table 16. Preliminary and final nitriding results for tantalum

Material	Holding temperature °C	Holding time minutes	Weight g	Weight change mg	Weight change per unit surface area mg/cm^2	Weight change ppm
Ta1	910	120	68.1400	18.3	0.6912	268.0
	860	60	68.0631	3.4	0.1286	49.9
	863	0	68.0665	0.5	0.0189	7.4
Ta2	910	120	68.2447	13.8	0.5205	202.0
	860	60	68.2012	5.1	0.1925	74.8
	863	0	68.2063	0.2	0.0075	2.9
Ta3	910	120	66.0338	7.9	0.3077	120.0
	860	60	65.9528	4.4	0.1716	66.7
	863	0	65.9572	0.1	0.0039	1.5
Ta4	900	0	88.3570	2.7	0.0791	30.6
	900	0	88.3597	0.7	0.0205	7.9
	900	0	88.3604	-0.8	0.0234	-9.0
	901	60	88.3600	0.4	0.0117	4.5
Ta5	900	0	88.4721	2.8	0.0819	31.6
	901	0	88.4749	1.1	0.0322	12.4
Ta6	947	120	88.4649	9.4	0.2750	106.3
Ta7	960	60	88.6249	5.6	0.1637	60.0
Ta8	960	30	67.4665	2.9	0.1106	43.0
Ta15	950	26	88.7020	5.4	0.1576	60.8
Ta16	950	26	88.7402	5.7	0.1662	63.1
Ta17	950	26	88.6735	5.3	0.1547	59.8
Ta19	950	58	88.5249	4.5	0.1315	49.7
Ta20	950	58	88.7022	4.3	0.1255	47.9
Ta22	950	58	88.6109	4.7	0.1371	51.3

Table 17. Summary of results of tensile testing niobium and tantalum

Sample	Composition ppm O	Composition ppm N	Interaction energy factor	Temp. °K	Strain rate $\times 10^{-3}$ %/sec.	Stresses - 1000 psi: Upper yield	Lower yield	Maximum	Fracture	Strain - %: Uniform[a]	Fracture	Reduction in area
30	34	24	1.0	77	10	114.2	---[b]	114.2	87.8	2.3	8.9	40.3
32	140	98	3.5	77	4.96	112.0	111.0	112.0	82.3	2.1	9.4	53.3
34	150	104	3.7	118	4.96	88.1	85.5	88.1	39.6	1.5	19.9	82.2
35	100	107	3.3	89	4.96	108.8	---[b]	108.8	97.3	0.6	5.2	41.1
36	94	100	3.1	98	4.96	106.7	100.0	106.7	51.9	0.9	11.0	66.3
37	183	264	7.4	93	4.96	--	102.8[c]	102.8	47.0	4.6	15.2	97.9
38	42	80	2.2	296	5.02	21.0	19.9	23.3	--[d]	4.7	4.7[e]	5.8
50	126	165	4.8	98	4.85	114.2	107.3	114.2	85.5	1.9	6.3	46.3
51	148	154	4.8	104	4.85	108.8	103.0	108.8	60.6	1.5	--	66.6
52	166	140	4.9	108	4.85	106.2	100.1	106.2	50.6	0.8	10.5	76.8
53	140	145	4.5	113	4.85	103.0	97.4	103.0	37.6	1.5	15.2	89.4
54	128	167	3.9	300	4.85	29.6	27.9	30.8	--[d]	7.8	8.4[e]	6.3
55	111	180	5.0	103	4.85	100.8	97.5	100.8	--[d]	1.9	6.3[e]	3.7
70	92	190	5.0	88	5.19		113.2	121.8	95.8	1.9	7.9	44.9
71	112	254	6.6	103	5.19	118.7	110.4	118.7	56.6	3.2	13.1	65.1
73	132	213	5.9	108	5.19	114.0	106.9	114.0	93.6	4.0	8.9	28.8
74	106	224	5.9	118	5.19	101.4	93.5	101.4	38.6	1.7	13.1	84.7

[a]Calculated from least change in diameter.

[b]Yield behavior obscured by twinning.

[c]Offset 0.2%.

[d]Test halted without fracture.

[e]Strain at maximum load.

Table 17. (Continued)

Sample	Composition ppm O	Composition ppm N	Interaction energy factor	Temp. °K	Strain rate x 10-3 %/sec.	Stresses - 1000 psi: Upper yield	Lower yield	Maximum	Fracture	Strain - %: Uniform[a]	Fracture	Reduction in area
75	104	258	6.6	113	5.19	106.1	98.2	106.1	64.6[d]	2.5	8.9	56.6
76	83	216	5.5	300	5.19	26.3	24.0	26.2	--[d]	9.7	10.0[e]	6.2
43	75	5	4.2	296	5.02	25.7	25.6	27.9	--[b]	5.5	8.9	40
44	32	10	3.8	101	5.02	102.8	100.0	102.8	2.3	0	15.2	95
45	57	18	4.1	119	5.02	95.6	93.2	96.6	2.3	0	15.7	95
46	42	14	4.6	107	5.02	98.2	96.0	98.0	23.3	2.5	12.1	95
47	88	17	6.4	87	5.02	100.4	97.1	100.4	2.3	0	12.1	95
63	30	25	4.6	93	5.05	112.2[b]	110.9[b]	114.2	44.6	12.5	16.8	95
66	34	35	5.4	108	5.05	--[b]	--[b]	103.3	31.0	1.8	18.9	95
67	34	26	4.9	113	5.05	--[b]	--[b]	96.7	25.8[d]	7.0	22.6	95
69	32	31	5.1	296	5.05	38.0	29.7	31.5	--[d]	8.9	15.2	20
170	34	27	4.9	103	5.05	101.8	90.6	101.0	27.9	0.9	17.3	95
83	170	100	15.1	152	5.03	74.3[b]	71.0	74.3	3.9	0.7	18.9	95
85	43	21	4.8	98	5.03	--[b]	99.4[b]	107.2	33.6	2.1	18.4	95
86	31	20	4.2	108	5.04	--[b]	--[b]	98.2	27.9[d]	3.0	21.5	95
87	31	26	4.6	296	5.04	--[b]	28.6[b]	30.0	--[d]	6.0	12.1	12.5
89	28	22	4.2	104	5.03	--[b]	--[b]	104.6	53.4	1.4	14.2	95

Table 18. Final annealing operations and results

Material	Sample	Temperature °C	Time minutes	Pressure x 10^{-6} mm Hg			Weight change ppm
				At hold	Maximum	Start	
Cb14	11	1690 ± 10	120	2.0 - 1.1	6.0	1.0	0
Cb14	12	1680 ± 10	120	0.9 - 0.9	2.3	0.9	-78
Cb14	13	1690 ± 5	120	1.6 - 1.3	2.9	1.8	-26
Cb14	14	1720 ± 40	120	1.4 - 1.3	2.0	1.3	+40
Cb14	15	1700 ± 15	240	2.1 - 1.3	2.3	1.2	+53
Cb14	16	1695 ± 10	240	1.7 - 1.4	2.2	1.4	-54
Cb14	17	1695 ± 10	240	1.7 - 1.6	2.7	1.6	+26
Cb14	18	1695 ± 10	240	1.6 - 1.2	2.4	1.3	0
Cb18	A	1700 ± 5	240	3.3 - 2.8	5.6	3.0	+20
Cb18	B	1715 ± 10	240	3.4 - 2.7	6.0	3.4	+27
Cb18	C	1700 ± 20	240	3.5 - 2.9	7.0	3.4	+33
Cb19	A	1720 ± 10	240	3.3 - 2.0	10.0	2.7	0
Cb19	B	1700 ± 50	240	3.3 - 2.9	6.4	3.0	+20
Cb19	C	1690 ± 20	242	3.4 - 2.6	6.6	2.5	0
Cb20	A	1710 ± 15	240	1.5 - 1.3	2.4	1.4	- 7
Cb20	B	1725 ± 10	248	1.6 - 1.2	2.3	1.3	- 7
Cb20	C	1695 ± 45	240	2.0 - 1.6	3.2	1.5	unknown
Cb22	A	1720 ± 15	240	4.4 - 3.0	10 +	3.0	+305
Cb22	B	1695 ± 35	247	3.9 - 3.1	8.6	3.3	+17
Cb22	C	1725 ± 20	240	3.6 - 3.0	6.8	3.2	+ 7
Cb23	A	1710 ± 10	240	3.4 - 2.8	5.0	3.0	+33
Cb23	B	1730 ± 25	242	4.0 - 2.9	4.3	3.0	+33
Cb23	C	1715 ± 15	240	4.5 - 3.0	8.8	3.3	+20
Cb24	B	1710 ± 15	61	2.2 - 1.7	3.6	1.8	-13
Cb27	A	1695 ± 15	240	3.5 - 3.0	10.0	3.2	+20
Cb27	B	1740 ± 10	240	3.8 - 2.8	4.3	3.0	+14
Cb27	C	1720 ± 40	245	3.6 - 3.0	4.5	3.4	+ 7

Table 18. (Continued)

Material	Sample	Temperature °C	Time minutes	Pressure x 10^{-6} mm Hg			Weight change ppm
				At hold	Maximum	Start	
Cb28	A	1710 ± 10	245	3.7 - 3.5	4.6	3.3	+20
Cb28	B	1710 ± 25	240	4.0 - 3.2	4.8	3.3	+33
Cb28	C	1715 ± 35	240	3.5 - 3.0	5.8	3.0	+20
Cb29	A	1710 ± 15	220	1.8 - 1.6	4.6	1.6	-40
Ta15	A	2120 ± 10	244	3.0 - 1.6	3.4	1.7	-56
Ta15	B	2095 ± 15	240	3.0 - 2.0	4.4	1.4	-17
Ta16	B	2105 ± 10	240	3.0 - 1.6	3.9	1.7	-37
Ta16	C	2090 ± 10	240	3.1 - 2.0	4.0	2.1	-52
Ta17	B	2090 ± 15	240	2.4 - 1.4	2.8	1.5	-50
Ta17	C	2105 ± 5	243	1.8 - 0.9	3.2	1.1	-42
Ta18	A	2085 ± 10	240	2.7 - 1.4	4.8	1.6	-52
Ta18	B	2095 ± 25	240	3.8 - 1.3	3.8	1.7	-132
Ta18	C	2087 ± 8	252	2.2 - 1.0	3.1	1.3	-69
Ta19	B	2085 ± 10	242	2.6 - 1.3	4.2	1.4	-77
Ta20	A	2095 ± 5	243	2.6 - 1.5	5.6	1.4	-100
Ta20	B	2075 ± 10	242	2.2 - 1.2	5.4	1.2	-59
Ta20	C	2090 ± 10	245	3.3 - 1.9	4.3	2.1	-45
Ta21	A	2080 * 5	243	2.0 - 1.3	3.4	1.5	-42
Ta21	B	2090 ± 5	240	2.5 - 1.3	4.1	1.9	-61
Ta21	C	2090 ± 15	240	2.0 - 1.4	3.1	1.4	-17
Ta22	B	2100 ± 5	247	2.4 - 1.2	4.8	1.8	-67
Ta23	A	2075 ± 15	120	1.7 - 1.3	3.2	1.2	-24

Table 19. Preliminary annealing operations and results

Material	Temperature °C	Time min.	Pressure x 10^{-6} mm Hg			Weight change ppm
			At hold	Maximum	Start	
			Niobium			
Cb1	1830 ± 20	60	3.4 - 2.7	6.9	3.8	--
Cb8	1480 ± 80	120	4.6 - 2.6	7.4	1.6	-5
Cb6	1510 ± 55	120	4.6 - 2.6	7.4	1.6	+5
Cb5	1685 ± 20	120	3.4 - 2.4	6.4	1.5	0
Cb10	1665 ± 10	180	3.1 - 1.1	4.8	1.6	-35
Cb7	1675 ± 5	180	2.6 - 1.4	10.0	1.0	-26
Cb9	1675 ± 5	180	3.3 - 2.0	4.2	1.8	0
Cb12	1695 ± 5	180	1.7 - 1.2	6.8	1.0	-5
Cb13	1675 ± 5	240	2.6 - 1.8	3.0	2.0	+13
Cb4	1705 ± 5	360	4.9 - 2.1	10.0	2.2	-24
			Tantalum			
Ta4	2000 ± 5	60	2.8 - 1.8	9.4	1.4	-9
Ta8A	1845 ± 20	120	2.4 - 1.6	5.0	2.5	0
Ta6	2055 ± 5	120	3.5 - 2.4	7.3	1.4	-11
Ta8B	1860 ± 25	240	2.4 - 1.6	6.0	1.4	-14
Ta7	2075 ± 20	240	3.1 - 1.4	13.0	1.5	-18
Ta5	1640 ± 15	360	4.8 - 2.7	10.0	2.8	+10